Mountain, G.S., Miller, K.G., Blum, P., et al., 1994
Proceedings of the Ocean Drilling Program, Initial Reports, Vol. 150

6. SITE 902[1]

Shipboard Scientific Party[2]

HOLE 902A

Date occupied: 11 June 1993

Date departed: 12 June 1993

Time on hole: 17 hr, 45 min

Position: 38°56.080′N, 72°46.349′W

Bottom felt (rig floor; m, drill-pipe measurement): 826.0

Distance between rig floor and sea level (m): 11.0

Water depth (drill-pipe measurement from sea level, m): 815.0

Total depth (rig floor; m): 857.0

Penetration (m): 31.0

Number of cores (including cores with no recovery): 4

Total length of cored section (m): 31.0

Total core recovered (m): 31.44

Core recovery (%): 101.4

Oldest sediment cored:
Depth (mbsf): 31.0
Nature: silty clay
Age: Quaternary
Measured velocity (km/s): 1.588

HOLE 902B

Date occupied: 12 June 1993

Date departed: 12 June 1993

Time on hole: 4 hr, 15 min

Position: 38°56.078′N, 72°46.364′W

Bottom felt (rig floor; m, drill-pipe measurement): 822.0

Distance between rig floor and sea level (m): 11.0

Water depth (drill-pipe measurement from sea level, m): 811.0

Total depth (rig floor; m): 832.5

Penetration (m): 10.5

Number of cores (including cores with no recovery): 1

Total length of cored section (m): 9.5

Total core recovered (m): 9.94

Core recovery (%): 104.6

Oldest sediment cored:
Depth (mbsf): 9.5
Nature: silty clay
Age: Quaternary
Measured velocity (km/s): 1.55

Comments: Drilled 0–1.0 mbsf

[1] Mountain, G.S., Miller, K.G., Blum, P., et al., 1994. *Proc. ODP, Init. Repts.,* 150: College Station, TX (Ocean Drilling Program).
[2] Shipboard Scientific Party is as given in the list of participants preceding the Table of Contents.

HOLE 902C

Date occupied: 12 June 1993

Date departed: 12 June 1993

Time on hole: 15 hr, 15 min

Position: 38°56.078′N, 72°46.364′W

Bottom felt (rig floor; m, drill-pipe measurement): 822.0

Distance between rig floor and sea level (m): 11.0

Water depth (drill-pipe measurement from sea level, m): 811.0

Total depth (rig floor; m): 952.0

Penetration (m): 130.0

Number of cores (including cores with no recovery): 16

Total length of cored section (m): 130.0

Total core recovered (m): 135.94

Core recovery (%): 104.6

Oldest sediment cored:
Depth (mbsf): 130.0
Nature: sandy silt
Age: late Miocene
Measured velocity (km/s): 1.57

HOLE 902D

Date occupied: 12 June 1993

Date departed: 18 June 1993

Time on hole: 5 days, 21 hr

Position: 38°56.079′N, 72°46.375′W

Bottom felt (rig floor; m, drill-pipe measurement): 819.0

Distance between rig floor and sea level (m): 11.0

Water depth (drill-pipe measurement from sea level, m): 808.0

Total depth (rig floor; m): 1559.1

Penetration (m): 740.1

Number of cores (including cores with no recovery): 82

Total length of cored section (m): 736.6

Total core recovered (m): 676.96

Core recovery (%): 91.9

Oldest sediment cored:
Depth (mbsf): 740.1
Nature: clayey nannofossil chalk with foraminifers
Age: late Eocene
Measured velocity (km/s): 2.067

Comments: Drilled 9.0–12.5 mbsf

Principal results: Site 902 (proposed Site MAT10) is in ~811 m of water on the upper continental slope off the New Jersey shore. It is located on CDP 1532 of *Maurice Ewing* Cruise 9009 (Ew9009) MCS Line 1027, 2 km north of, and slightly upslope from, the COST B-3 stratigraphic test well. The primary objective of Site 902 was to core and log a post-lower Eocene section containing seismic reflections that can be traced to sequence boundaries beneath the adjacent continental shelf. Shipboard paleontologic and paleomagnetic analyses provide preliminary ages for many of these surfaces; physical, chemical, and sedimentological descriptions, along with downhole log measurements, characterize the sedimentary facies. In combination with results from Sites 903 (proposed Site MAT11), 904 (proposed Site MAT12A), and 906, these data make possible a detailed study of the effect of glacioeustatic change on the stratigraphic record of siliciclastic passive margins.

Hole 902A began on 11 June 1993 after a seismic tie-in and a detailed bathymetric survey were completed (see Chapter 4, this volume). Continuous advanced hydraulic piston coring (APC) with 101.4% recovery to 31 mbsf sampled Holocene green muds and middle Pleistocene gray sandy silty clay. Operations ended when a core barrel became stuck at the bit face and could not be retrieved.

Hole 902B was offset 20 m west and APC operations resumed. Irregular seafloor topography led to miscalculation of true water depth, and the first core failed to recover the mud line.

Hole 902C was spudded without further offset, the mud line was recovered, and APC coring continued to refusal at 130 m with 104.5% recovery. These cores recovered a thin cover of Holocene green muds overlying thick middle Pleistocene gassy, gray sandy silty clays that include several thin slump/debris-flow deposits. Shipboard correlations of the GRAPE and biostratigraphic data indicate that this unit was nearly complete from within oxygen isotopic stage 5 to stage 13, with a possible hiatus within stage 10. Three seismic reflections apparently correlate with Pleistocene transitions from interglacial to glacial stages; slumps, reflections, and the possible stage 10 hiatus correlate with glacioeustatic lowerings. Upper Miocene sediments were recovered at the base of the hole (123–130 mbsf).

Hole 902D was offset another 20 m to the west and began with APC coring to 145 mbsf and 99.1% recovery. Coring with the extended core barrel (XCB) began at that depth and continued with extraordinarily high recovery (90.0%) to a total depth of 736 mbsf. The hole was logged with separate runs of the sonic-induction, lithoporosity, and Formation MicroScanner tools. The site was plugged and abandoned on 18 June 1993.

Six lithostratigraphic units are recognized at Site 902 that can be correlated with similar units at Sites 903, 904, and 906. One unit (II) that was defined at Site 903 was not found at Site 902. Units I through VI are primarily siliciclastic upper Pleistocene to upper Oligocene sediments, consisting of clays and silts with sporadic interbeds of fine- to medium-sized quartz and glauconitic quartz sands. Fragments of woody material are common in the Miocene section. These units indicate high terrigenous input. In contrast, Unit VII is a biogenic carbonate interval without significant terrigenous influence. Preliminary seismic correlations indicate that the boundaries between these units correspond to reflections, and that several other reflections match glauconite sand layers within the units. The units include the following:

Unit I (0–121.1 mbsf): Holocene to middle Pleistocene (stage 13 and younger), gray sandy silty clays with several thin slump/debris-flow units at Hole 902C;

Unit III (121.1–152.5 msbf): poorly fossiliferous upper Miocene gray silty clays with scattered layers of glauconite sands;

Unit IV (152.5–403.7 mbsf): upper and middle Miocene homogeneous gray silty clay and clayey silt with occasional siderite nodules/bands and abundant plant and wood fragments. Pyrite is present in disseminated and nodular form. Calcareous fossils are generally absent, and diatoms and dinoflagellates provide stratigraphic control;

Unit V (403.7–594.8 mbsf): middle to lower Miocene gray glauconitic silty clays and clayey silts, clay siltstone, and sandy silts with glauconite sand beds;

Unit VI (594.8–680.9 mbsf): lower Miocene to uppermost lower Oligocene silty claystones and silty clays distinguished by their brownish color, greater induration than is found in overlying units, and common nannofossils and diatoms; and

Unit VII (680.9–736.4 mbsf): upper Eocene siliceous nannofossil clayey chalks containing foraminifers. The striking lithologic contact between this and the overlying unit corresponds to an unconformity between the uppermost lower Oligocene and the upper Eocene. This boundary marks a significant change in depositional regime from pelagic, carbonate-dominated deposition during the Eocene to predominantly terrigenous deposition in the early Oligocene.

Calcareous microfossils are abundant to common in the Pleistocene and lower Miocene to Eocene sediments, and in these intervals they provide good biostratigraphic resolution. In contrast, calcareous microfossils are generally absent from the upper and middle Miocene silty clays; diatoms and dinoflagellates provide stratigraphic control for these sections. Dinoflagellates provide the only zonal control in cores barren of calcareous microfossils and nonsignificant diatom assemblages. Rich benthic foraminifer assemblages indicate transport of material from the shelf during the Pleistocene, with little in situ fauna found; in contrast, Eocene to lowermost Miocene benthic foraminifer assemblages are predominantly in situ and indicate a shallowing from middle bathyal (600–1000 m) to upper bathyal (200–600 m), respectively.

Determining the magnetic stratigraphy at Site 902 was hampered by weak intensities of magnetization, downhole changes in the stability of magnetization under alternating-field (AF) demagnetization, and suspected diagenetic changes in the magnetic mineralogy of the sediments. Remanent magnetization from the upper part of Holes 902C and 902D indicate a thick Brunhes polarity interval; dominantly reversed polarity magnetizations between 130 and 400 mbsf may represent a discontinuous record of the upper middle to upper Miocene. Polarity reversals in the lower middle Miocene to Eocene section suggest that further study will yield correlations to the time scale.

High concentrations of methane (as high as 64%) were measured in headspace samples from Site 902; heavier volatile hydrocarbons (C_2–C_5) were detected in trace levels. However, elevated C_1/C_2 ratios and correspondingly high interstitial water alkalinity values (30 mM) indicate the gas was biogenically generated. Rapid sedimentation rates caused by mass flows and slumping off the continental shelf plus an abundant supply of terrestrially derived organic matter have produced total organic carbon (TOC) values that range from 0.3% to 3.9%. Low carbonate contents (<0.8%) between 150 and 550 mbsf are associated with scarce calcareous microfossils; low pH values in this interval indicate that carbonate has been dissolved during diagenesis.

Chloride ions and salinity increase with depth at Site 902, and this trend is associated with a sharp drop in pH to a minimum value of 6.5 at 609 mbsf. These slightly acidic pH values are associated with rare occurrences and ghosts of calcareous microfossils. The return to higher pH at 640 mbsf corresponds to a downward increase in calcareous microfossils. A similar increase in salinity was observed at nearby DSDP Site 612, indicating that the migration or diffusion of a salt brine came from greater depths.

Bulk density varies cyclically downhole, and values determined with GRAPE are used for Pleistocene correlations to the SPECMAP time scale; they also show significant variations in the Miocene section. Magnetic susceptibility peaks are also associated with GRAPE maxima in the Pleistocene section. Water content and porosity vary inversely with bulk density, but closely mirror trends in bulk density. This relationship suggests that most variations in bulk density are the result of variations in porosity. The ADARA temperature shoe was deployed at Site 902, and 18 sub-bottom temperature equilibration data sets were collected in the depth range of 22 to 140 mbsf. Preliminary temperature estimates indicate a linear gradient of 40°C/km.

Initial logging efforts ended at an impenetrably narrow section (bridge) at 216 mbsf in Hole 902D. The side-entry sub (SES) was then deployed to enable logging tools to reach the bottom of the hole. Three logging runs were completed: sonic induction from 30 m above seafloor (through the pipe) to 676 mbsf, lithoporosity from 508 to 710 mbsf, and Formation MicroScanner (FMS) from 502 to 689 mbsf. Despite the incomplete coverage, these logging data provide valuable correlations between the borehole and the seismic profiles that pass through this site. Four log units are recognized:

Unit 1 (66–465 mbsf) begins at the bottom of the drill pipe with relatively high and variable resistivity values (generally above 1.0 Ωm) and low velocities (1620 m/s). Values of both measurements decrease with depth to 300 mbsf, at which point velocities increase rapidly and remain roughly 1700 m/s to the bottom of the unit. The base of this unit is marked by a bridge.

Unit 2 (465–604 mbsf) displays resistivity values that decrease with depth from 0.6 to 0.45 Ωm, with several thin intervals with higher values. Natural gamma-ray values are higher than in the overlying unit. Sonic velocities increase steadily to about 1733 m/s and correspond with other log peaks in this unit.

Unit 3 (604–681 mbsf) is characterized by changes in density and velocity. Densities are higher and more variable than they are in Unit 2, whereas velocities are highly variable and range from 1940 to 2900 m/s.

Unit 4 (681–689 mbsf) corresponds to the siliceous nannofossil clayey chalks of lithologic Unit VII and was logged only with the gamma-ray tool and FMS.

The principal result from Site 902 is that sequence boundaries traced from beneath the shelf to the slope can be recognized as stratal surfaces and dated at Site 902. Numerous (~17) potential sequence boundaries are observed within the Ew9009 MCS grid on the shelf. Some of these were originally defined by Greenlee and Moore (1988) and refined by Greenlee et al. (1992) based on studies of a grid of seismic data acquired by Exxon Production Research. Others have been added based on an ongoing study of data collected by Lamont-Doherty Earth Observatory (G.S. Mountain, K.G. Miller, and N. Christie-Blick, unpubl. data, 1990). To avoid the possibility of having to reassign correlations between these two parallel and evolving data sets, we adopted a strictly local set of reflector names tied to the Leg 150 cores. For example, we correlated reflector m6 with the surface separating the lower lower Miocene from the uppermost Oligocene (hiatus ~23–26 Ma) and with the pink-3 sequence boundary on the shelf. Similarly, reflector m5 separates the lower and middle Miocene (~16 Ma) and is the same surface as the shelf sequence boundary Green of Greenlee et al. (1992). Other reflectors observed on Line Ew1027 and their ages include the following: p1, stage 7/6 transition; p2, stage 9/8 transition; p3, stage 11/10 boundary; p4, an unconformity between the middle Pleistocene and upper Miocene; m0.5, intra-upper Miocene; m0.7, within lower upper Miocene; m1, near the middle/upper Miocene boundary; m2, within the middle middle Miocene; m3, within middle middle Miocene; m4, near the lower middle Miocene boundary; m5, near the lower/middle Miocene boundary; m5.2, lower Miocene; m5.4, lower Miocene; m6, an unconformity separating upper Oligocene from lower Miocene strata; and o1, an unconformity separating uppermost Eocene from upper lower Oligocene strata.

BACKGROUND AND OBJECTIVES

Site 902 was the first site drilled by Leg 150 on the New Jersey continental slope. It is located 145 km (79 nmi) east-southeast of Barnegat Inlet, New Jersey, in a region of steeply sloping topography (generally 1:20, 3°) and incised slope canyons. Bathymetric control for this region is provided by SeaMARC (Farre and Ryan, 1987), SeaBeam (W. Ryan and D. Twitchell, unpubl. data, 1989), and Hydrosweep bathymetric data (G.S. Mountain and K.G. Miller, unpubl. data, 1990). Site 902 is in 802 m water depth on *JOIDES Resolution* PDR profiles (see Chapter 4, this volume); it is located 3.7 km (2 nmi) southwest of the thalweg of Berkeley Canyon on the southwest interfluve of an unnamed slope canyon ("middle Berkeley"; Fig. 1).

The geological background, hydrographic setting, and scientific justification for slope drilling are described in Chapters 1 and 2 (this volume). Due to the complexity of slope stratigraphy (e.g., Poag, Watts, et al., 1987), Leg 150 was designed to recover the Oligocene-Holocene "Icehouse" interval on the slope with a composite, stacked section from four sites as free of hiatuses as possible. Each borehole

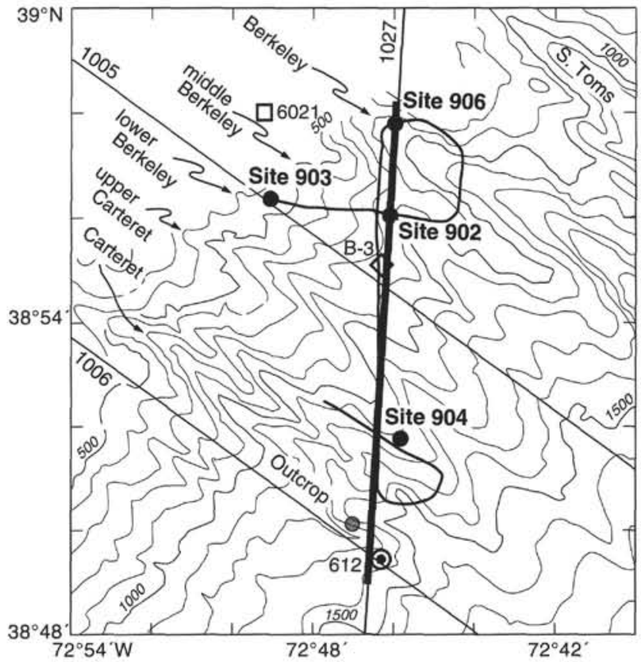

Figure 1. SeaBeam bathymetry with Leg 150 survey tracks near Sites 902, 903, 904, and 906. Heavy line indicates *Maurice Ewing* Cruise 9009 (Ew9009) MCS Line 1027 (shown in Fig. 2). Canyons are indicated by arrows. The outcrop indicated near DSDP Site 612 was sampled using the *Alvin* in 1989.

targeted different parts of the Oligocene-Holocene section; each was selected for its optimum thickness and clarity of seismic expression. Site 902 focused on the upper Oligocene and upper middle to upper Miocene sections.

The primary scientific objectives addressed at Site 902 and other slope sites are (1) to date Oligocene-Holocene "Icehouse" seismic sequences traced from the continental shelf, and (2) to evaluate correlation of these sequence boundaries with glacioeustatic age estimates obtained from the $\delta^{18}O$ record. Secondary goals are to determine ages of major Eocene "Doubthouse" unconformities and to test the link between sea-level change and slope failure.

The oldest strata to be drilled by Leg 150 are lower Eocene near the target reflector Red-3 (= the 49.5-Ma sequence boundary of Greenlee and Moore, 1988). This target was selected to complement drilling of Eocene strata at nearby DSDP Site 612, at the onshore sites at Island Beach and Atlantic City (see Chapters 1 and 2 in Miller et al., 1994), and to provide information on "Doubthouse" sequences. We have traced reflector Red-3 to Site 902 from DSDP Site 612, where it is associated with the top of a diagenetic front near the lower/middle Eocene boundary (Poag, Watts, et al., 1987).

Site 902 is located 2 km north (and slightly upslope) of the COST B-3 well, a stratigraphic test drilled in 819 m of water to a total depth of 3991 mbsf (Scholle, 1980). Greenlee et al. (1992) used samples from the COST B-3 well to estimate the ages of Miocene seismic sequences (see Figs. 5–6 in Chapter 2, this volume). Stratigraphic details were limited at COST B-3 because samples came from cuttings and a modest number of sidewall cores, the first of which were not recovered until 329 mbsf (middle Miocene and older). Seismic profiles connecting COST B-3 and Site 902 (Fig. 2) show the following:

1. The upper Miocene section above the Tuscan sequence boundary of Greenlee et al. (1992; ~10.5 Ma; herein designated m1) is thicker at Site 902 than at the COST B-3 well.

2. The middle Miocene section is thick between the Tuscan and Pink-2 reflectors of Greenlee et al. (1992; herein designated m3) at

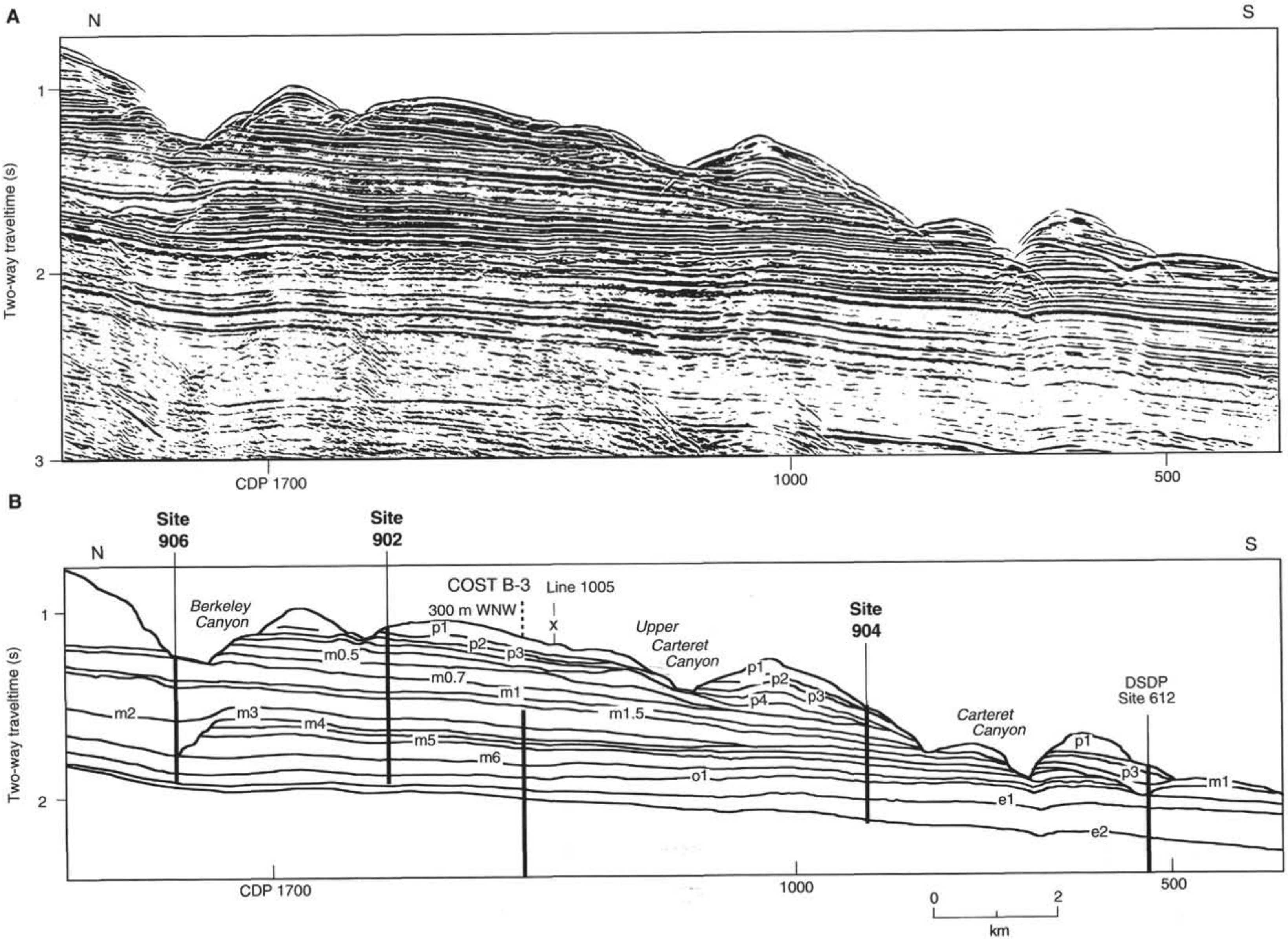

Figure 2. Cruise Ew9009 MCS Line 1027, an oblique dip profile shown as heavy line in Figure 1. **A.** Uninterpreted seismic section. **B.** Line drawing interpretation connecting ODP Sites 906, 902, and 904, the COST B-3 well (projected from ~300 m west-northwest), and DSDP Site 612. Reflectors (e.g., p1, p2) are described in the "Seismic Stratigraphy" section (this chapter). CDP = common depth point. Location of crossing with Line 1005 (Fig. 1) is shown (x). See also Plate 1 (back-pocket foldout).

both Site 903 and COST B-3; this was one of the primary criteria for selecting this site.

3. The upper Oligocene–lower middle Miocene section at COST B-3 is thin and punctuated by hiatuses (Scholle, 1980). This section also thickens away from COST B-3 toward Site 902, particularly between Pink-2 and Green of Greenlee et al. (1992; ?16 Ma; herein designated m4), and we anticipated a thicker upper Oligocene to lower Miocene section at Site 902.

4. The Eocene section at COST B-3 and Site 902 should be similar, although truncation of both the middle and upper Eocene section occurs between these sites and DSDP Site 612. Because of this, we placed a lower priority on reaching the top of the lower Eocene at this site than at Site 904.

Based on COST B-3 results and the Ew9009 seismic grid, Site 902 was predicted to penetrate a moderately thick (~300 m) upper Neogene (<10 Ma), a thick (200 m) upper middle Miocene section, a moderately thick (225 m) lower middle Miocene to upper Oligocene section, and a thin (75 m) middle to upper Eocene section.

OPERATIONS

Transit from Lisbon to Site 902

The vessel departed at 1045 hr (Universal Time Coordinated [UTC]), 28 May 1993, from Lisbon, Portugal. A rhumb-line course was set nearly due west for the operating area. The great-circle route was not taken because of the possibility of encountering icebergs and because it would have been directly into the main flow of the Gulf Stream current. Almost from the beginning, rough weather conditions prevailed, with 25- to 35-kt winds from the southwesterly quadrant the rule, and gusts to 66 kt that forced the ship onto a southwesterly course for 3 hr on 5 June. Weather conditions improved for the final 3 days of the transit, but opposing Gulf Stream currents limited speed over ground. The two days gained by the brief port call were lost on the Atlantic crossing. Average transit speed for the 2952 nmi (5404 km) from Lisbon to the survey way point was only 9.2 kt.

At 1415 hr, 10 June, speed was reduced and the seismic profiling gear was deployed. A preliminary survey was conducted to tie in the navigation of previous surveys used for reference in locating the drill sites (proposed Sites MAT10–14; see Chapter 4, this volume).

Hole 902A

The first drill site of Leg 150 is located on the continental slope, about 79 nmi (145 km) off Barnegat Inlet, New Jersey, in approximately 800 m of water. The irregular bathymetry of the continental slope resulted in a discrepancy of 24 m between the corrected precision depth recorder (PDR) reading and the actual seafloor depth below the vessel. That, in turn, caused a loss of ~1 hr in "feeling for bottom" and a premature spud attempt that recovered only water.

At 1845 hr, Hole 902A was spudded with an advanced hydraulic piston corer (APC) "shot" from 819.5 m below driller's datum, the dual elevator stool (DES), to 829 m. Just under 3 m of core were recovered (Table 1), so water depth was set at 826 m. Continuous APC coring then began in clay that became quite stiff within 1 m of the seafloor. Temperature measurements with the "ADARA" shoe and magnetic core orientation were begun with Core 150-902A-3H.

The APC was being lowered for Core 150-902A-4H while the hole was being reamed to the depth of the top of the core interval when the coring assembly inadvertently was landed at the outer core barrel (OCB). The impact of landing caused the APC shearpins to fail and the corer to extend outside the bit. Attempts to recover the APC were unsuccessful, and a round trip of the drill string was necessary to recover the APC assembly.

Hole 902B

Hole 902B was spudded at 0430 hr, 12 June, with a 20-m west offset relative to Hole 902A. The bit was positioned at 823 m for the "mud-line" core to maximize core length while still recovering the seafloor interface. A full core barrel was recovered, indicating that the bit had been positioned below the seafloor for the shot. It was decided to start a new hole with no additional offset and try to recover the mud line.

Hole 902C

At Hole 902C, the corer was actuated from 818 m and found the seafloor at 822 m below DES (811 m below sea level) to begin continuous coring. Orientation and ADARA temperature-shoe measurements again began with Core 150-902C-3H. Full stroke could be achieved through only the upper 43 m in the exceptionally stiff silty clay. Orientation and temperature work were suspended after short cores and plastic liner failures on Cores 150-902C-6H and -7H to protect the instrumentation from impact damage. Though full-stroke indication was not regained, a lithology change to siltier material produced better coring conditions on the ensuing cores. Coring continued on an advance-by-recovery basis, but the majority of the liners were full. Cores were quite gassy below the heavy clay, and much of the "recovery" was a result of numerous gas separations and "puffing" of the core. One additional temperature measurement was attempted on Core 150-902C-10H at 78 mbsf and was successful.

An isolated occurrence of relatively heavy gases of suspected thermogenic origin was noted in association with thin sand beds around 90 mbsf. Geochemical studies later indicated a biogenic origin (see "Organic Chemistry" section, this chapter). The total gas concentration already was decreasing at that depth, however, and gas quantity fell off sharply below about 120 mbsf.

At 130 mbsf, liner failures and decreasing penetration indicated that the effective penetration refusal point was near. Coring was terminated with 104.6% recovery (Table 1) to begin the scheduled deeper APC/XCB hole, and the bit was pulled above the seafloor.

Hole 902D

After an additional offset of 20 m west, a seafloor APC core fixed water depth at 819 m below driller's datum (808 m below sea level). To provide stratigraphic overlap, a 3.5-m interval was drilled from 9.0 to 12.5 mbsf. This later proved unnecessary because the topography apparently offset the stratigraphic sections sufficiently relative to the seafloor. Continuous coring began with Core 150-902D-2H and proceeded to penetration refusal at 145 mbsf (Core 150-902D-17H). Incomplete stroke began with Core 150-902D-5H, and all subsequent APC cores were on an advance-by-recovery basis. The temperature shoe was deployed on Cores 150-902D-6H to -16H with good success despite the repeated high impacts.

Coring continued with the extended core barrel (XCB) system. The fifth XCB barrel to be dropped came to an abrupt halt because of a damaged joint of pipe. Coring resumed after a 1 hr delay. A high rate of penetration (ROP) and good core recovery continued until coring was halted at 507 mbsf for the first logging stage. The hole was flushed with drilling mud, and a "wiper" trip was started at 1015 hr, 14 June, to condition the hole. No significant overpull was felt as the bit was raised to 75 mbsf and started back down the hole, but a solid obstruction was encountered at 291 mbsf on the down-trip. It yielded to circulation and rotation after the top drive was reinstalled. The top drive was then left in the string, and the hole was found to be clean down to total depth. After an additional mud flush, the bit was pulled to logging depth at 82 mbsf.

Table 1. Coring summary, Site 902.

Core no.	Date (June 1993)	Time (UTC)	Depth (mbsf)	Length cored (m)	Length recovered (m)	Recovery (%)
150-902A-						
1H	11	1900	0.0–3.0	3.0	2.70	90.0
2H	11	1930	3.0–12.5	9.5	9.91	104.0
3H	11	2100	12.5–22.0	9.5	9.87	104.0
4H	12	0100	22.0–31.0	9.0	8.96	99.5
Coring totals				31.0	31.44	101.4
150-902B-						
*****Drilled 0.0–1.0 mbsf*****						
1H	12	0500	1.0–10.5	9.5	9.94	104.6
Coring totals				9.5	9.94	104.6
150-902C-						
1H	12	0530	0.0–5.5	5.5	5.37	97.6
2H	12	0615	5.5–15.0	9.5	9.94	104.0
3H	12	0730	15.0–24.5	9.5	9.93	104.0
4H	12	0830	24.5–34.0	9.5	10.26	108.0
5H	12	0930	34.0–43.5	9.5	10.08	106.1
6H	12	1110	43.5–45.0	1.5	1.50	100.0
7H	12	1245	45.0–50.0	5.0	5.28	105.0
8H	12	1335	50.0–59.5	9.5	10.02	105.5
9H	12	1410	59.5–69.0	9.5	9.88	104.0
10H	12	1505	69.0–78.5	9.5	10.25	107.9
11H	12	1600	78.5–88.0	9.5	11.23	118.2
12H	12	1635	88.0–97.5	9.5	9.23	97.1
13H	12	1700	97.5–105.5	8.0	8.29	103.0
14H	12	1730	105.5–115.0	9.5	10.03	105.6
15H	12	1810	115.0–121.0	6.0	5.66	94.3
16H	12	1920	121.0–130.0	9.0	8.99	99.9
Coring totals				130.0	135.94	104.6
150-902D-						
*****Drilled 9.0–12.5 mbsf*****						
1H	12	2200	0.0–9.0	9.0	8.94	99.3
2H	12	2300	12.5–22.0	9.5	8.79	92.5
3H	12	2320	22.0–31.5	9.5	9.68	102.0
4H	12	2340	31.5–41.0	9.5	9.97	105.0
5H	13	0000	41.0–50.5	9.5	7.38	77.0
6H	13	0100	50.5–60.0	9.5	10.30	108.4
7H	13	0200	60.0–69.5	9.5	10.93	115.0
8H	13	0300	69.5–79.0	9.5	10.29	108.0
9H	13	0400	79.0–88.5	9.5	9.42	99.1
10H	13	0500	88.5–98.0	9.5	7.41	78.0
11H	13	0545	98.0–107.5	9.5	10.51	110.6
12H	13	0630	107.5–117.0	9.5	11.47	120.7
13H	13	0730	117.0–126.5	9.5	6.92	72.8
14H	13	0815	126.5–131.0	4.5	4.38	97.3
15H	13	0930	131.0–135.0	4.0	3.80	105.3
16H	13	1200	135.0–140.0	5.0	4.93	98.6
17H	13	1245	140.0–145.0	5.0	5.13	102.6
18X	13	1355	145.0–152.0	7.0	7.81	111.6
19X	13	1430	152.0–161.5	9.5	4.21	44.3
20X	13	1500	161.5–170.9	9.4	10.01	106.5
21X	13	1520	170.9–180.3	9.4	10.00	106.4
22X	13	1650	180.3–190.2	9.9	9.84	99.4
23X	13	1710	190.2–199.8	9.6	9.87	102.8
24X	13	1730	199.8–209.4	9.6	9.86	102.7
25X	13	1755	209.4–219.1	9.7	9.85	101.5
26X	13	1830	219.1–228.8	9.7	9.91	102.2
27X	13	1900	228.8–238.4	9.6	9.88	102.9
28X	13	1920	238.4–248.1	9.7	9.84	101.0
29X	13	1945	248.1–257.7	9.6	9.91	103.0
30X	13	2015	257.7–267.3	9.6	9.90	103.0
31X	13	2045	267.3–277.0	9.6	9.89	103.0
32X	13	2115	277.0–286.6	9.6	9.90	103.0
33X	13	2145	286.6–296.3	9.7	6.39	65.9
34X	13	2215	296.3–305.9	9.6	4.16	43.3
35X	13	2245	305.9–315.5	9.6	9.84	102.0
36X	13	2315	315.5–325.1	9.6	9.85	102.0
37X	13	2340	325.1–334.8	9.7	9.91	102.0
38X	14	0000	334.8–344.4	9.6	9.35	97.4
39X	14	0030	344.4–354.0	9.6	8.89	92.6
40X	14	0100	354.0–363.6	9.6	9.93	103.0
41X	14	0130	363.6–373.3	9.7	9.89	102.0
42X	14	0200	373.3–382.9	9.6	9.50	98.9
43X	14	0230	382.9–392.6	9.7	9.73	100.0
44X	14	0300	392.6–402.2	9.6	9.22	96.0
45X	14	0330	402.2–411.9	9.7	2.95	30.4
46X	14	0415	411.9–421.2	9.3	9.71	104.0
47X	14	0500	421.2–430.6	9.4	8.97	95.4
48X	14	0545	430.6–440.0	9.4	8.39	89.2
49X	14	0620	440.0–449.3	9.3	8.46	90.9
50X	14	0650	449.3–458.9	9.6	9.84	102.0
51X	14	0745	458.9–468.6	9.7	9.66	99.6
52X	14	0830	468.6–478.2	9.6	9.56	99.6
53X	14	0855	478.2–487.9	9.7	9.87	102.0
54X	14	0920	487.9–497.6	9.7	9.83	101.0
55X	14	1000	497.6–507.2	9.6	9.98	104.0
56X	15	0400	507.2–517.0	9.8	8.78	89.6
57X	15	0500	517.0–526.0	9.0	8.73	97.0
58X	15	0530	526.7–536.0	9.3	9.94	107.0
59X	15	0600	536.0–545.5	9.5	6.16	64.8
60X	15	0630	545.5–555.0	9.5	6.24	65.7
61X	15	0715	555.0–564.6	9.6	9.82	102.0
62X	15	0830	564.6–574.4	9.8	9.94	101.0
63X	15	0940	574.4–584.0	9.6	9.80	102.0
64X	15	1045	584.0–593.7	9.7	9.93	102.0
65X	15	1200	593.7–603.3	9.6	3.32	34.6
66X	15	1340	603.3–613.0	9.7	9.60	98.9
67X	15	1500	613.0–622.2	9.2	9.87	107.0
68X	15	1700	622.2–631.9	9.7	9.82	101.0
69X	15	1740	631.9–641.6	9.7	9.80	101.0
70X	15	1830	641.6–651.2	9.6	9.83	102.0
71X	15	1915	651.2–660.9	9.7	9.94	102.0
72X	15	2000	660.9–670.5	9.6	9.93	103.0
73X	15	2115	670.5–680.2	9.7	8.33	85.9
74X	15	2245	680.2–689.9	9.7	8.05	83.0
75X	16	0115	689.9–699.5	9.6	4.89	50.9
76X	16	0300	699.5–709.2	9.7	9.80	101.0
77X	16	0530	709.2–718.8	9.6	3.36	35.0
78X	16	0730	718.8–722.8	4.0	1.33	33.2
79X	16	1000	722.8–728.4	5.6	3.69	65.9
80X	16	1300	728.4–733.4	5.0	0.72	14.4
81X	16	1510	733.4–736.1	2.7	0.29	10.7
82X	16	1700	736.1–740.1	4.0	0.33	8.3
Coring total				736.6	676.96	91.9
Drilled (9.0–12.5 mbsf)				3.5		
Total penetration				740.1		

The logging sheaves were rigged, and a sonic-induction gamma-ray tool string was run for the first logging attempt. The tool descended freely until it met an obstacle at 215 mbsf. Efforts to work the tool past the bridge or ledge were unsuccessful, so logs were recorded over the available open-hole interval. To maximize the log interval, the blocks were raised until the bit was only 53 mbsf. Further logging attempts were deferred until the hole reached total depth.

As the performance of the XCB system had been exemplary beyond 500 mbsf, the decision was made to continue deepening Hole 902D. When the logging sheaves had been rigged down, the drill string was run back to total depth. No sign of the obstacle at 215 mbsf was noted on the rig's weight indicator, but the bit again was stopped at 288 mbsf (later identified as sands correlated to reflector m1). Several minutes were required to open the hole using circulation only. Use of the top drive was avoided deliberately for the down-trip to determine if the side-entry sub (SES) could be used to place the logging tools below the obstructions. Two other minor bridges were cleared at 424 and 462 mbsf by means of the circulating head. Five meters of fill or tight hole were found at total depth.

Coring with the XCB resumed at midnight 14/15 June. One of the main bit's polycrystalline diamond compacts was recovered intact in the top of Core 150-902D-66X from 603 mbsf. Excellent core recovery and ROP continued to 681 mbsf, at which point the lithology changed to chalk. Both recovery and ROP fell off rapidly in the chalk and became worse as induration increased with depth. Sufficient water could not be delivered to the XCB cutting shoe to "lubricate" it because small passages in the shoe became plugged. Consequently, the cores became jammed off in the shoes. The bottom-hole assembly (BHA) weight was supported by the jammed-off core and was not applied to the cutting structure of either the bit or the cutting shoe. Coring was discontinued 70 m short of the ultimate target when Cores 150-902D-81X and -82X produced only about 30 cm of core each and 4 hr of rotating time were required to advance 6.7 m. Average recovery for Hole 902D was 91.9% (Table 1).

Preparations for logging included a wiper trip, circulating bridges or ledges out at 292 and 448 mbsf, flushing 10 m of accumulated fill from the hole, and making up the SES into the string. The first logging tool (sonic-induction gamma ray) was started down the pipe at 0530 hr, 17 June. An attempt was made to run the logging tool down into open hole after three stands of pipe had been run, but the tool came to rest on an obstruction only 55 m below the bit. After the tool was pulled back inside the drill string, the string was lowered until fill was tagged 10 m short of total depth. A successful log then was recorded from 677 to 103 mbsf as the tool followed the drill string back up the hole.

The same technique (SES) was used to obtain a log from 710 to 121 mbsf with the lithoporosity combination tool string. After a false start caused by failure of the Formation MicroScanner (FMS) tool, the backup tool was deployed for a successful log from 698 to 506 mbsf in a deteriorating hole. Caliper log records showed the hole to be in poor condition above about 500 mbsf, with numerous washouts and irregularities. Two or three restrictions in the hole almost certainly would have precluded logging without the use of the SES.

While the logging tools were being rigged down, the "ADARA" temperature recorder was deployed on the coring line for a check on the seafloor baseline temperature. Downhole measurements were completed at 1030 hr, 18 June.

The bit was returned to a solid obstruction at 677 mbsf, from which the hole was displaced with 10 lb/gal mud. After the mud had been emplaced, the string was pulled to 141 mbsf and cement slurry was spotted from about 141 to 120 mbsf before the bit was pulled from the hole. When the residual cement slurry had been flushed from the drill string, the recallable positioning beacons were recovered. The drill string then was tripped for a bit change and the dynamic positioning (DP) move to Site 903 began. Site 902 was abandoned officially at 1730 hr, 18 June.

LITHOSTRATIGRAPHY

A total of 740 m of section was penetrated and continuously cored at Site 902. Of the four holes drilled at Site 902 (see "Operations" section, this chapter), the stratigraphic section recovered at Hole 902D is the focus of the lithologic description. Holes 902A to 902C recovered mostly Pleistocene strata, which are also present in Hole 902D. Because the lithologies are similar at each of the four sites drilled on the slope during Leg 150, we have maintained the same unit designation at each location.

The sedimentary succession recovered has been divided into six major lithologic units (I and III through VII), ranging from upper Pleistocene to Eocene in age (Figs. 3–4). The lithostratigraphic column is not complete at Site 902 (when compared with Site 903), as Unit II is missing. Units I and III through VI (0–681 mbsf) comprise upper Pleistocene to uppermost lower Oligocene sediment, which primarily consists of clays and silts with sporadic interbeds of fine- to medium-sized quartz and glauconitic sands. These units reflect a high terrigenous input. The biosiliceous microfossils are mainly diatoms and sponge spicules; calcareous biogenic remains are mainly nannofossils and rarely foraminifers. Lithologic contacts between the units have been defined primarily by the occurrence of basal mass-transport deposits and coarse-grained sediment such as glauconite sands. The origin of glauconite is thought to be shallow marine (McRae, 1972). Therefore, glauconite sands were most likely transported by gravity-flow processes to Site 902. Large amounts of glauconite sands occur near the top of the Pliocene at DSDP Sites 612 and 613 (Poag, Watts, et al., 1987), in the New Jersey continental margin. Glauconite may also have been transported downslope to DSDP Sites 612 and 613 (Scott, 1987). Contacts between the lithologic units of Site 902 mark unconformities and appear to correlate with seismic reflections (see "Seismic Stratigraphy" section, this chapter).

Unit VII (681–736.4 mbsf) is the deepest unit at Site 902 and consists of upper Eocene clayey siliceous nannofossil chalks containing foraminifers. The striking lithologic contact between Units VI and VII corresponds to an unconformity between the uppermost lower Oligocene and the uppermost Eocene. This contact also represents a significant change in sediment depositional regime from pelagic, carbonate-dominated deposition during the Eocene to predominantly hemipelagic deposition in the Oligocene (Table 2).

The bulk rock mineralogy, identified with XRD in 21 samples from Unit I, between 2 and 123.3 mbsf in Hole 902C, is shown in Figure 5. Sixty-eight samples were studied from Units III through VII between 128.59 to 736.33 mbsf in Hole 902D (Fig. 6). Seven major minerals are identified: quartz, feldspar, calcite, dolomite, siderite, pyrite, and opal-CT. Clay minerals also occur, but further studies will be required for accurate identification. Mineral distribution is plotted according to the intensity of the main diffraction peak. Glauconite, quartz, and calcareous and siliceous microfossil abundances were estimated in smear-slide observations (Fig. 3). The inorganic carbonate content of the sediment was measured by coulometry. The calculated percentage of $CaCO_3$ assumes all inorganic carbon is present as calcite (Fig. 3) (see "Organic Geochemistry" section in Chapter 3, this volume).

Unit I

Intervals: Cores 150-902A-1H to -4H; Core 150-902B-1H; Core 150-902C-1H to Section 150-902C-16H-1, 113 cm; Core 150-902D-1H to Section 150-902D-13H-3, 110 cm
Depth: Hole 902A, 0–31 mbsf; Hole 902B, 1–10.5 mbsf; Hole 902C, 0–122.1 mbsf; Hole 902D, 0–121.1 mbsf
Age: upper to middle Pleistocene

This unit is characterized by hemipelagic sediment punctuated by intervals of mass-transport deposits (slumps and debris flows) as evidenced by contorted beds and contacts and deformed clay clasts (Fig. 7). Mass-transport deposits are interbedded with thick-bedded units (30–100 cm thick) and with thin (0–30 cm thick) intervals of color banding. Greenish gray silty clay is the major lithologic component of this unit. Very fine sand is a minor component. Quartz and feldspar are the major constituent minerals of the silty clay, and their abundances correlate throughout the unit except toward the base of the unit where feldspar abundance is greater (Fig. 5). Calcite (detrital and biogenic) is abundant near 38, 45, and 82 mbsf; it then decreases toward the base of the unit. The greatest abundance of calcite is observed near 38 mbsf (Fig. 5). Small amounts of dolomite are typical of this unit. Dolomite occurs together with abundant feldspars and traces of amphibole. This relationship suggests a detrital origin for the dolomite. Pyrite and opal-CT are minor constituents that occur sporadically throughout the unit.

Total carbonate content for Unit I at Hole 902D reaches a maximum of 30% at 40 mbsf; it then decreases downhole to <5% near the base of the unit at 126.5 mbsf (Fig. 3). Calcareous microfossils are also most abundant (~30%) near 40 mbsf; they range from 10% to 20% downward throughout the rest of the unit. Siliceous microfossils first occur near 40 mbsf and then range from 10% to 50% between 40 and 126.5 mbsf (Fig. 3).

A sharp color change from light to dark greenish gray (10Y 4/2 to N4) separates Holocene soft muds from stiffer muds at approximately 1 mbsf (Cores 150-902A-1H, 150-902B-1H, and 150-902C-1H). Greenish gray silty clay is interbedded with lighter and darker, thin color bands (5Y 4/1, 10Y 5/1, N3 to N5) and is bioturbated from 0 to approximately 69.5 mbsf. Burrows in this unit are, for the most part, filled with sand. The sand found in the burrows in some instances is stained black by hydrotroilite (iron sulfide) and/or is composed of pyrite.

Mass-flow units occur from 16 to 19 mbsf in Hole 902D (Core 150-902D-2H) and from 7 to 19 mbsf in Hole 902C (Cores 150-902C-2H and -3H). These mass-flow units are identified on the basis of contorted beds with variable dip directions and light to dark gray and pinkish green light to dark gray color variations (N3 to N4 and 10YR 3/1 to 10YR 4/1). A bed of medium to fine, normally graded sand with a sharp base occurs from 30.3 to 30.4 mbsf (Section 150-902D-3H-6, 90 cm). Slump and/or debris flows occur from 44 to 47

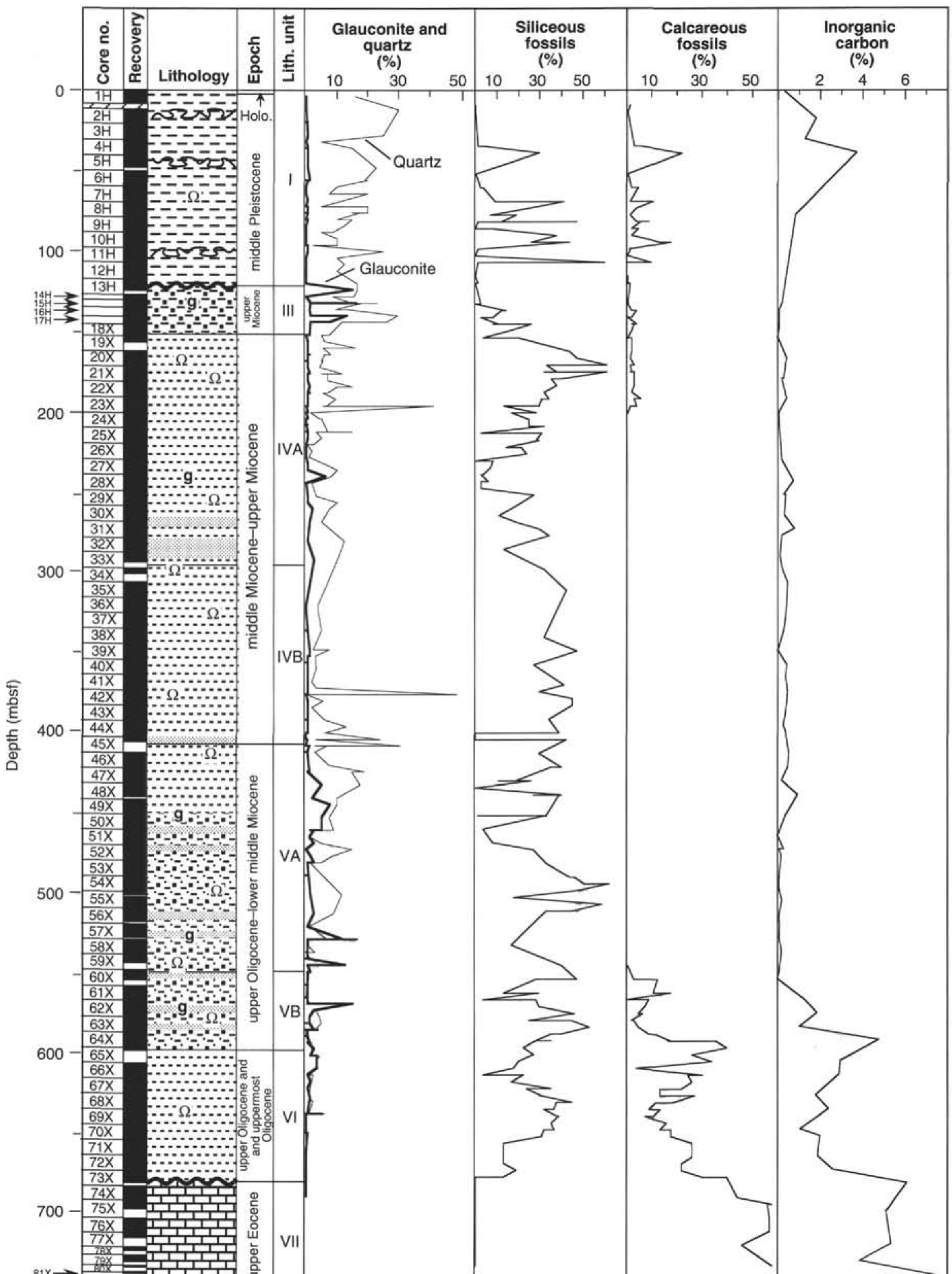

Figure 3. Generalized summary lithologic column for Hole 902D showing glauconite and quartz, siliceous (diatoms and sponge spicules) and calcareous fossil content (based on smear slides), and inorganic carbon (see "Organic Geochemistry" section, this chapter). See also Plate 2 (back-pocket foldout).

Table 2. Lithostratigraphy, Site 902.

Unit or subunit	Series	Depth (interval)	Lithology	Process
I	upper to middle Pleistocene	0–122.1 mbsf (Hole 902C) (150-902C-1H-1, 0 cm, through -16H-1, 113 cm) 0–121.1 mbsf (Hole 902D) (150-902D-1H-1, 0 cm, through 13H-CC-3, 110 cm)	Greenish gray silty clay to clayey silt.	Hemipelagic, rare mass-transport deposits.
		Major disconformity		
III	upper Miocene	122.1–TD (Hole 902C) (150-902C-16H-1, 113 cm, to -16H-CC, 19 cm) 126.5–152.5 mbsf (Hole 902D) (150-902D-14H-1, 0 cm, through -19X-1, 50 cm)	Silty clay with abundant glauconite.	Predominantly hemipelagic deposits and gravity controlled flows; rare mass-transport deposits (slumps, debris flows).
IVA	upper Miocene to middle Miocene	152.5–293.0 mbsf (Hole 902D) (150-902D-19X-1, 50 cm, through -33X-CC, 40 cm)	Homogeneous silty clay and clayey silt with siderite nodules and bands, and land plant debris.	Predominantly hemipelagic and rare gravity-controlled flows; alteration of sediments by flows; alteration of diagenetic processes.
IVB	middle Miocene	293.0–403.7 mbsf (150-902D-34X-1, 0 cm, through -45X-1, 150 cm)	This subunit has the same lithologic composition as Subunit IVA, but it is further characterized by the occurrence of thin sand beds near the base.	
VA	lower middle Miocene and lower? Miocene	403.7–551.7 mbsf (150-902D-45X-1, 150 cm, through -60X-CC, 49 cm)	Glauconitic silty clay, clayey silt, sandy silt, and dark brown silty claystone with abundant diatoms.	Predominantly hemipelagic with gravity-controlled flows.
VB	middle? and lower Miocene	551.7–594.8 mbsf (150-902D-61X-1, 0 cm, through -65X-1, 108 cm)	This subunit has the same lithologic composition as Subunit VA, but it is further characterized by an increase in calcite content and carbonate microfossils.	
VI	lower Miocene, upper Oligocene, uppermost lower Oligocene	594.8–680.9 mbsf (150-902D-65X-1, 108 cm, through -74X-1, 74 cm)	Dark brown silty clay and silty claystone with abundant diatoms and nannofossils.	Predominantly hemipelagic with gravity-controlled flows.
		Major disconformity		
VII	upper Eocene	680.9–TD (736.4 mbsf) (150-902D-74X-1, 74 cm, through -82X-CC, 33 cm)	Siliceous, nannofossil chalk with abundant foraminifers and clay.	Predominantly pelagic.

mbsf (Sections 150-902D-5H-3 and -4) and were recognized by the occurrence of dark gray silty-clay clasts, which are supported in a light gray clay matrix (N4 to N5).

Disseminated sand is an important constituent of the silty clays between 69.2 and 69.7 mbsf (Section 150-902D-7H-7, 88–142 cm). Black to dark gray, mottled silty clay is interbedded with light gray, calcareous silty clay (5Y 4/1 to 5Y 4/2) from 79 to 88.5 mbsf (Core 150-902D-9H). Thick beds (30–100 cm thick) of homogeneous, bioturbated clay, silty clay, and sandy silty clay occur from 88.5 to 117 mbsf (Cores 150-902D-10H through -12H).

Thin slump/debris-flow deposits recognized by clay clasts in a clay matrix or contorted strata occur between 98 and 105.5 mbsf (Core 150-902D-11H). Thin (<5 cm), normally graded beds of fine- to medium-sized, micaceous sand are present near 110 mbsf (Section 150-902D-12H-3). Mass-flow deposits occur from 110 to approximately 122 mbsf in Hole 902C (Cores 150-902C-14H and -15H and Section 150-902C-16H-1) and from 113 to 121 mbsf in Hole 902D (Cores 150-902D-12H and -13H). Mass-flow deposits are recognized by contorted, thin color bands and by deformed clay clasts supported in a silty clay matrix. The base of these mass-flow intervals at both Holes 902C and 902D mark the boundary between Units I and III. This boundary may also represent an unconformity between the middle Pleistocene and upper Miocene that appears to correlate with reflector p4 (purple) (see "Seismic Stratigraphy" section, this chapter).

Unit III

Interval: Sections 150-902C-16H-1, 113 cm, to -16H-CC, 20 cm; Sections 150-902D-14H-1, 0 cm, to -19X-1, 50 cm
Depth: Hole 902C, 122–130 mbsf; Hole 902D, 126.5–152.5 mbsf
Age: upper Miocene

The distinctive lithologic characteristic of this unit is the abundance of glauconite sand from 126.5 to 135 mbsf (Cores 150-902D-14H and -15H) and from 140 to 152.2 mbsf (Cores 150-902D-17H and -18X). Silty clay is a major component of Unit III. Abundant detrital quartz and feldspar (mainly albite), along with occasional pyrite, occur throughout this unit (Fig. 6). Total carbonate content decreases from 5% near the top of the unit to near zero at the base (Fig. 3). Calcareous microfossils are rare. Siliceous microfossils occur predominantly toward the base of the unit, where their abundance increases from 10% to 30% (Fig. 3).

The silty clay is greenish gray (5Y 4/1) and heavily bioturbated from 126.5 to 135 mbsf (Cores 150-902D-14H and -15H). Burrows are filled with glauconite. Dark gray, silty clay with matrix-supported light gray mud clasts may be a slump/debris-flow unit at ~135.5 mbsf (Section 150-902D-16H-1). Homogeneous greenish gray silty clay (5Y 4/1) with no apparent structures is interbedded with glauconite-bearing sandy silts from 140.0 to 152.2 mbsf. The lithologic boundary between Units III and IV is gradational and is defined by the lowest

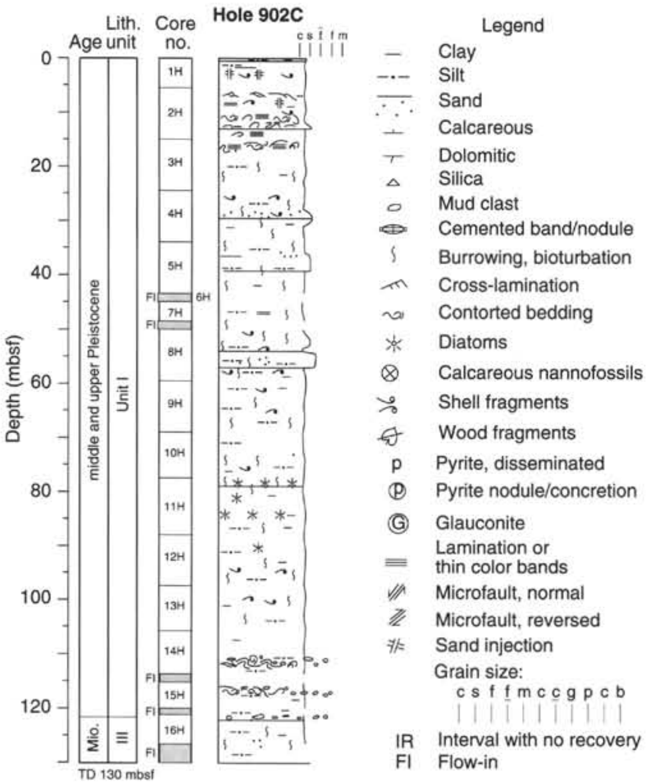

Figure 4. Detailed summary lithologic columns, Holes 902C and 902D.

occurrence of glauconite-, quartz-, and feldspar-rich sands. This lithologic boundary appears to correlate with reflector m0.5 (Red) (see "Seismic Stratigraphy" section, this chapter). Sediments in this unit are upper Miocene (see "Biostratigraphy" section, this chapter).

Unit IV

Interval: Sections 150-902D-19X-1, 50 cm, to -45X-1, 150 cm
Depth: 152.5–403.7 mbsf
Age: upper to middle Miocene

Subunit IVA

Interval: Sections 150-902D-19X-1, 50 cm, to -33X-CC, 40 cm
Depth: 152.5–293.0 mbsf

Subunit IVB

Interval: Sections 150-902D-34X-1, 0 cm, to -45X-1, 150 cm
Depth: 293.0–403.7 mbsf

The major lithologies in this unit are homogeneous, moderately bioturbated, greenish gray silty clay and clayey silt (5Y 4/1). Quartz and feldspar are abundant and mica fragments are common. Calcareous microfossils are not present; however, siliceous microfossil abundances range from 30% to 40%. Diatoms and sponge spicules predominate. Total carbonate is less than 5% throughout this unit (Fig. 3).

The distinctive features of Unit IV indicate a change in the depositional and diagenetic environment. These features include an abundance of terrestrial plant and wood fragments, cream-colored nodules and thin bands, pyrite nodules, black laminae (millimeter thick), and burrows (centimeter size) with black rims. Unit IV is further divided into Subunit IVA (152.5–293.0 mbsf), the base of which is defined by a glauconite quartz sand, and Subunit IVB (293.0–403.7 mbsf).

The highest occurrence of nodules is noted from 152.5 to 156 mbsf (Core 150-902D-19X). Cream-color bands and nodules are common from 210 to 400 mbsf (Cores 150-902D-25X through -44X) (Fig. 8A). X-ray diffraction (XRD) analyses show that the nodules are composed of siderite and that siderite and pyrite occur throughout Unit IV (Fig. 6). A change in the chemistry of the nodules occurs with depth. Between 152.5 and 156 mbsf, the nodules consist of microcrystalline siderite, calcite, and pyrite framboids. Below 260 mbsf, the nodules consist of siderite and pyrite. The disappearance of calcite corresponds broadly with slightly acidic interstitial waters (see "Inorganic Chemistry" section, this chapter). Different degrees of diagenesis are observed because siderite nodules and color bands are sharply defined in some intervals (228.8–277.0 mbsf; Cores 150-902D-27X to -31X), but in others they have diffuse boundaries (305.9–325.1 mbsf; Cores 150-902D-35X to -36X).

The highest occurrence of plant and wood debris is noted from 209 to 219 mbsf (Core 150-902D-25X). Occasional laminations (up to 10 cm thick) formed by plant and wood debris occur between 210 and 219 mbsf (Core 150-902D-25X), suggesting gravity-flow activity. Plant and wood fragments occur otherwise disseminated throughout the cores. Pyrite nodules (millimeter size) are present from 267 to 278 mbsf (Sections 150-902D-30X-7 through -31X-4), and from 308 to 313 mbsf (Sections 150-902D-35X-2 through -5). The pyrite nodules have a cream-colored halo between 267.3 and 273.3 mbsf.

Moderate bioturbation occurs throughout this unit. Burrow forms include *Chondrites, Planolites,* and *Zoophycos.* Burrows (centimeter size) are marked by black rims and are filled with sand and/or glauconite from 305.9 to 334.8 mbsf (Cores 150-902D-35X through -37X). Burrows are primarily parallel or subparallel to bedding. Black laminae (millimeter scale) are common from 305.9 to 315.5 mbsf (Core 150-902D-35X). The occurrences of burrows with black rims and black laminae between 305.9 and 334.8 mbsf also corresponds to an increase in pyrite as revealed by XRD.

Silty sand and sandy silt layers separated by 8 m of gray clay are present from 257.7 to 293 mbsf (Cores 150-902D-30X and -33X) (Fig. 8B). Quartz, feldspar, and glauconite are abundant between 279.21 and 293 mbsf. The sand at the base of this interval is distinctive because it contains abundant granule-sized quartz grains. The presence of loose sand at 289.0 mbsf and throughout Core 150-902D-33X, together with the incomplete core recovery, suggests the existence of a thicker sand layer at this level. This sand bed is the base of Subunit IVA, and it appears to correlate with reflector m1 (Tuscan) (see "Seismic Stratigraphy" section, this chapter).

Thin sand beds (0–10 cm thick) occur in Cores 150-902D-42X through -44X) and are characteristic of the base of Subunit IVB. Sand is also present from 402.2 to 403.7 mbsf (Core 150-902D-45X), and only two core sections were recovered. Poor core recovery suggests that more sand was present in this interval and was probably washed out during coring. The basal sand unit marks the boundary between Units IV and V. The base of the sand unit at this depth apparently correlates with reflector m2 (Yellow-2) (see "Seismic Stratigraphy" section, this chapter).

Unit V

Interval: Sections 150-902D-45X-1, 150 cm, to -65X-1, 108 cm
Depth: 403.7–594.8 mbsf
Age: lower middle Miocene

Subunit VA

Interval: Sections 150-902D-45X-2, 50 cm, to 150-902D-60X-CC, 49 cm
Depth: 403.7–551.7 mbsf

Subunit VB

Interval: Sections 150-902D-61X-1, 0 cm, to 150-902D-65X-1, 108 cm
Depth: 549.4–594.8 mbsf

Clayey siltstones with glauconite-rich sands characterize Unit V. The major lithologies of this unit are glauconitic silty clays, clayey silts, clayey siltstones, and sandy silts. Quartz decreases from the top to the base (Fig. 6). Feldspars occur throughout this unit, but they are

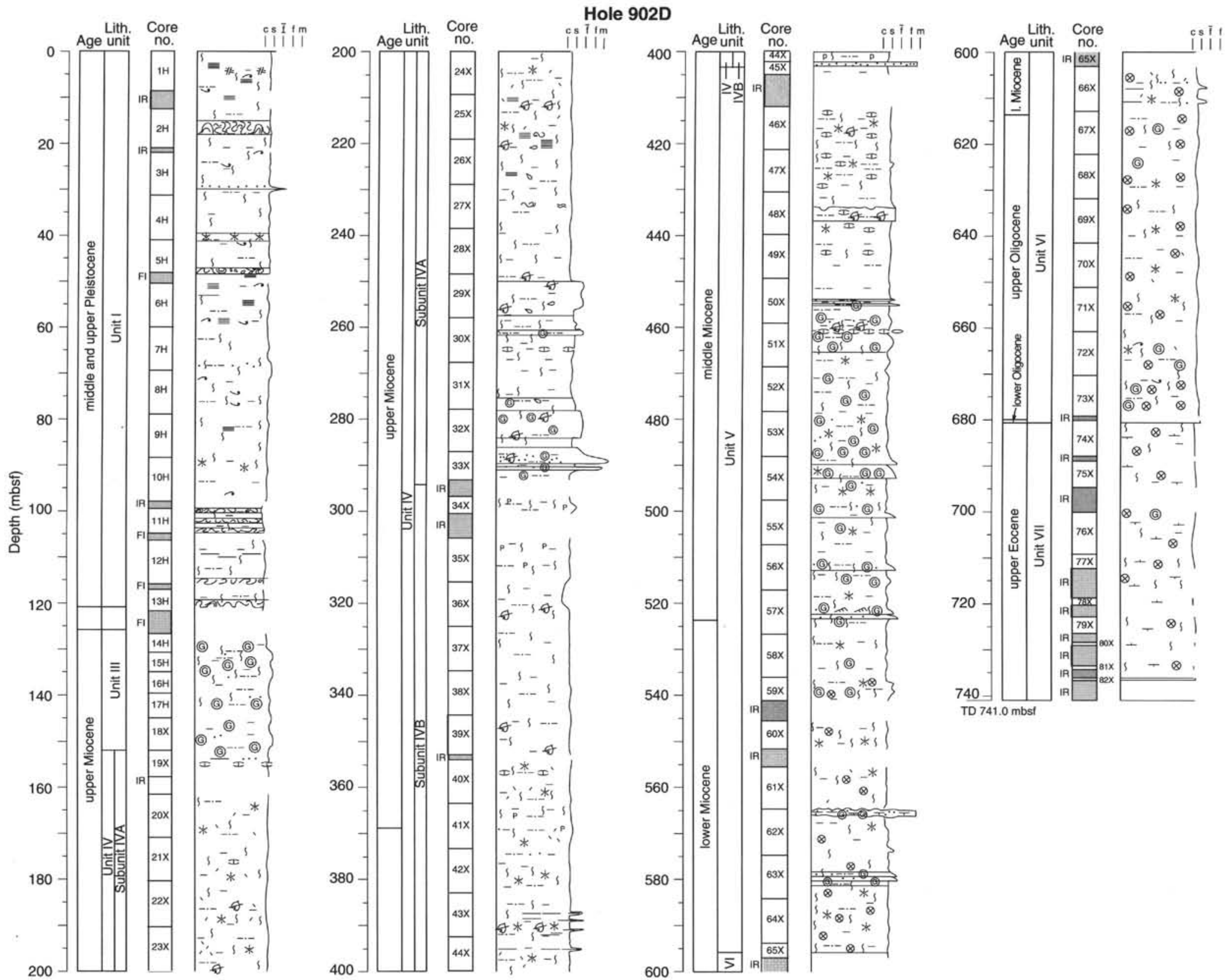

Figure 4 (continued).

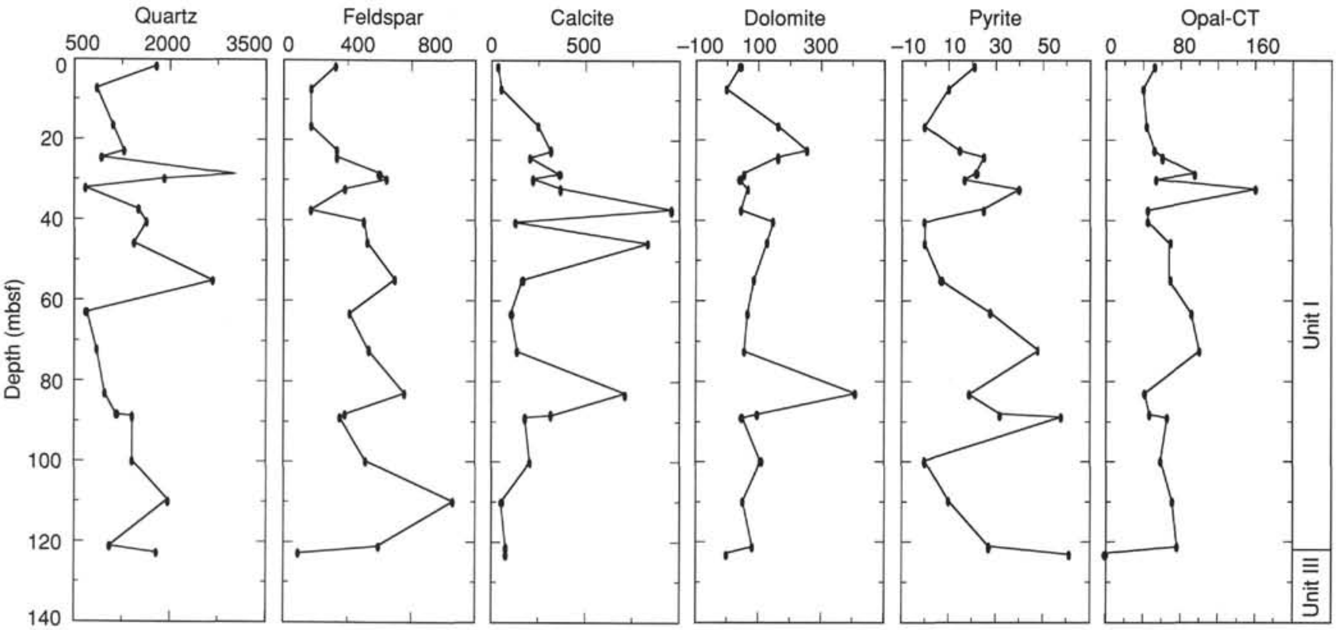

Figure 5. X-ray diffraction analyses for Hole 902C plotted according to the intensity of the mineral's main diffraction peak: quartz (3.33Å), feldspar (3.25Å), calcite (3.03Å), dolomite (2.89Å), pyrite (2.71Å), and opal-CT (4.05Å–4.10Å).

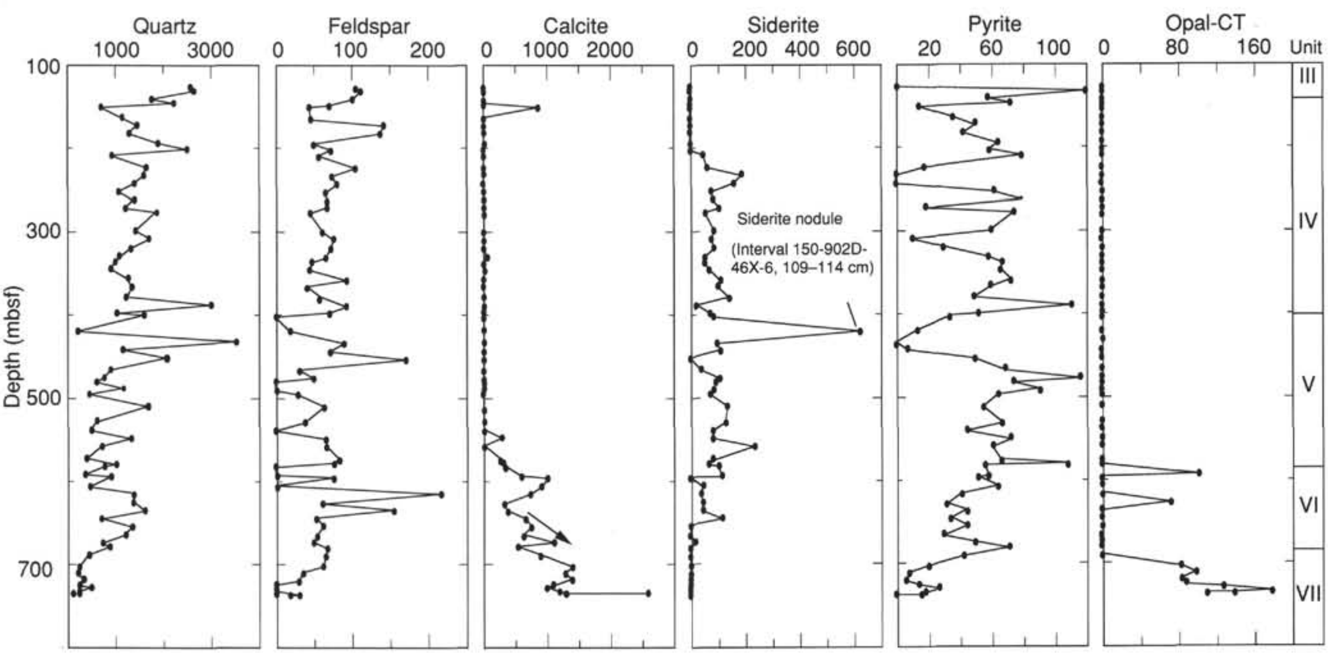

Figure 6. X-ray diffraction analyses for Hole 902D plotted according to the intensity of the mineral's main diffraction peak: quartz (3.33Å), feldspar (3.25Å), and calcite (3.03Å), siderite (2.80Å), pyrite (2.71Å), and opal-CT (4.05Å–4.10Å).

less abundant than in Units I, III, and IV. Siderite and pyrite also occur in this unit and increase regularly downward to its base (Fig. 6). Siderite nodules with different degrees of induration and at different stages of morphologic evolution are also noted from 412 to 448 mbsf (Cores 150-902D-46X through -49X). Siliceous microfossils are common in this unit, and their abundances range from 20% to 30% (Fig. 3). This unit can be divided into two subunits based on the occurrence of calcite: Subunit VA from 403.7 to 549.41 mbsf (Core 150-902D-60X), which has no calcite, and Subunit VB from 549.41 to 594.8 mbsf, which has up to 30% total carbonate (Fig. 3).

Glauconite sand beds are common in Subunits VA and VB occurring intermittently from ~455 to ~580 mbsf (Cores 150-902D-50X to -63X). The sand beds are 10–90 cm thick, normally graded fine- to coarse-sized, and commonly display sharp bases. The glauconite occurs in both subunits as well-rounded, fine- to medium-sized sand, dark green to black in color.

The silty clays and clayey silts are dark greenish gray, homogeneous, and slightly to moderately bioturbated. Bioturbation has caused color mottling. Burrow forms include *Chondrites, Planolites,* and *Zoophycos* (Fig. 8C). The silty clays typically are thick bedded, but locally (449.3–457.4 mbsf; Core 150-902D-50X), are intercalated with thin color bands.

Subunit VB is characterized by the occurrence of calcite, noted from 549.41 mbsf (Core 150-902D-60X) and below. Calcite increases regularly downward toward the base of this subunit (Fig. 6). Total carbonate increases from <1% at 545.5 mbsf to 40% at 595.4 mbsf (Fig. 3). Nannofossil abundances show a similar increase toward the base of the unit (Fig. 3).

The degree of cementation from silty clays to silty claystones may be influenced by the appearance of calcite. Within the cemented intervals, dolomite rhombohedrons (100 μm scale) are the dominant cement. The rhombohedrons are zoned from iron-poor in the center to iron-rich on the margins. Dolomite has totally replaced the matrix, resulting in an idiotopic fabric. Diatom fragments have been incorporated into the dolomite rhombohedrons. The degree of cementation is not uniform downhole. Silty claystones occur from 545.5 to 564.6 mbsf (Cores 150-902D-60X and -61X). Silty clays occur between 574.4 and 584.0 mbsf (Cores 150-902D-62X and -63X). Two beds of very indurated, gray (5Y 6/1) glauconitic sandy siltstone occur between 564.6 and 573.4 mbsf (Core 150-902D-62X). As the lithologies become increasingly indurated downhole, drilling disturbance during XCB coring forms drilling "biscuits" throughout each core. A gradual but obvious color change occurs from 560.4 to 574.4 mbsf (Section 150-902D-63X-5) from dark greenish gray to dark brown (5Y 3/2 to 10YR 2/2) silty clay.

The base of this unit is defined by a marked color change from dark brown to brownish green (10YR 2/2 to 5Y 3/2), which corresponds to a further marked increase in calcite (Fig. 6), carbonate (as much as 40%; Fig. 9), and calcareous microfossils (Fig. 3). This basal contact also corresponds to an increase in opal-CT cementation. The base of this unit appears to be about 15 m above a composite reflection from m5.6 (true blue) and m6 (pink-3) (see "Seismic Stratigraphy" section, this chapter).

Unit VI

Interval: Sections 150-902D-65X-1, 108 cm, to -74X-1, 74 cm
Depth: 594.8–680.9 mbsf
Age: lower Miocene, upper Oligocene, and uppermost lower Oligocene

The major lithologies in this unit are silty claystones and silty clays. Distinctive characteristics of Unit VI are the degree of lithification from silty clay to silty claystone and the occurrence of abundant nannofossils and diatoms. Unit VI is also characterized by a decrease in pyrite, the occasional occurrence of opal-CT, and minor siderite (Fig. 6). Variations in color occur throughout the unit and range from dark brown to light brownish green (10YR 2/2 to 5Y 3/2). Calcite content decreases gradually in the upper part of the unit and is correlated with an increase in detrital quartz and feldspar (Fig. 6). An increase in quartz and feldspar corresponds to a glauconitic sandy silt layer from 609.3 to 612.4 mbsf (Core 150-902D-66X). This interval correlates with an unconformity between the upper Oligocene and the lower Miocene (see "Biostratigraphy" section, this chapter). This level also appears to correlate with the reflector m6 (pink-3) (see "Seismic Stratigraphy" section, this chapter).

Calcite content increases toward the base of the unit. Total carbonate abundances throughout the unit range between 20% and 30% (Fig. 3). Siliceous microfossil abundances range from 30% to 40% (Fig. 3). A lithologic change marks the boundary between Units VI and VII from silty claystones above to siliceous nannofossil chalks below at 681.7 mbsf in Section 150-902D-74X-1 (Fig. 10A). This lithologic change includes an abrupt increase in calcite (XRD) and calcium carbonate (coulometry). This boundary also represents an unconformity between the uppermost lower Oligocene and upper Eocene (see "Biostratigraphy" section, this chapter). Reflector o1 (green-2) apparently correlates with this boundary (see "Seismic Stratigraphy" section, this chapter).

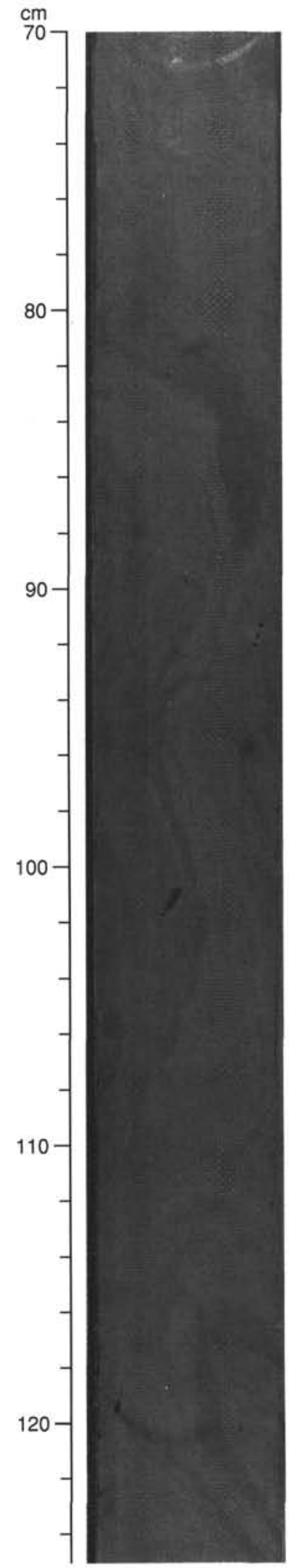

Figure 7. Mass-transport deposits are recognized by contorted bedding in upper to middle Pleistocene sediment from Unit I (Interval 150-902C-3X-2, 70–125 cm).

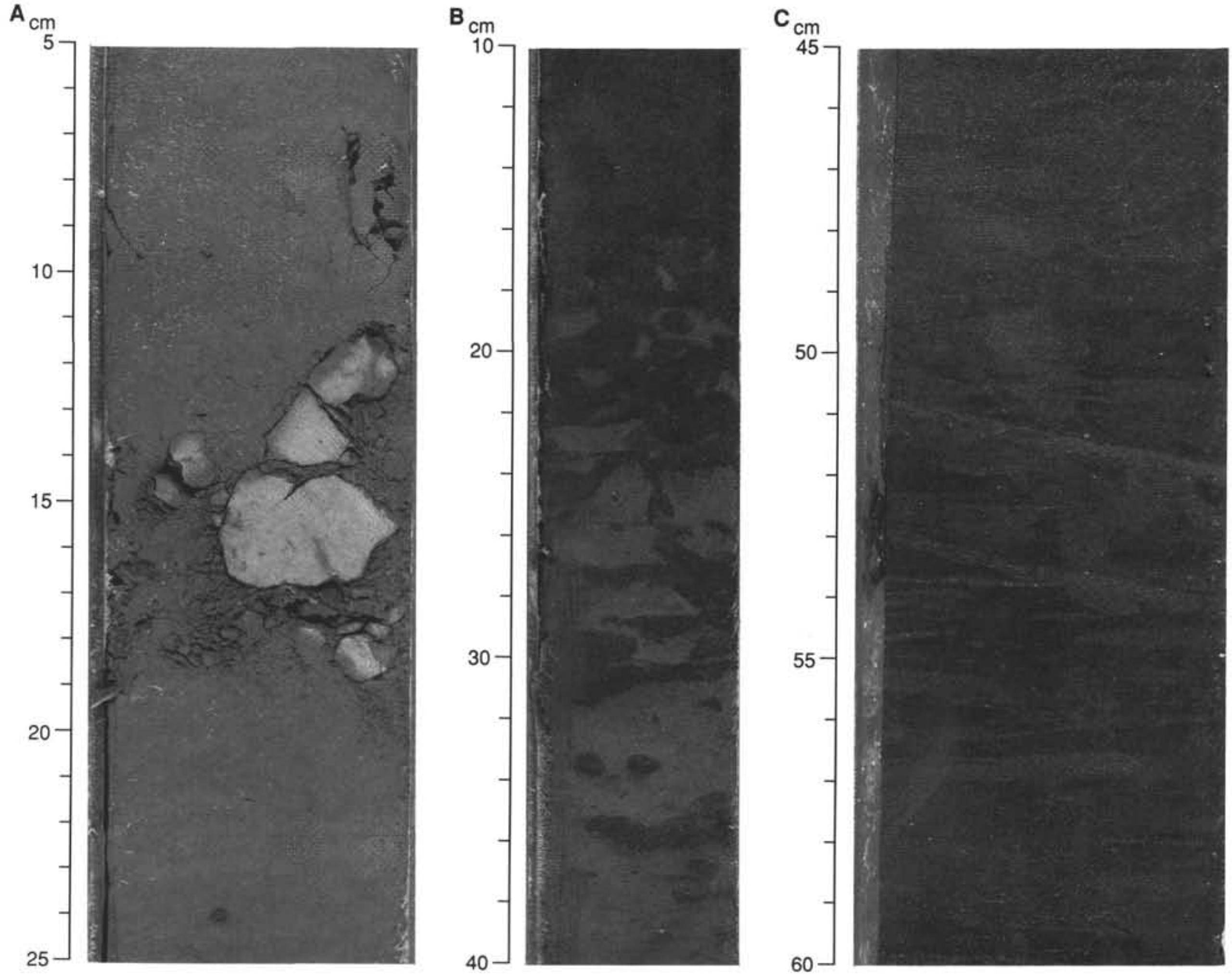

Figure 8. Miocene sediment from Units IV and V. **A.** Example of a nodule composed of microcrystalline siderite, calcite, and pyrite commonly found in Miocene sediment of Hole 902D (Interval 150-902D-30X-6, 5–25 cm). **B.** Bioturbated contact at the base of a glauconite-rich bed (Interval 150-902D-30X-4, 10–40 cm). **C.** Moderately bioturbated, dark brown silty clay from the lower Miocene. Common trace fossils include *Chondrites, Planolites,* and *Zoophycos* (Interval 150-902D-62X-1, 45–60 cm). Note differences in scale.

Unit VII

Interval: Sections 150-902D-74X-1, 74 cm, to -82X-CC, 33 cm
Depth: 680.9–736.4 mbsf
Age: upper Eocene

Unit VII consists of upper Eocene clayey siliceous nannofossil chalks containing foraminifers (Fig. 10B). This unit is characterized by marked increase in nannofossils and opal-CT (Figs. 3 and 6). Calcium carbonate content ranges from 40% to 50%, reaching a maximum abundance of 60% at 740.1 mbsf (Fig. 3). The noncarbonate fraction is composed of opal-CT and clay. The clayey siliceous chalk is homogeneous, semi-indurated, and light greenish gray (5Y 6/1). Biogenic opal or opal-A is an amorphous open-structured hydrous silica. During silica diagenesis, opal-A is transformed into opal-CT, a disordered, low temperature (25°–60°C) cristobalite/tridymite structure (Jones and Segnit, 1972; Weaver and Wise, 1972). Silica diagenesis was studied in correlative sediments from DSDP Sites 612 and 613 (Thein and von Rad, 1987; Wilkens et al., 1987), and the results indicated that opal-CT coupled with carbonate cementation are the source for matrix cementation in the chalk and porcellanite. The presence of opal-CT in the chalks of Hole 902D indicates that silica is a cement in the semilithified sediment.

The sediment is moderately burrowed. Burrows are delineated in light to dark shades of greenish gray (5Y 6/1 to 5Y 6/2). Most burrows are oriented subparallel to original bedding because of compaction. Burrow forms include *Planolites, Chondrites,* and *Zoophycos.* Because of the moderately strong degree of induration of this unit, recovery at the base of each core was poor.

BIOSTRATIGRAPHY

Summary

A discontinuous 736.40-m-thick upper Eocene to Pleistocene section was recovered at Site 902. It consists primarily of Neogene and Oligocene silty clays (0–680.9 mbsf; lithologic Units I and III through VI) and upper Eocene clayey chalks (680.9–736.4 mbsf; lithologic Unit VII). Microfossils occur at all levels, but their distribution is highly variable. Calcareous microfossils are common to abundant in the Pleistocene and lower Miocene to Eocene sediments, for which they provide good biostratigraphic resolution. They are mostly absent from the upper and middle Miocene silty clays, for which diatoms and dinoflagellates provide stratigraphic control. Dinoflagellate cysts provide the only zonal control in cores without calcareous microfossils or age-diagnostic diatom assemblages (e.g., in Cores 150-902D-14H and

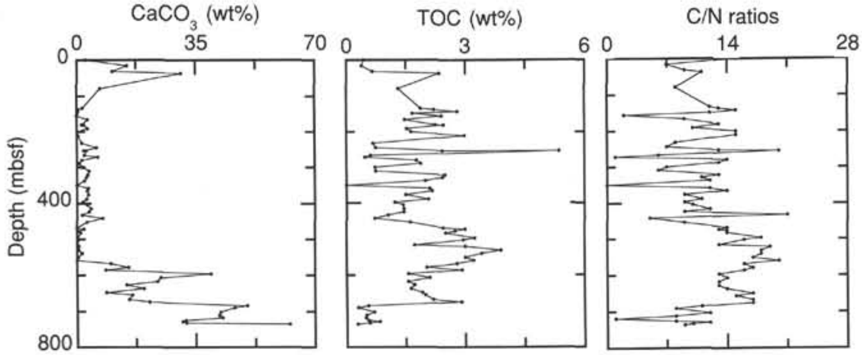

Figure 9. Carbonate concentration (calculated as percent $CaCO_3$), total organic carbon (percent TOC), and organic C/N atomic ratios vs. depth for sediment samples from Hole 902D.

-15H; 126.50–134.80 mbsf), and allow a fine zonal subdivision of the middle Miocene interval recovered from Hole 902D. Rich benthic foraminifer assemblages indicate extensive downslope transport during the Pleistocene; they also indicate largely in situ deposition and a shallowing from the late Eocene (middle bathyal; 600–1000 m) to the early Miocene (upper bathyal; 200–600 mbsf).

Four holes were drilled at Site 902. Holes 902A (Cores 150-902A-1H to -4H; 0–31 mbsf) and 902B (Core 150-902B-1H; 0–10.5 mbsf) were terminated in the middle and upper Pleistocene, respectively. Hole 902C (Cores 150-902C-1H to -16H; 0–129.99 mbsf) was terminated in upper Miocene sediments slightly below a Pleistocene/upper Miocene contact in Section 150-902C-16H-1, 113 cm (122.13 mbsf; contact between lithologic Units I and III; see "Lithostratigraphy" section, this chapter). Hole 902D (Cores 150-902D-1H to -82X; 0–740.1 mbsf), which terminated in upper Eocene clayey chalks, provides the biostratigraphic means for determining the ages of Miocene and older seismic reflectors (see "Seismic Stratigraphy" section, this chapter).

Holocene to upper middle Pleistocene sediments (lithologic Unit I, see "Lithostratigraphy" section, this chapter) were recovered in Sections 150-902D-1H to -13H-CC (0–123.92 mbsf); however, the interval between 121 and 123.92 mbsf is flow-in. They belong to the *Pseudoeunotia doliolus* Zone (diatom; Cores 150-902D-1H to -11H; 0–107.50 mbsf; Table 3) and extend from calcareous nannofossil Zone NN21 to the upper part of Zone NN19. This is in agreement with the fact that Cores 150-902D-1H to -13H (0–121 mbsf) are of normal polarity (see "Paleomagnetism" section, this chapter), indicating that the Pleistocene interval recovered from Hole 902D represents part of the Brunhes Chron.

A 428.5-m-thick, upper to upper lower Miocene section was recovered from Hole 902D (between Sections 150-902D-14H-CC and -60X-CC; 126.5–551.74 mbsf). It corresponds to lithologic Units III, IV, and V (partim) (see "Lithostratigraphy" section, this chapter) and consists primarily of noncalcareous, diatom- and organic-rich silty clays. Dinoflagellate stratigraphy indicates that the upper part of the section is middle upper Miocene. Sections 150-902D-14H-CC and -15H-CC, (130.88–134.80 mbsf) belong to Zone H (see below). This agrees with the co-occurrence of the silicoflagellate species *Mesocena diodon diodon* and *Distephanus crux* in Section 150-902D-16H-CC (139.93 mbsf). According to Perch-Nielsen (1985), these two taxa have their last occurrence datum in the middle late Miocene (in the *Corbisema triacantha* Biochron). This also agrees with assignment of Section 150-902D-17H-CC (145.13 mbsf) to dinoflagellate Zone G, of Section 150-902D-19X-CC (190.60 mbsf) to the *Coscinodiscus yabei* diatom zone, and of Interval 150-902D-23X-1, 39–41 cm (190.60 mbsf), to planktonic foraminifer Zone N16–N17 based on the occurrence of *Neogloboquadrina acostaensis.* Furthermore, the highest occurrence of *Denticulopsis hustedtii* in Section 150-902D-19X-CC (156.21 mbsf) suggests a stratigraphic position no younger than Chron 10 (= Chron C5Ar). Burckle et al. (1982) established that the LAD of this species in the equatorial Pacific occurred in mid-Chron 10. An early late Miocene age for Section 150-902D-19X-CC (156.21 mbsf), however, is contradicted by the occurrences in Section 150-902D-21X-CC (180.90 mbsf) of *Globorotalia cibaoensis* and *Globorotalia* sp. aff. *G. margaritae,* suggestive of a latest Miocene age (Chron 5 = C3An; BKV85; see below).

The upper and middle Miocene section recovered between 156.21 mbsf (Section 150-902D-19X-CC) and 584.20 mbsf (Section 150-902D-63X-CC) comprises the *Coscinodiscus yabei* Zone (Sections 150-902D-19X-CC to -41X-CC; 156.21–373.49 mbsf), the *Rhizosolenia barboi* Zone (Sections 150-902D-42X-CC to -52X-CC; 382.80–478.15 mbsf), and the *Coscinodiscus lewisianus* Zone (Sections 150-902D-53X-CC to -63X-CC; 487.07–584.20 mbsf). The absence of the *Rhizosolenia praebarboi* and *Denticulopsis praedimorpha* zones (Baldauf, 1984) indicates that the upper and middle Miocene section recovered from Hole 902D may be discontinuous. However, the use of Baldauf's (1984) zonation may not be appropriate on the New Jersey margin and shipboard analysis may not have allowed recognition of important marker species.

Dinoflagellate Zone G (from Sections 150-902D-17H-CC to -31X-CC; 145.13–267.59 mbsf), Zone F (from Sections 150-902D-32X-CC to -49X-CC; 286.90–448.46 mbsf), Zone E (from Sections 150-902D-50X-1, 93–98 cm, to -51X-1, 14–19 cm; 450.25–459.05 mbsf), Zone D (from Sections 150-902D-51X-5, 95–100 cm, to -53X-CC; 465.90–488.07 mbsf), and Zone C (from Sections 150-902D-54X-CC to -56X-CC; 497.73–515.98 mbsf) were identified. The lower part of Zone B (from Sections 150-902D-58X-CC to -61X-CC; 536.64–564.82 mbsf), and Zone A (from Sections 150-902D-62X-CC to -65-1; 38–41 cm; 574.54–594.10 mbsf) were identified between Cores 150-902D-17H and -60X (145.13–551.74 mbsf). Only the lower part of Zone B was identified, and there may be a gap between Cores 56 and 58 (515.98–536.64 mbsf). The thinness of Zone E suggests an unconformable contact. In addition, the thinness of Zones D and C, which together correspond to a complex glauconitic interval (Cores 150-902D-51X to -53X, 458.90–488.07 mbsf; see "Lithostratigraphy" section, this chapter), and the possible absence of the *Rhizosolenia praebarboi* Zone (diatom), suggest an unconformity in the lower part of Core 150-902D-54X. Although difficult to interpret, the preliminary magnetic record between Cores 150-902D-48X and -64X (see "Paleomagnetism" section, this chapter) may reflect a discontinuous stratigraphic record.

The stratigraphic position of Cores 150-902D-57X to -60X (525.73–551.74 mbsf) is uncertain. Based on the diatom stratigraphy, they belong to the lower or lower middle Miocene (*Coscinodiscus lewisianus* Zone). Based on dinoflagellate stratigraphy, they are lower Miocene (Zone A). Core 150-902D-58X-CC (536.64 mbsf) yields rare long-ranging calcareous nannofossil taxa that do not further resolve the stratigraphic position at this level.

The interval between Sections 150-902D-61X-CC and -73X-1, 74 cm (564.82–671.24 mbsf) extends from the lower Miocene (upper Zone NN2) to the upper lower Oligocene (upper Zone NP23). Calcareous

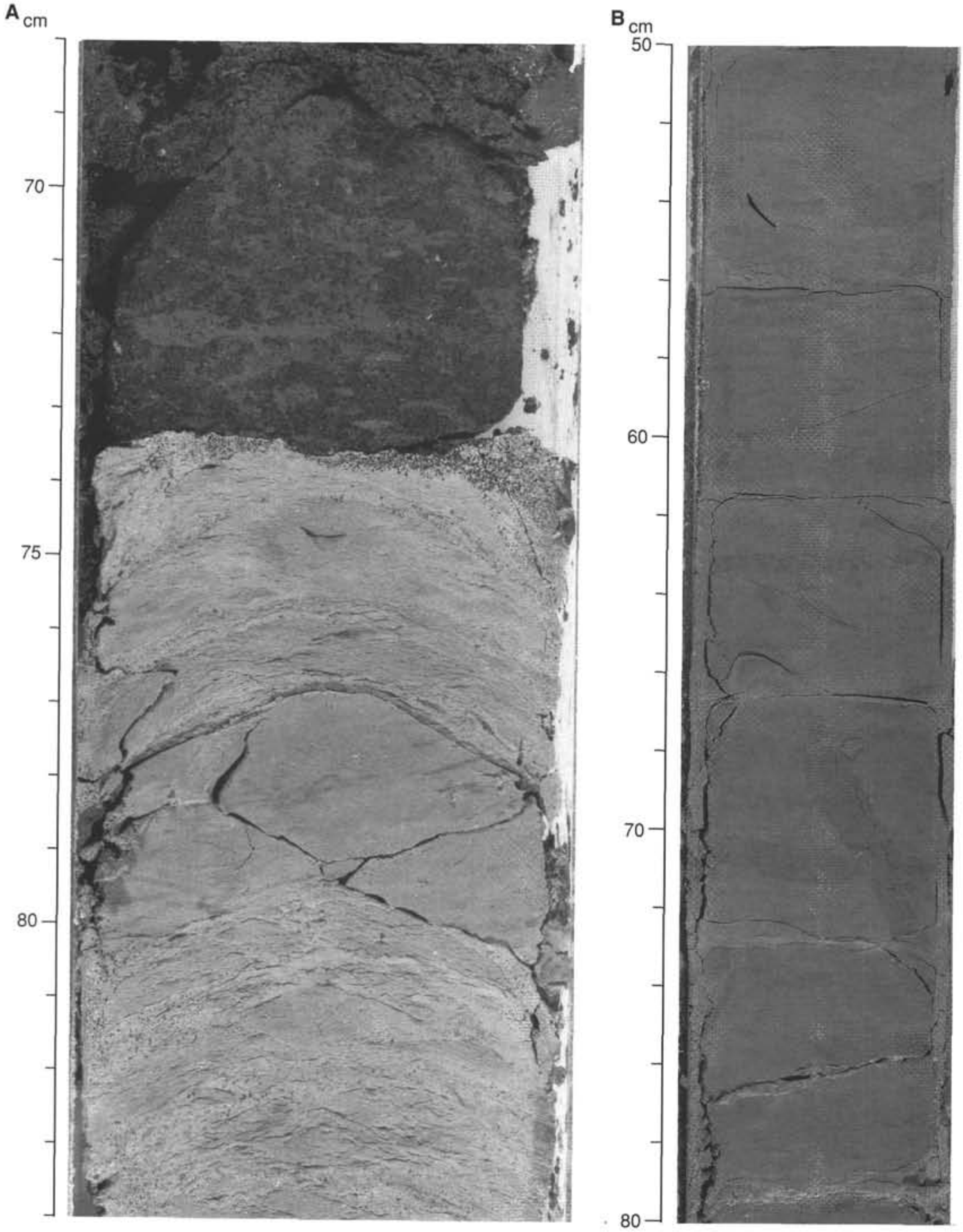

Figure 10. **A.** The striking lithologic contact between Units VI and VII corresponds to an unconformity between the uppermost lower Oligocene and the upper Eocene. This boundary marks a significant change in the depositional environment from pelagic, carbonate-dominated deposition during the Eocene to predominantly terrigenous deposition for the lower Oligocene (Interval 150-902D-74X-1, 68–84 cm). **B.** Upper Eocene clayey siliceous nannofossil chalks. These chalks are extensively burrowed (Interval 150-902D-75X-3, 50–80 cm). Note differences in scale.

nannofossils provide the main stratigraphic control in close (but not complete) agreement with planktonic foraminifer and dinoflagellate stratigraphies. The Oligocene/Miocene contact, which occurs between Sections 150-902D-66X-CC and -66X-5, 29–35 cm (at ~611 mbsf) may be unconformable. The youngest Oligocene sediments in Section 150-902D-66X-CC (612.90 mbsf) belong to Zone NP25 and are correlative with, or older than, Chron C7N; the oldest Miocene sediments belong to the lower part of calcareous nannofossil Zone NN2 or to Zone NN1 and to planktonic foraminifer Subzone N4b. Integration of the calcareous and dinoflagellate stratigraphies suggest a possible unconformity within Core 150-902D-65X (593.70–597.02 mbsf). However, this possible unconformity could be accounted for by the 6.28 m of core loss in Core 150-902D-65X, to which must be added 9.6 m of unsampled Core 150-902D-66X. The oldest Oligocene sediments above the upper Eocene/Oligocene contact in Section 150-902D-74X-1, 74 cm (680.9 mbsf) belong to the upper part of Zone NP23.

The lower part of the section recovered from Hole 902D consists of upper Eocene gray clayey chalks (Sections 150-902D-73X-1, 74 cm, to 150-902D-82X-CC; 680.9–736.43 mbsf). They correspond to lithologic Unit VII (see "Lithostratigraphy" section, this chapter) and are unconformable with the Oligocene silty clays that constitute the lower part of lithologic Unit VI. The sequential disappearances of three calcareous nannofossil species (*Discoaster saipanensis, D. barbadiensis,* and *Reticulofenestra reticulata*) indicate that this is a continuous upper Eocene section deposited at high sedimentation rates.

The biostratigraphic framework described herein serves as a basis for estimating the age of hiatuses associated with the unconformities and for assessing the ages of their surfaces (see "Sedimentation Rates" section, this chapter).

Planktonic Foraminifers

Planktonic foraminifer assemblages were used to date Pleistocene sediments and to interpret glacial/interglacial depositional cycles. The most persistent and commonly occurring taxa include *Neogloboquadrina pachyderma* (both dextrally and sinistrally coiled), *Globigerina bulloides, Globorotalia inflata, Globorotalia truncatulinoides,* and *Globigerinoides ruber.* High relative abundances of *N. pachyderma,* particularly if dextrally coiled forms predominate, indicate colder conditions inferred to reflect glacial episodes. Relative, rather than absolute, abundances of these forms have been emphasized because dilution by terrigenous sediments during glacial episodes can markedly reduce the number of specimens per unit volume of sediment. Nonglacial conditions are characterized by increased relative abundances of *G. bulloides* and *G. inflata.* The occurrence of *G. ruber* and *G. truncatulinoides,* species associated with warm waters, indicate full interglacial periods. Patterns in Hole 902C are the focus of the following discussion.

Although greater sampling density will more accurately resolve cyclic variations in faunal composition, shipboard sampling delineates several glacial/interglacial cycles. Modest total abundances and low-diversity faunas, numerically dominated by *N. pachyderma,* indicate glacial intervals in Sections 150-902C-1H-CC (5.37 mbsf), -3H-5 (21–22.5 mbsf), -6H-1, 45 cm (43.95 mbsf), and -10H-CC (79.25 mbsf); interglacial episodes, marked by greater abundance and diversity, occur in Sections 150-902C-4H-CC (34.76 mbsf), -5H-CC (44.08 mbsf), -9H-CC (69.38 mbsf), -11H-CC (88.23 mbsf), and -12H-CC (97.23 mbsf) (Fig. 11). Glacial faunas are associated with higher percentages of sand and displaced shallow-water benthic foraminifers, particularly *Elphidium* spp. Planktonic assemblages assignable to the Pleistocene extend downward to Core 150-902C-13H (105.74 mbsf). Glauconitic sands of Sample 150-902C-16H-CC (129.99 mbsf) are barren.

A similar Pleistocene sequence was encountered in Hole 902D, to which the remainder of this discussion is devoted. Pleistocene sediments of Hole 902D extend downward through Core 150-902D-13H (0–126.5 mbsf), below which an unfossiliferous interval was encountered. Planktonic foraminifers were next encountered in Sample 150-902D-21X-CC (180.90 mbsf), in which the assemblages include *Globoquadrina dehiscens, Globorotalia cibaoensis,* and forms that appear to be transitional between *Globorotalia juanai* and *G. margaritae.* Both *G. ciboaensis* and *G. margaritae* had a first appearance datum (FAD) in Chron 5 (BKV85) and so indicate a zonal assignment to upper Miocene Zone N17 or lower Pliocene Zone N18, which does not agree with the dinoflagellate and diatom evidence. Because these groups occur more abundantly and consistently than the foraminifers, the N17–N18 zonal assignment must be considered tentative pending more detailed post-cruise sampling and additional study. Samples 150-902D-22X-3, 83–85 cm (184.13 mbsf), and -23X-1, 39–41 cm (190.60 mbsf), also yield upper Miocene assemblages. These can be constrained only to Zones N16–N17, which encompass the dinoflagellate-diatom assignment for this interval. Planktonic foraminifers include *Globorotalia plesiotumida* (FAD in Chron C5A), *Neogloboquadrina acostaensis* (FAD in Chron C5n according to BKV85), and a variety of longer ranging species.

Table 3. Biostratigraphic zonations and datum levels, Site 902.

Zone (base unless specified) and/or datum level	Code	Sample number	Depth (mbsf)
LO *P. doliolus*	Dm	150-902D-11H-CC	108.51
NN19–20	Cn	150-902C-15H-1, 71–73 cm, to -15H-1, 132–134 cm	115.73 to 116.34
Dinocyst Zone H	Df	150-902C-16H-CC	129.99
FO *G. truncatulinoides*	Pf	150-902D-11H-CC	107.50
NN19–20	Cn	150-902D-15H-1, 71–73 cm 150-902D-15H-1, 132–134 cm	131.73 to 132.34
Dinocyst Zone H	Df	150-902D-15H-3, 82–87 cm	133.57
HO *D. hustedtii*	Dm	150-902D-19X-CC	139.93
HO *T. grunowii*	Dm	150-902D-19X-CC	156.21
N17–N18	Pf	150-902D-21X-CC	180.90
N16–N17	Pf	150-902D-22X-3, 83–85 cm	184.15
Dinocyst Zone G	Df	150-902D-31X-CC	267.59
HO *D. novaecaesaraea*	Dm	150-902D-33X-CC	292.99
HO *D. punctata hustedtii*	Dm	150-902D-41X-CC	373.49
Dinocyst Zone F	Df	150-902D-49X-CC	448.46
Dinocyst Zone E	Df	150-902D-51X-1, 14–19 cm	459.09
Dinocyst Zone D	Df	150-902D-53X-CC	488.07
Dinocyst Zone C	Df	150-902D-56X-CC	515.98
Dinocyst Zone B	Df	150-902D-61X-CC	564.82
HO *C. lewisianus*	Dm	150-902D-63X-CC	584.20
HO *R. marylandicus*	Dm	150-902D-63X-CC	
NN11–NN12	Cn	150-902D-64X-CC	593.93
Dinocyst Zone A	Df	150-902D-65X-1, 38–43	594.00
N5	Pf	150-902D-65X-CC	597.02
N4b	Pf	150-902D-66X-CC	612.90
NP25–NN1	Cn	150-902D-66X-CC	
NP24–NP25	Cn	150-902D-68X-CC	632.02
Dinocyst Zone Pre-A	Df	150-902D-68X-CC	632.02
P21–P22	Pf	150-902D-73X-CC	678.83
NP19–NP23	Cn	150-902D-73X-CC	
P16–P17	Pf	150-902D-74X-1, 138–140 cm	681.60

Note: Dm = diatom, Cn = calcareous nannofossil, Df = dinocyst, and Pf = planktonic foraminifer. LO = lowest occurrence, HO = highest occurrence.

Sediments from Samples 150-902D-23X-CC through -64X-CC (200.07–593.93 mbsf) are diatomaceous silty clays with occasional pulses of glauconite and quartz sands. No calcareous fauna is present in this entire sequence, so no age assignments based on planktonic foraminifers could be attempted.

Sediments from Samples 150-902D-65X-1, 118–123 cm, through -66X-CC (594.90–612.90 mbsf) contain planktonic taxa indicative of Aquitanian to lower Burdigalian. Samples from Core 150-902D-65X (594.90 mbsf) are assignable to Zone N5. The assemblage includes *Globorotalia fohsi peripheroronda, G. siakensis, Globoquadrina praedehiscens, G. dehiscens,* and *Globigerinoides altiaperturus.* Based upon the FADs and LADs of these taxa, the assemblage indicates Chron C6A (BKV85). Specimens of *Globorotalia opima nana* are interpreted to be reworked. Sample 150-902D-66X-CC (612.90 mbsf), which contains *Globorotalia* cf. *G. kugleri* and *Globoquadrina dehiscens* but lacks *Globorotalia fohsi peripheroronda,* is tentatively assigned to Zone N4b. Based on the calcareous nannofossil stratigraphy, this level belongs to the upper Oligocene Zone NP25.

Samples from 150-902D-67X-CC through -73X-CC (622.87–678.83 mbsf) contain Oligocene assemblages that are numerically dominated by such taxa as *Catapsydrax unicavus, C. dissimilis, Globigerina ciperoensis, Subbotina tripartita,* and *Globorotalia opima nana. Globorotalia opima opima* occurs in the lower part of this interval. This assemblage indicates the upper Oligocene (within but not necessarily encompassing all of Zones P21–P22). There is no indication of lower Oligocene sediments.

Sediments from Sample 150-902D-74X-1, 138–140 cm (681.60 mbsf) yield an assemblage indicative of the upper Eocene (Zones P16–17). Diagnostic taxa include *Hantkenina* spp. and *Globorotalia cerroazulensis cerroazulensis,* both of which had an LAD in Chron C13r (BKF85). Samples below this level to the bottom of Hole 902D (681.60–736.43 mbsf) are assignable to the upper Eocene. In Sample 150-902D-82-CC (736.43 mbsf), taxa indicative of the upper middle Eocene are mixed with upper Eocene assemblages. Most importantly,

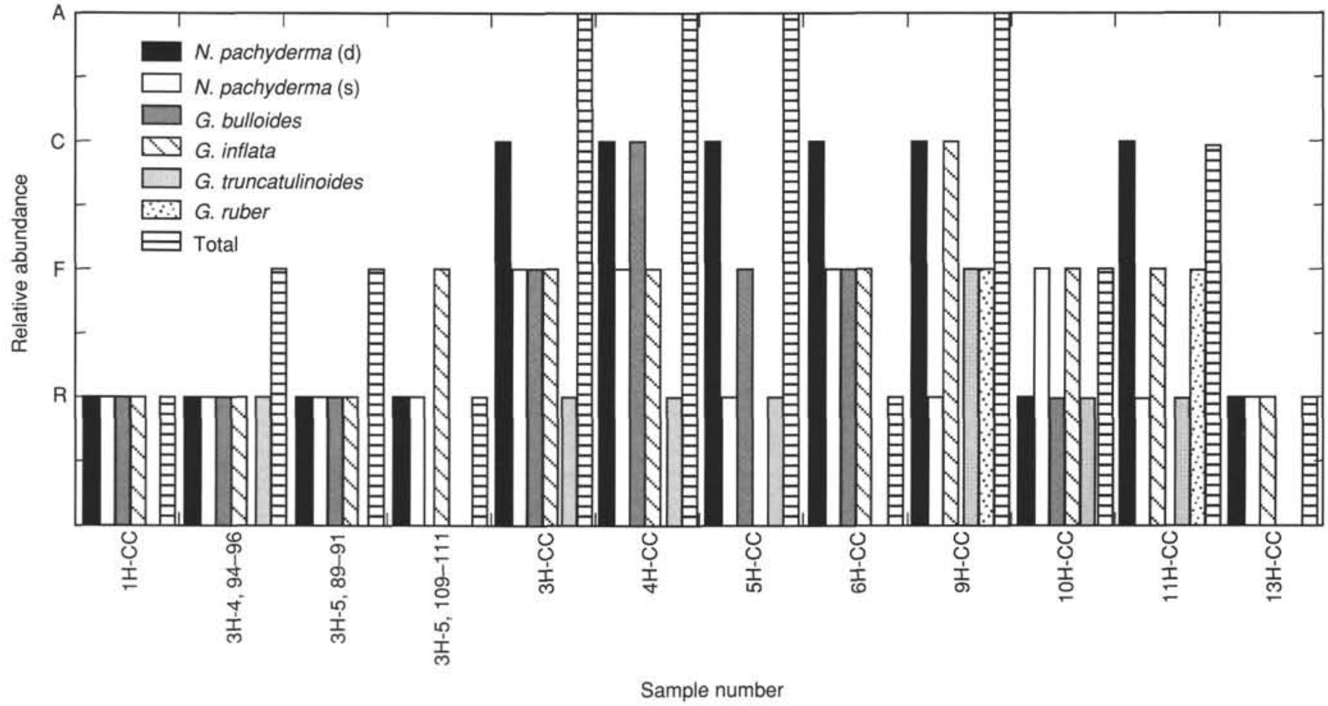

Figure 11. Relative abundances of selected planktonic foraminifers indicating cold, cool temperate, and warm waters during the Pleistocene in Hole 902C. A = abundant, C = common, F = few, and R = rare.

species of *Truncorotaloides* and *Acarinina,* which both had an LAD within Chron C17n (BKF85), occur in some abundance. The specimens are interpreted to be reworked, but very good preservation coupled with their numerical abundance indicates that they were not transported far from the original site of deposition.

The main planktonic foraminifer datums delineated in the upper Eocene to Pleistocene section recovered at Site 902 are given in Table 4.

Benthic Foraminifers

Benthic foraminifer assemblages were used to identify episodes of transported and in situ sedimentation in the Pleistocene sections. Virtually all benthic foraminifers from the Pleistocene sections of Holes 902A through 902D were downslope transported. The water depth at Hole 902D is 811 m (middle bathyal); therefore, the presence of neritic (0–200 m) and upper bathyal (200–600 m) benthic foraminifer assemblages in high relative abundances indicates downslope transport in the Pleistocene. Common elements of the transported faunas include both shelf species and upper bathyal fauna (Table 5). Transported shallow-water shelf taxa include *Buccella frigida, Bulimina marginata, Cassidulina* sp., *Cibicides lobatulus, Cibicides* spp., *Eggerella* spp., *Elphidium* spp., *Fursenkoina* spp., *Islandiella* spp., miliolids, and *Rosalina* spp. Transported deeper water (outer shelf–upper bathyal) fauna include *Melonis barleeanum* and *Bulimina elongata.*

Glacial assemblages were differentiated from interglacial assemblages primarily by high relative abundances of *Elphidium* spp. Long associated with inner neritic (<30 m) depths, high relative percentages (25%–30%) of *Elphidium* spp. were found on the modern continental shelf off Long Island, New York, between 66.5 and 85.5 m (Gevirtz et al., 1971), where they are interpreted as tests in relict glacial sediments. Poag et al. (1980) reported dominant *Elphidium* spp. on the continental shelf. Because *Elphidium* spp. are dominant along the modern western Atlantic continental shelf in association with *C. lobatulus, Eggerella advena, Fursenkoina fusiformis,* and *Saccamina difflugiformis* (Poag et al., 1980), the presence of these species in association with high relative abundances of *Elphidium* spp. indicates a shelf source of transported material. The interpretation of glacial age of these transported assemblages is corroborated by the presence of a cold-water planktonic fauna. Additional support for the glacial, transported interpretation includes the presence of wood fragments, echinoid spines, glauconite, subangular to angular quartz sand grains, high percentages of mica and the absence of in situ elements. *Elphidium* spp. are also present on the western North Atlantic slope (Streeter and Lavery, 1982), although not in the high abundances noted on the shelf.

Cores 150-902D-14H to -64X (130.88–593.93 mbsf) contain no benthic foraminifers, with the exception of Cores 150-902D-21X (171.61 mbsf) and -22X (180.90 mbsf), which contain transported inner shelf benthic foraminifer assemblages (*Bulimina curta, Uvigerina juncea,* and *Nonionellina pizzarensis*). In addition, the presence of in situ, probably Miocene, slope material is indicated by *Martinotiella* cf. *communis.* The presence of glauconite, mica, and wood fragments provides further evidence of transport in this interval.

Samples examined in and below Core 150-902D-65X contained primarily in situ benthic foraminifer assemblages. There is little evidence of downslope transport in this section.

Samples 150-902D-65X-CC (597.02 mbsf) and -66X-CC (612.90 mbsf) (lower Miocene to uppermost Oligocene) contain bathyal benthic foraminifer assemblages that are characterized by *Bulimina mexicana, Cibicidoides bradyi, Globocassidulina subglobosa, Gyroidinoides* spp., *Hoeglundina elegans, Lenticulina* spp., *Melonis barleeanum, Melonis pompilioides, Oridorsalis* spp., *Plectofrondicularia* sp., polymorphinids, *Pullenia* spp., *Siphonina tenuicarinata, Sphaeroidina bulloides, Stilostomella* spp., and *Uvigerina* spp. The presence of *Cibicidoides mundulus* and *Planulina renzi* indicates an approximate upper depth limit of 200 m, whereas the presence of *Cibicidoides dutemplei* indicates a lower depth limit of 600 m (van Morkhoven et al., 1986), placing these samples within the upper bathyal zone (i.e., slightly shallower than at present).

Benthic foraminifer faunas examined from Samples 150-902D-67X-CC through -73X-CC (622.87–678.83 mbsf) (upper Oligocene)

Table 4. Planktonic foraminifer datums in the upper Eocene to Pleistocene section recovered at Site 902.

Core, section, interval (cm)	Depth (mbsf)	Zone/Age	Species	Datum
150-902C-				
11H-CC	88.0	Pleistocene	*Globorotalia truncatulinoides*	FAD below base of Olduvai at 1.9 Ma
150-902D-				
11H-CC	107.5	Pleistocene	*Globorotalia truncatulinoides*	FAD below base of Olduvai at 1.9 Ma
21X-CC	180.3	upper N17/N18	*Globorotalia cibaoensis*	FAD at 6.7 Ma
			Transitional forms of *G. juanai* to *G. margaritae* (?)	FAD in Chron 5 at 5.6 Ma
22X-3, 83–85	184.2	N16/N17	*Globorotalia plesiotumida*	FAD at base of Zone 17a
			Neogloboquadrina acostaensis	FAD in Chron 11 at 10.2 Ma
65X-1, 118–123	594.9	N5	*Globorotalia peripheroronda*	FAD at base of Zone N4b
and 65X-CC	603.3		*Globoquadrina dehiscens*	FAD in Chron C6B at 23.2 Ma
			Globoquadrina praedehiscens	LAD in lower Zone N6
			Globigerinoides altiaperturus	FAD at top of Chron C6A at 20.9 Ma
66X-CC	613.0	N4b	*Globorotalia* cf. *G. kugleri*	FAD in middle of Chron 6C a 23.7 Mat
			Globorotalia opima nana	LAD in Zone N4b
73X-CC	680.2	P21/P22	*Globorotalia opima opima*	LAD in Chron C9 at 28.2 Ma and FAD in Chron C12 at 32.7 Ma
74X-1, 138–140	681.6	P16/P17	*Globorotalia cerroazulensis*	LAD in Chron C13 at 36.6 Ma
			Hantkenina spp.	LAD in Chron C13 at 36.6 Ma

Notes: The datums listed should be considered provisional because of the large barren intervals. Sporadic and isolated occurrences restrict the reliability of the datums as delineated.

are similar to the lower Miocene assemblages discussed above, including *Bulimina mexicana, Cibicidoides* spp., *Gyroidinoides* spp., *Lenticulina* spp., *Melonis barleeanum, Melonis pompilioides, Plectofrondicularia* sp., *Pleurostomella* sp., polymorphinids, *Pullenia* spp., *Stilostomella* spp., and *Uvigerina* spp. In addition, *Alabamina* sp. and *Planulina costata* are common in the upper Oligocene section. *Planulina renzi* indicates an upper depth limit of 200 m, and *Planulina costata* and *Siphonina tenuicarinata* a lower limit of 1000 m (van Morkhoven et al., 1986), suggesting that this part of the section was probably deposited in the upper to middle bathyal zone. *Cibicidoides dutemplei* was used to estimate the upper bathyal paleodepth of the overlying lower Miocene section; however, its global first occurrence is in planktonic foraminifer Zone N5 (van Morkhoven et al., 1986), eliminating this as a potential depth-diagnostic species in the upper Oligocene section. In the absence of other depth-indicative taxa, the paleobathymetric estimate for the upper Oligocene section is upper to middle bathyal (200–1000 m).

Samples 150-902D-74X-CC (688.25 mbsf), -75X-CC (694.79 mbsf), -76X-CC (709.30 mbsf), and -80X-CC (729.12 mbsf) (upper Eocene) contain bathyal assemblages that include *Bulimina alazanensis, Bulimina* spp., *Cibicidoides bradyi, Cibicidoides micrus, Cibicidoides praemundulus, Globocassidulina subglobosa, Gyroidinoides* spp., *Hanzawaia ammophila, Lenticulina* spp., *Nonion havanensis, Osangularia* sp., *Plectofrondicularia* spp., *Pleurostomella* sp., polymorphinids, *Pullenia* spp., *Stilostomella* spp., and *Uvigerina havanensis. Planulina costata* and *Siphonina tenuicarinata* in these samples indicate a lower limit of 1000 m (van Morkhoven et al., 1986). The presence of *Cibicidoides robertsonianus* in Sample 150-902D-74X-CC (688.25 mbsf) places an upper paleodepth limit of 600 m (van Morkhoven et al., 1986) on this sample, indicating that it was probably deposited in the middle bathyal zone.

The benthic foraminifers in the upper Eocene through lower Miocene section indicate a paleobathymetric shallowing upsection. Upper Eocene middle bathyal (600–1000 m) faunas are overlain by upper Oligocene, upper to middle bathyal (200–1000 m) assemblages. The overlying lower Miocene assemblages indicate upper bathyal paleodepths (200–600 m).

Calcareous Nannofossils

Calcareous nannofossils are rare to common and moderately preserved (because of partial dissolution) in the Pleistocene and lower Miocene to Oligocene silty clays recovered at Site 902. They are abundant and generally well preserved in the upper Eocene marls. They are absent in the upper and middle Miocene interval, except at a few levels that yield impoverished assemblages.

The upper and middle Pleistocene is represented by the *Emiliania huxleyi* Zone (Zone NN21) and the *Gephyrocapsa oceanica* Zone (Zone NN20). The *E. huxleyi* Acme Zone (top of Zone NN21) was identified only at the top of the sediment section (Section 150-902A-1H-1, 20 cm; 0.2 mbsf). Some 77 cm below this level, *Emiliania huxleyi* is present but is no longer dominant, thus indicating an age in excess of 75–83 ka (oxygen isotope stage 5) from this level downward. *Emiliania huxleyi* becomes progressively rarer, and its lowest occurrence is just short of 45 mbsf (Samples 150-902C-5H-4, 83.5 cm, and 150-902D-6H-CC). Thus, this level yields an age estimate of approximately 270 ka (oxygen isotope stage 8). The entire interval above this datum belongs to Zone NN21. Zone NN20 extends from this same level (45 mbsf) to approximately 113.7 mbsf (Sample 150-902C-15H-1, 132–134 cm), where very rare *Pseudoemiliania lacunosa* were recorded. Because calcareous nannofossils are generally rare in the Pleistocene sediments at Site 902, delineation of the NN19/NN20 zonal boundary between Samples 150-902C-15H-1, 71–73 cm (115.72 mbsf), and 150-902C-15H-1, 132–134 cm (116.33 mbsf) is tentative. The section below this level has an age estimate greater than 474 ka (oxygen isotope stage 12). Just below the contact between lithologic Units I and III in Hole 902C (see "Lithostratigraphy" section, this chapter), at approximately 122.25 mbsf (Section 150-902C-16H-1, 125 cm), a sparse assemblage with *Reticulofenestra pseudoumbilicus* and *Discoaster brouweri* occurs. Thus, the youngest sediments below the contact in Hole 902C can be constrained to the NN10–NN15 zonal interval (mid-Pliocene to upper Miocene; older than 3.5 Ma; Fig. 12). Non-age-diagnostic assemblages were recovered at 170.9, 180.3, and 190.2 mbsf in Samples 150-902D-20X-CC, -21X-CC, and -22X-CC, respectively. No calcareous nannofossils were recovered between Sections 150-902D-22X-CC (190.2 mbsf) and -60X-CC (555.0 mbsf), except in Sample 150-902D-58X-CC (536.64 mbsf), which yields *Cyclicargolithus floridanus* and *Discoaster deflandrei,* indicating the middle or lower Miocene.

An early Miocene assemblage indicative of Zone NN2 was recovered in Section 150-902D-61X-CC (564.82 mbsf). This assemblage contains *Triquetrorhabdulus carinatus,* a variety of forms assignable to *Discoaster druggi* and *Discoaster calculosus,* as well as *Discoaster deflandrei.* Shipboard biostratigraphers (M.-P. Aubry [MPA] and Steve Gartner [SG] disagree on interpretation of the extent of Zone NN2. Zone NN2 extends down to at least Section 150-902D-65X-CC (597.02 mbsf) (MPA). In Samples 150-902D-64X-CC and -65X-CC (593.7 and 597.02 mbsf), respectively, *Dictyococcites abisectus* was recorded, indicating a probable earliest Miocene age (Biochron NN1) (SG).

Sample 150-902D-66X-CC (612.90 mbsf) belongs to Zone NP25 (upper Oligocene). The simultaneous highest occurrences of *Zygrhablithus bijugatus, Reticulofenestra bisecta,* and *Sphenolithus ciperoen-*

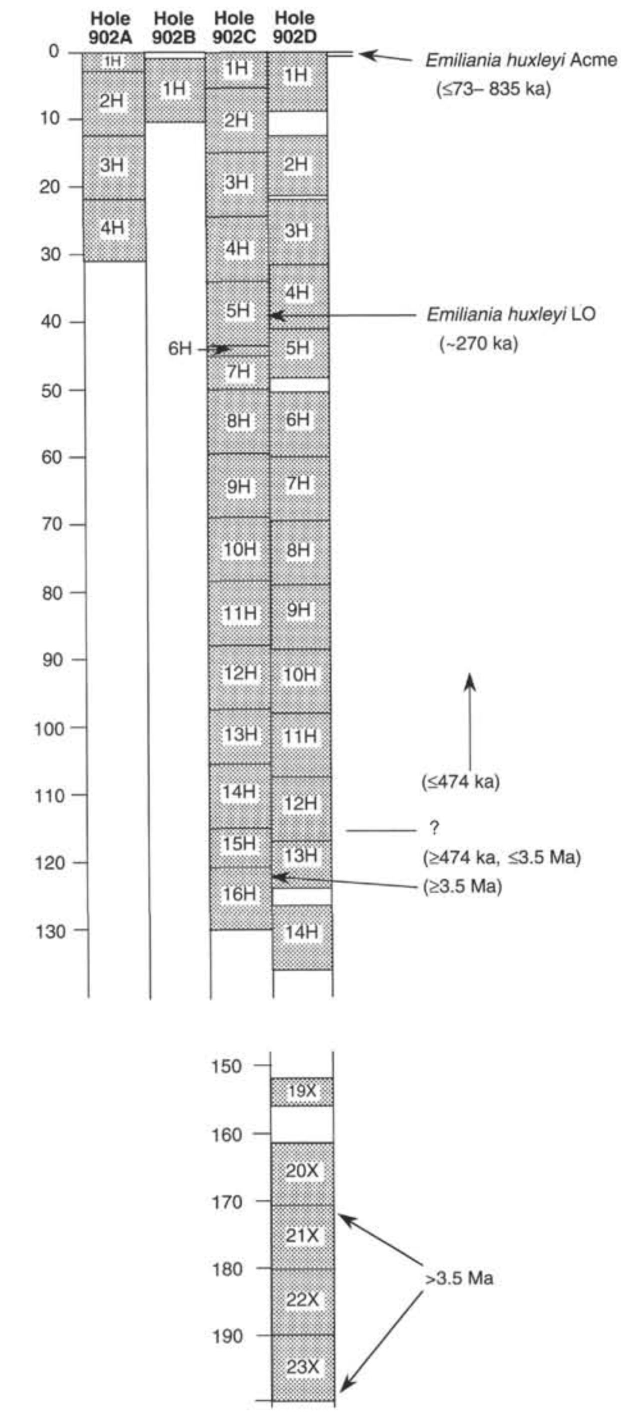

Figure 12. Chronological framework based on calcareous nannofossil biochronology for the Pleistocene section recovered at Site 902.

sis between Sections 150-902D-66X-CC (612.90 mbsf) and -66X-5, 29–31 cm (609.60 mbsf) indicates an unconformity between these two levels, the upper part of Zone NP25 being truncated. Zone NP25 extends down to Section 150-902D-71-CC (661.94 mbsf). The highest occurrence of *Sphenolithus distentus* in Section 150-902D-72X-CC (670.83 mbsf) and the lowest occurrence of *S. ciperoensis* in Section 150-902D-73X-CC (678.83 mbsf) delineate Zone NP24. Few *Sphenolithus predistentus* were observed in Samples 150-902D-74X-1, 1 cm and 73 cm (680.21 and 680.93 mbsf, respectively), which are tentatively assigned to Zone NP23. Poor preservation at these levels may account for the absence of *S. ciperoensis*.

The clayey chalks recovered between Sections 150-902D-74X-1, 74 cm, and -82X-CC (680.94–736.43 mbsf) yield abundant, rich calcareous nannofossil assemblages of Zone NP19–20. The sequential highest occurrences of *Discoaster saipanensis* (in Sample 150-902D-74X-1, 74 cm; 680.94 mbsf), *D. barbadiensis* (in Sample 150-902D-74X-CC; 688.25 mbsf), and *Reticulofenestra reticulata* (in Sample 150-902D-75X-CC; 694.79 mbsf) indicate a complete uppermost Eocene section (Fig. 13).

Table 5. Characterization of calcareous nannofossil, planktonic foraminifer, and benthic foraminifer assemblages in Hole 902C and their glacial interval and oxygen isotope stages.

Core, section, interval (cm)	Calcareous nannofossil assemblage	Planktonic foraminifer assemblage	Benthic foraminifer assemblage	Interpreted glacial interval	Oxygen isotope stage
150-902C-					
1H-2, 140	Warm			Interglacial	5.3
1H-CC		Cooler	?Cool	Glacial	5.4
2H-3, 140	Warm			Interglacial	5.5
2H-5, 50	Very cool			Glacial	
2H-CC			Shallow	Glacial	6.2
3H-4, 94–96	Warm	Warm	Deeper	Interglacial	6.3
3H-5, 89–91		?Cool	?Shallow	Glacial	6.3/6.4
3H-5, 109–111		Cool	Shallow	Glacial	6.4
3H-CC	Cool	Warm		Interglacial	6.5
4H-4	Pelagic			?Interglacial	6.5
4H-5	Mild, detrital			?Glacial	7.0
4H-CC		Warm		Interglacial	7.1
5H-CC	Mild	Warm		Interglacial	7.5
6H-1, 45	(Stage 8)	Cool		Glacial	8.2
8H-CC			Deeper	Interglacial	8.5
9H-CC		Warm	Deeper	Interglacial	8.5
10H-CC		Cool		Glacial	9.2
11H-CC		Warm	Deeper	Interglacial	11.3
12H-CC	(NN20)	Warm	Deeper	Interglacial	11.3
13H-CC			Shallow	Glacial	12.2
14H-CC			Shallow	Glacial	12.4
16H-CC		Barren	Barren		

Notes: Calcareous nannofossil and planktonic foraminifer assemblages were characterized as either warm or cool. Benthic foraminifer assemblages were characterized as transported shallow-water material (shallow) or transported outer shelf to upper bathyal (deeper) material. Oxygen isotope stage assignments are tentative and based on calibration of bulk density data with the SPECMAP oxygen curve (see "Sedimentation Rates" section, this chapter).

Diatoms

Hole 902A

At Hole 902A, we recovered a 31-m-thick Pleistocene section. Samples 150-902A-1H-CC to -4H-CC (0–31 mbsf) are placed in the upper–middle Pleistocene *Pseudoeunotia doliolus* Zone. This is based upon the presence of *P. doliolus* and the absence of *Nitzschia reinholdii*, which indicates that sediments recovered from Hole 902A were deposited entirely in the Brunhes Chron. Other species include *Actinoptychus senarius, Coscinodiscus asteromphalus, C. marginatus, Cyclotella stylorum, Thalassionema nitzschioides,* and *Thalassiosira oestrupii*. Diatom abundances range from nil (barren) to common; preservation, where diatoms are present, is generally moderate. Most samples, however, are barren of diatoms.

Hole 902B

At Hole 902B, we recovered a 9.5-m-thick section with no diatoms.

Hole 902C

At Hole 902C, we recovered a 130-m-thick section of upper–middle Pleistocene sediments as well as a lower barren section that may be as old as upper Miocene. Sections 150-902C-1H-CC to -12H-

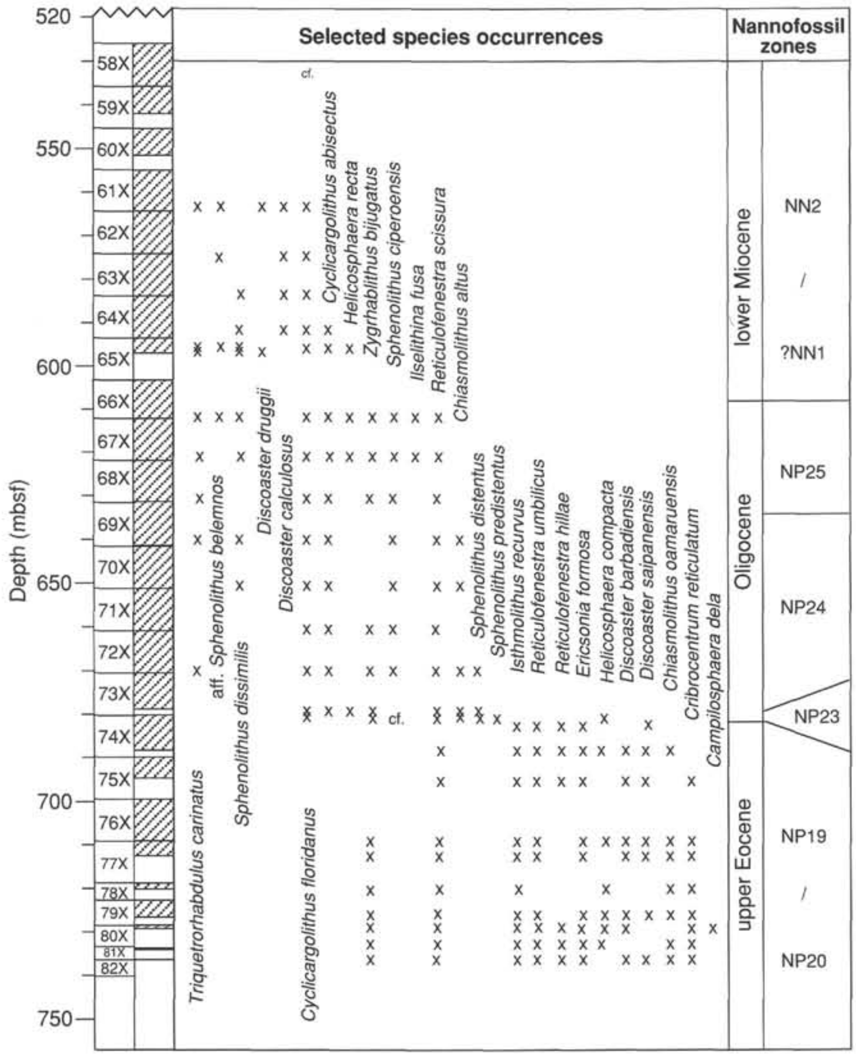

Figure 13. Distribution of selected calcareous nannofossil species in the lower Miocene to upper Eocene sediments recovered from Hole 902D.

CC (0–97.23 mbsf) belong to the *P. doliolus* Zone based upon the presence of the nominate taxon and the absence of *N. reinholdii.* Other species include *Actinoptychus senarius, Azpeitia nodulifera, Coscinodiscus asteromphalus, C. marginatus, Cyclotella stylorum, Hemidiscus cuneiformis, Roperia tesselata, Stephanopyxis* spp., *Thalassionema nitzschioides,* and *Thalassiosira oestrupii.* Diatom abundances range from nil (barren) to common, and the preservation is generally moderate. Sections 150-902C-13H-CC to -16H-CC (105.74–129.99 mbsf) are barren of diatoms, but rare fragments of what are very likely radiolarians are present.

Hole 902D

At Hole 902D, we recovered a 740-m-thick section of upper Pleistocene to Eocene sediments. Sections 150-902D-1H-CC to -11H-CC (0–108.51 mbsf) belong to the *P. doliolus* Zone based upon the presence of the nominate taxon and the absence of *N. reinholdii.* Other species include *Actinoptychus senarius, Azpeitia nodulifera, Coscinodiscus asteromphalus, C. marginatus, Cyclotella stylorum, Hemidiscus cuneiformis, Rhyzosolenia hebetata, Roperia tesselata, Stephanopyxis* spp., *Thalassionema nitzschioides,* and *Thalassiosira oestrupii.* Diatom abundances range from nil (barren) to common, and the preservation is generally moderate. Alternations of diatom-rich and diatom-poor intervals occur in Core 150-902D-9H (79–88.42 mbsf); the diatom-rich intervals are characterized by abundant *C. marginatus,* whereas the diatom-poor intervals, which contain more carbonate, are characterized by a mixed assemblage, *P. doliolus, T. nitzschioides,* and *T. oestrupii* being the most common. The absence of a diatom datum level (FAD of *Nitzschia reinholdii*) places these alternations at younger than 600 ka, whereas the calcareous nannofossil datum levels constrain them between approximately 275 and 450 ka (i.e., approximately between oxygen isotope stages 8 and 12). The *C. marginatus*-dominated assemblage suggests a more boreal environment, whereas the higher diversity, lower abundance assemblage suggests a warmer water environment.

Samples 150-902D-12H-CC to -15H-CC (118.97–134.80 mbsf) contain rare to no diatoms and rare fragments of radiolarians and sponge spicules. This interval may represent the Pliocene or uppermost Miocene. We are unsure of the age of Samples 150-902D-16H-CC to -18X-CC (139.93–152.81 mbsf). Although few to common diatoms are present, no age-diagnostic indicators were observed. Indeed, the diatom zones that have been reported from upper Miocene to lower Pliocene sediments of the North Atlantic (*Nitzschia porteri–N. miocenica, Thalassiosira convexa, Nitzschia jouseae* [Burckle, 1972], and *Nitzschia marina* [Baldauf, 1984]) are not present at Hole 902D. One species, *Actinocyclus ingens,* suggests that these samples cover part of the upper Miocene. *Actinocyclus ingens* occurs in Neogene sediments in the equatorial Pacific up to about the middle of the upper Miocene. Its presence in Sample 150-902D-16H-CC (139.93 mbsf) suggests an age older than middle late Miocene. A Miocene age for this sample is also supported by the co-occurrence of the silicoflagellates *Mesocena diodon diodon* and *Distephanus crux*. This age assignment is supported by the diatoms present in the next lowest sample (150-902D-19X-CC; 156.21 mbsf). In addition to *A. ingens*, this sample also includes the last occurrence datum of *Denticulopsis hustedtii*. This species disappears from equatorial Pacific sediments during the early middle part of the late Miocene (the middle part of Chron 10 [Chron C4Ar]; Burckle et al., 1982).

Although the zonal markers were not always observed, the interval from Samples 150-902D-19X-CC to -41X-CC (156.21–373.49 mbsf) probably belongs to the *Coscinodiscus yabei* Zone of Baldauf (1984). In addition to the nominate taxon, this zone contains *Actinocyclus ellipticus, A. ingens, A. senarius, A. tenellus, Coscinodiscus endoi, Cymatosira immunis, D. hustedtii, Mediaria splendida, Rhizosolenia barboi, T. nitzschioides,* and *Thalassiosira grunowi*. Also of note is the fact that diatom zonal markers from the east coast (U.S.) also occur in this zone. For example, the last occurrence of *Delphineis novaecaesaraea* is in Sample 150-902D-33X-CC (292.99 mbsf). The lowest occurrence of this species is in East Coast Diatom Zone (ECDZ) 3-4, and it ranges through ECDZ 5, 6, and 7 (Andrews, 1988). The *Denticulopsis praedimorpha* Zone, which was described by Baldauf (1984), does not appear to be present in Hole 902D. The nominate taxon, *D. praedimorpha*, is not present in the interval below the *C. yabei* Zone. Instead, the last occurrence of *Denticula punctata* var. *hustedtii*, which defines the base of this zone, is at Sample 150-902D-41X-CC (373.49 mbsf). In the equatorial Pacific, Burckle et al. (1982) noted the last occurrence of this variety in magnetic Chron 12 (Chron C5r; late middle Miocene).

Samples 150-902D-42X to -52X-CC (382.80–478.15 mbsf) span the *Rhizosolenia barboi* Zone of Baldauf (1984). In addition to the nominate taxon, this zone also includes *A. ellipticus, A. ingens, A. tenellus, C. endoi, D. hustedtii, D. punctata* var. *hustedtii, R. miocenica, R. alata, Hemidiscus cuneiformis, Stephanopyxis grunowii, Thalassiosira grunowii,* and two species that are also used to subdivide the Miocene sediments of the east coast: *Delphineis penelliptica* and *D. novaecasaeraea*. The last occurrence of these latter two species is used to identify ECDZ 6 and 7 (Andrews, 1988). The *Denticulopsis nicobarica* Zone of Baldauf (1984) is not present in Hole 902D; the *Coscinodiscus lewisianus* Zone (Baldauf, 1984) lies directly beneath the *R. barboi* Zone. This former zone extends from Sample 150-902D-53X-CC to at least Sample 150-902D-63X-CC (488.07–584.20 mbsf). In addition to the nominate taxon, this zone contains *A. ingens, A. tenellus, C. endoi, D. hustedtii, D. punctata* var. *hustedtii, R. miocenica,* and *Stephanopyxis grunowii*. The top of the zone, defined by the highest occurrence of *C. lewisianus*, also contains *Rhaphidodiscus marylandicus*, a species that usually has its highest occurrence well below the top of the zone. Samples below 150-902D-63X-CC to -73X-CC (584.20–678.83 mbsf) are characterized by progressive fragmentation and silica dissolution; as a result, it is difficult to identify species and assign ages, although some samples contain robust specimens of *Stephanopyxis* spp.

A continuous record was not recovered in Hole 902D. According to the diatoms, the lower Pleistocene and all of the Pliocene are missing or truncated; in any event, the levels that should approximate these intervals are barren of diatoms. Similarly, no diatom record exists for the latest Miocene. The lower part of the upper Miocene section appears to be expanded as is the interval straddling the middle/upper Miocene boundary. We identify a stratigraphic gap below this, the upper middle Miocene resting unconformably on the lower Miocene. In the lower Miocene, increased dissolution and diatom fragmentation have compromised our ability to identify zonal markers and to recover a biochronology. Regional paleoceanography can be determined from a preliminary consideration of the occurrence of diatom assemblages and their species composition. The occurrence of alternating zones of diatom-rich and diatom-poor sediments is likely related to glacial/interglacial changes during the Pleistocene. The fact that the diatom-rich interval contains a more boreal assemblage suggests that it represents glacial conditions. If one rules out the slumped portion of Hole 902D, then most of the (upper–middle) Pleistocene that was recovered contains a record of these alternations. The presence of early to late Miocene diatoms in Hole 902D is a record of past high oceanic productivity, likely caused by upwelling or the presence of nutrient-rich waters. Finally, as at least some of Andrew's zonal markers are present, it will be possible to correlate sediment in holes recovered during Leg 150 with the ECDZ of Andrews (1988).

Dinoflagellate Cysts

Dinoflagellate cyst (dinocyst) assemblages at this site are diverse and moderately to well preserved in the Pleistocene, Miocene, and Oligocene intervals (Table 6). Most palynological analyses were restricted to the Miocene section that contains calcareous microfossils in only a few intervals. However, marine and nonmarine palynological assemblages are probably also preserved in the Eocene section. Sieving sediment samples at 25 µm undoubtedly resulted in the loss of all the small angiosperm pollen and some acritarchs and fungal spores (see Chapter 3, this volume).

The Pleistocene section is not subdivided using dinocyst biostratigraphy but is recognized by the presence of *Ataxiodinium choanum*, at least to Sample 150-902C-8H-CC (60 mbsf).

Many as-yet-undescribed taxa, particularly peridinioids, are present in low numbers throughout the Miocene recovered at Site 902. Several of these have been encountered in coeval deposits in Maryland and Virginia and are currently under study by de Verteuil. Some of these undescribed species are biostratigraphically important, but in most instances only published species are cited in this report.

Hole 902A

Three of the four core-catcher samples analyzed yield dinocysts (Samples 150-902A-1H-CC [2.70 mbsf], -2H-CC [12.91 mbsf], and -3H-CC [22.37 mbsf]; Sample 150-902A-4H-CC [30.63 mbsf] is barren). All have well-preserved, low-diversity assemblages of late Pleistocene taxa with mixed ecological preferences. The assemblage at 22 mbsf (Sample 150-902A-3H-CC) for example, includes *Nematosphaeropsis lemniscata, Impagidinium patulum,* and *Bitectatodinium tepikiense,* as well as *Selenopemphix quanta, Protoperidinium avellana, P. leonis,* and *Polykrikos schwartzii*. The presence of neritic taxa, rare Compositae pollen, and common terrestrial palynodebris indicates that some elements of the flora were transported across the shelf to the site of deposition.

Hole 902C

We recovered well-preserved Pleistocene assemblages from six core-catcher samples between 44.08 and 115.53 mbsf (Sections 150-902C-5H-CC through -14H-CC). In addition to taxa found in the Pleistocene of Hole 902A, assemblages contain *Spiniferites elongatus, S. frigidus, S. membranaceous, S. bentorii, S. mirabilis, S. ramosus* complex, *A. andalousiensis, Filisphaera filifera, Operculodinium centrocarpum* s.l., and *Lingulodinium machaerophorum*. These gonyaulacoid taxa co-occur with *Polysphaeridium zoharyi*, brown diplopsiloid cysts, and *Polykrikos* sp. cf *P. kofoidii*. Several specimens of *L. machaerophorum* have the short, wide, rounded processes characteristic of abnormal salinity concentrations. The co-occurrence of the tropical to subtropical *P. zoharyi* with *S. frigidus* and other cold-temperate species is also incongruous. Thus, during the Pleistocene, the indigenous dinocyst flora was augmented by taxa transported to this site from the north, south, and west. Although floral mixing has clearly occurred, this should not preclude future quantitative studies from recognizing Pleistocene climatic cycles and paleoceanographic events and may, in fact, aid such research.

Middle upper Miocene sediments of dinocyst Zone H, which extends between 115.53 and 129.99 mbsf, unconformably underlie the

Table 6. Distribution of selected calcareous nannofossil species in the lower Miocene to upper Eocene sediments recovered from Hole 902D.

Core, section, interval (cm)	Depth (mbsf)	Zone	Lowest occurrence	Age	Highest occurrence	Age
150-902A-						
1H-CC	2.70	Pleistocene				
2H-CC	12.90	Pleistocene				
3H-CC	22.40	Pleistocene				
4H-CC	31.00					
150-902C-						
5H-CC	44.08	Pleistocene				
6H-CC	45.00	Pleistocene				
7H-CC	50.28	Pleistocene				
8H-CC	60.12	Pleistocene				
10H-CC	79.25	Pleistocene				
14H-CC	115.53	Pleistocene				
16H-CC	129.99	H				
150-902D-						
13H-CC	123.92	Pleistocene				
14H-CC	130.88	H			*L. truncatum*	8.5*1
15H-3, 82–87	134.50	H	"*Barssidinium*" sp.	8*1		
17H-CC	145.00*	G			*S. soucouyantiae*	9*1
20X-CC	171.61	G				
22X-CC	190.14	G				
28X-CC	248.24	G				
31X-CC	267.59	G				
32X-CC	286.90	F			*C.* sp . cf. *C. utinensis*	11*2
33X-CC	292.99	F				
35X-CC	315.74	F				
38X-CC	344.15	F				
43X-CC	393.75	F				
44X-CC	401.82	F				
45X-CC	405.15	F				
49X-CC	448.46	F	*C.* sp. cf. *C. utinensis*	12*2		
50X-1, 93–98	450.30	E				
51X-1, 14–19	459.00	E				
51X-5, 95–100	465.90	D			*S. placacantha/ancyrea* complex	14*1
52X-CC	478.15	D				
53X-CC	488.07	D	*H. tectata, U. aquaeductum*	15*1		
54X-CC	497.73	C				
55X-CC	507.58	C			*D. paradoxum*	15*0.5
56X-CC	515.98	C	*L. truncatum*	17.5*1		
58X-CC	536.64	B				
61X-CC	564.82	B				
62X-CC	574.54	A			*C. cantharellum*	18*1
63X-3, 32–37	577.70	A				
63X-5, 94–95	581.40	A				
65X-1, 38–43	594.00	A	*S. soucouyantiae*	18*2		
65X-2, 43–48	595.70	pre-A			*H. vallum, Chiropteridium* spp., M. aspinatum	23*2
66H-CC	612.90	pre-A	*H. truncana*	25*1		
68H-CC	632.02	pre-A	*T. vancampoae, B. sphaerica* complex	27*1		

Note: Item marked with an asterisk (*) in the "Depth" column indicates that no APC core catcher could be found in the scratch file.

upper Pleistocene in Hole 902C (see "Calcareous Nannofossils," this section). A single core-catcher sample from 129.99 mbsf (150-902C-16H-CC) contains a diverse middle late Miocene assemblage that includes the age-diagnostic species *Hystrichosphaeropsis obscura, Dapsilidinium pseudocolligerum, Labyrinthodinium truncatum,* and *Barssidinium evanglineae.* These taxa constrain this sample to dinocyst Zone H. The rare occurrence of *Paleocystodinium golzowense,* which generally has a highest occurrence in the underlying Zone G, suggests that the sample may be from the base of Zone H or that it may contain minor reworking.

Hole 902D

Thirty-four samples (mostly core catcher), between 123.92 and 632.02 mbsf (Cores 150-902D-13H to -68X), were processed and studied for palynomorphs. We recognized eight dinocyst zones in the Miocene section, with Pleistocene sediments (Sample 150-902D-13H-CC; 123.92 mbsf) unconformably overlying middle upper Miocene strata (Sample 150-902D-14H-CC; 130.88 mbsf).

Dinocysts in Section 150-902D-13H-CC (123.92 mbsf) occur in low concentrations compared with other Pleistocene samples from Hole 902C. The diversity at this level is low but otherwise similar to that of assemblages described (above) from Hole 902C. In general, Miocene and Oligocene samples have high concentrations of organic matter and are very productive with respect to palynomorphs.

Dinocyst Zone H occurs from the Pleistocene/Miocene contact down to 135 mbsf (Sample 150-902D-15H-3, 82–87 cm). In addition to the diagnostic taxa already cited for the equivalent interval in Hole 902C, other recorded taxa include *O. centrocarpum* sensu stricto, *Reticulatosphaera actinocoronata, L. machaerophorum, Habibacysta tectata, Tectatodinium pellitum, Impagidinium paradoxum, Nematosphaeropsis lemniscata, Spiniferites pseudofurcatus, Trinovantedinium papulum, T. harpagonium, Erymnodinium delectabile, Selenopemphix brevispinosa brevispinosa,* and *Tuberculodinium vancampoae.* The further occurrence of *Batiacasphaera sphaerica* s.s., and *Heteraulacacysta campanula* may be of stratigraphic significance (Table 5).

The interval from the base of Zone H to 267.59 mbsf (Sample 150-902D-31X-CC) belongs to dinocyst Zone G on the basis of the occurrence of *Sumatradinium soucouyantiae* and the absence of *Cannosphaeropsis* cf. *C. utinensis.* These assemblages are similar to those in Zone H, but they have fewer outer neritic/oceanic taxa and specimens of *Impagidinium* and *Nematosphaeropsis.* Additional taxa of interest that occur in Zone G are *Paleocystodinium golzowense, Selenopemphix dionaeacysta, Trinovantedinium? xylochoporum, T. ferugnomatus, Cristadinium diminutivum,* and *Xandarodinium xanthum* sensu Head et al. 1989b (pars.; pl. 3, fig. 12). The highest occurrence in Zone G of *Cordosphaeridium minimum* sensu Benedek and Sarjeant 1980 may be of stratigraphic significance.

Zone F comprises a thick section at Hole 902D that extends down from the base of Zone G to 448.46 mbsf (Sample 150-902D-49X-

CC). *Cannosphaeropsis* cf. *C. utinensis* occurs in every sample examined from the zone. Assemblages within Zone F vary in composition in relation to the amount of terrestrial constituents in the kerogen. In general, however, they are quite similar to those of Zone G but with some intervals having abundant *Polysphaeridium zoharyi,* which indicates the presence of warm-water masses on the shelf at least intermittently. Zone F is also characterized by a high diversity of peridinioid taxa, including *Leipokatium invisitatum.*

The narrow interval from 450.25 to 459.05 mbsf belongs to dinocyst Zone E (Samples 150-902D-50X-1, 93–98 cm, and -51X-1, 14–19 cm). The zone is recognized by the absence of *Cannosphaeropsis* sp. cf. *C. utinensis* (lowest occurrence in Zone F) and the *S. placacantha–S. ancyrea* complex (highest occurrence in Zone D). A distinct change occurs in this interval from palynofacies dominated by terrigenous kerogens in the overlying sequences (Zones F and G), which indicates a deltaic influence on the New Jersey continental slope, to palynofacies dominated by amorphous marine sapropelic kerogen below. The Zone E assemblage is diverse and well preserved. It contains a higher proportion of specimens of *Impagidinium* spp. than the overlying Zones F and G assemblages, which is consistent with inferred regional shallowing during deposition of the overlying middle Miocene sequences (Greenlee et al., 1992). However, several typical oceanic taxa are not present in any of the E, F, and G zonal intervals.

Dinocyst Zone D is recognized from the base of Zone E to 478.15 mbsf (Sample 150-902D-53X-CC). The zone is easily recognized by the highest downhole occurrence of the *S. placacantha–S. ancyrea* complex. This datum marks the last appearance of the genus *Systematophora* in the western North Atlantic. Specimens of this complex are common in almost every sample from this level until well into the Oligocene, and elsewhere they range at least to the base of the Cenozoic. The highest occurrence of *Systematophora* spp. is an important regional datum, therefore. *Habibacysta tectata* occurs at the base of Zone D and persists in the basin throughout the Miocene (de Verteuil and Norris, 1992). At Site 902, Zone D is also characterized by the restricted occurrence of *Unipontidinium aquaeductum.* This species has not been found beneath the lower middle Miocene. It is characteristic of outer neritic and further offshore environments. The last appearance of *U. aquaeductum* is not well constrained, but its range up to the top of Zone D in Hole 902D (Sample 150-902D-51X-5, 95–100 cm; 465.9 mbsf) may be truncated; this would be consistent with the evidence for increased deltaic influence in the rest of the Miocene section at this site.

The interval from 497.73 mbsf (Sample 150-902D-54X-CC) to 515.98 mbsf (Sample 150-902D-56X-CC) belongs to dinocyst Zone C on the basis of the co-occurrence of *L. truncatum* and *D. paradoxum.* The highest occurrence of the distinctive *Hystrichokolpoma*? sp. 1 (= Dinocyst sp. 6 of Manum et al., 1989) at this level in Hole 902D is consistent with other North Atlantic occurrences and marks an important biostratigraphic event. The genus *Aptiodinium* has a highest occurrence at Site 902 in Zone C.

No samples were examined for dinocysts between 516 and 536 mbsf. At 536.64 mbsf (Sample 150-902D-58X-CC), the assemblage recovered belongs to the lower part of Zone B and includes *Cribroperidinium tenuitabulatum.* The lower boundary of Zone B is constrained by the highest occurrence of *Cordosphaeridium cantharellum* at 574.54 mbsf. Sample 150-902D-62X-CC marks the top of Zone A, which extends down to 594.10 mbsf (Sample 150-902D-65X-1, 38–43 cm). The Zone A assemblage is characterized by a flora comprising some short-ranging early Miocene species like *Hystrichokolpoma truncana, Stoveracysta conerae,* and other undescribed taxa, a few Paleogene holdovers like *C. cantharellum* and *Operculodinium* sp. I of Manum 1976, and the absence of several typical Miocene taxa that evolved later on.

Samples taken at 595.65 and 612.90 mbsf (Samples 150-902D-65X-2, 43–48 cm, and -66X-CC) are from dinocyst Zone Pre-A based on the occurrence in both of *Chiropteridium* spp. Other taxa in the assemblage that are characteristic of this zone are *H. truncana, Homotryblium vallum,* and *Caligodinium amiculum.* In both samples, *H. vallum* is the dominant species. *Membranophoridium aspinatum* is also present, but it is common in the lower sample and rare in the upper one.

The Oligocene/Miocene contact occurs between 612.90 and 632.02 mbsf (Samples 150-902D-66X-CC and -68X-CC). The assemblage from the latter level is generally similar to that in the former level, but it is dominated by lenticular cysts (*Chiropteridium lobospinosum, C. mespilanum,* and *M. aspinatum*), with fewer occurrences of *H. vallum.* The absence of *Thalassiphora*? *pansa,* however, indicates that this level (632.02 mbsf) is still within Zone Pre-A. The assemblage also includes rare thick-walled specimens of the *Batiacasphaera sphaerica* complex and sporadic occurrences of *Tuberculodinium vancampoae.* Together, these taxa suggest that this level is upper Oligocene or younger. We also recorded *Riculacysta perforata* in this assemblage, a species that is found in the northern part of Blake Plateau, ranges from the upper part of the *Paragloborotalia opima opima* Zone (planktonic foraminifers) to the upper part of the *Globigerina ciperoensis* Zone (Stover, 1977). The co-occurrence of *T. vancampoae* and *R. perforata,* together with the absence of *T*? *pansa,* (which occurs commonly in middle and upper Oligocene sediments in the basin), constrains the age of this assemblage to a narrow interval in the later part of the late Oligocene.

PALEOMAGNETISM

Paleomagnetic measurements made at Site 902 followed the methods outlined in Chapter 3 (this volume). Holes 902A, 902B, 902C, and the upper part of 902D (Cores 150-902D-1H through -18H) were APC cored and oriented using data from the tensor tool. The XCB was used to core the remainder of Hole 902D (Cores 150-902D-19X through -78X). We measured natural and demagnetized remanent magnetization: (1) of whole sections using the pass-through method, and (2) of individual 6-cm^3 shipboard samples. We measured magnetic susceptibility of the shipboard samples to supplement the routine susceptibility measurements using the multisensor track (MST). These latter measurements were made at 10-cm intervals on the cores before they were split. On representative samples, we performed isothermal remanent magnetization (IRM) acquisition and "back-field" demagnetization experiments for the preliminary examination of magnetic mineralogy.

Determination of a magnetic stratigraphy at Site 902 is hampered by weak intensities of magnetization (generally <1 mA/m) and low stability under alternating-field (AF) demagnetization. In general, demagnetization to 15 mT was required for removal of a secondary magnetization often of steep negative inclination. However, the residual signal in pass-through cores was equal to or less than the practical limit in sensitivity of the cryogenic magnetometer (expressed as magnetization intensity, this limit is about 0.1 mA/m). The smaller volume of discrete cube samples (6 cm^3) requires a material of higher magnetization intensity to enhance the signal, estimated to be about 1 mA/m (see Chapter 3, this volume). However, the intensity of natural remanent magnetization in discrete cube samples at Site 902 is often 1 mA/m or less. In addition, XCB coring disturbed thick intervals of silty clays in Hole 902D, forming "biscuit" structures surrounded by a slurry of core cuttings. This limited our ability to extract any detailed information from the pass-through data. In the intervals where magnetization intensity was relatively strong and stability to demagnetization acceptable, we based our determination of magnetic polarity on downhole changes in inclination; declination changes were often irregular throughout Hole 902D and thus of little use in judging polarity. Holes 902A, 902B, and 902C were entirely APC cored, and we excluded from our pass-through data the steep negative (nearly vertical) inclination values that were directly correlative with "flow-in" material often present at the bottoms of the APC cores.

The four cores taken at Hole 902A and the one at Hole 902B are entirely normal in polarity at 15-mT AF demagnetization. Pass-

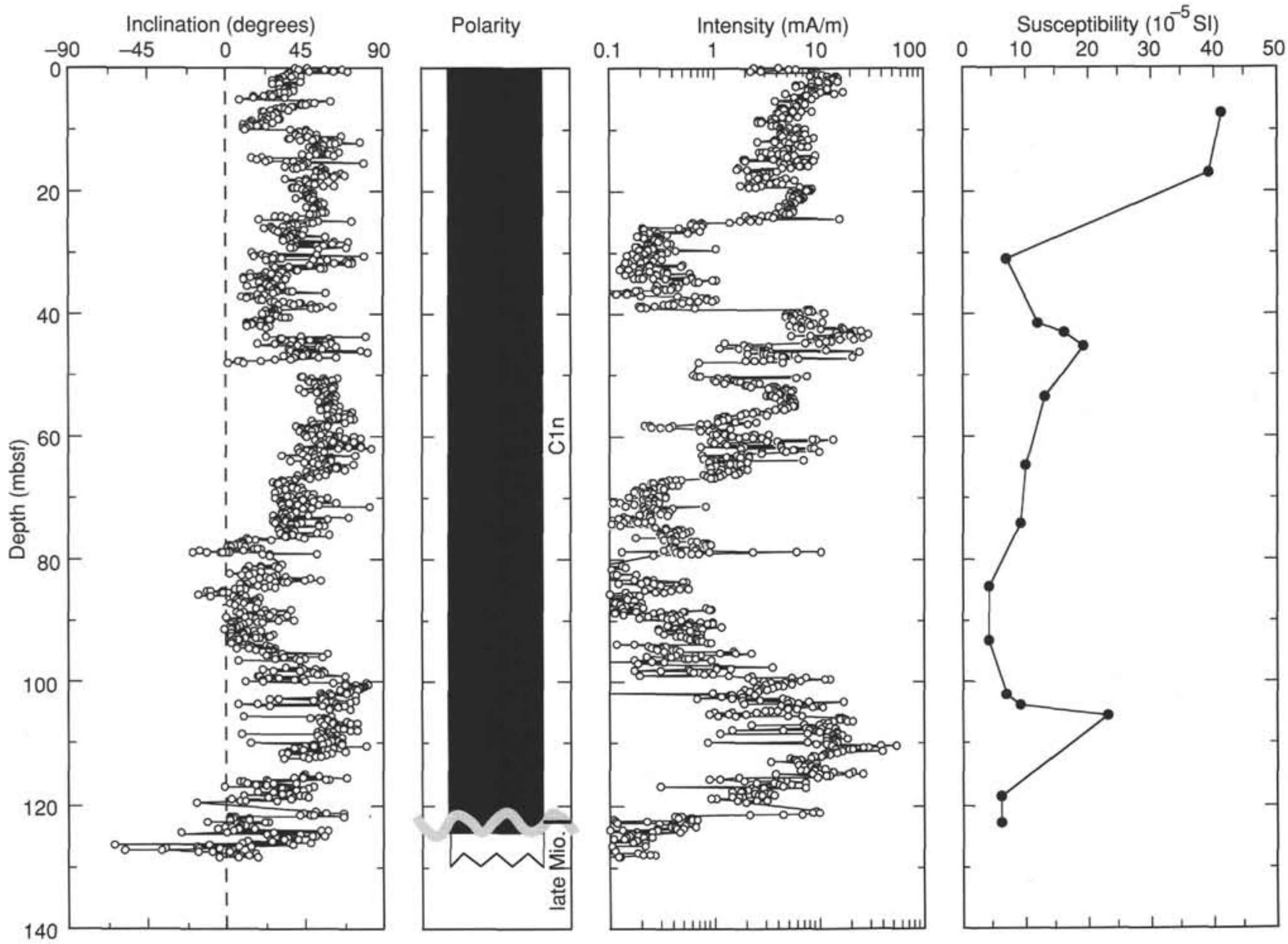

Figure 14. Inclination, magnetic polarity zones, magnetization intensity, and volume susceptibility, Hole 902C. Demagnetized magnetization intensity from discrete (open circles) and pass-through (closed circles) sample measurements; volume susceptibility from discrete sample measurements. In the polarity column, black = normal polarity and white = reversed polarity.

through measurements and demagnetization of the sediments recovered from Hole 902C (0–130 mbsf; Fig. 14), and measurements and demagnetization of 6-cm^3 samples from Hole 902D (Fig. 15) yield a fairly uniform zone of normal polarity magnetizations from 0 to 125 mbsf (Fig. 15). The overall range of magnetization intensity (at 15 mT) is 0.1–10 mA/m, and within the upper 20 m there is a gradual decrease from 10 to 2 mA/m downhole (Hole 902C; Fig. 14). In general, the discrete cube samples (Hole 902D) are stable under AF demagnetization to 50 or 70 mT. The range of susceptibility at Site 902 is 0 to 250×10^{-5} SI, with low average values (1 to 20×10^{5} SI) typical of marine sediments. Downhole changes in magnetization intensity and susceptibility parallel one another in their general trends; in fact, we can make correlations to within 1 m using magnetic susceptibility at Holes 902A, 902C, and 902D. We note that in the upper 120 m in these three holes, trends in susceptibility are also comparable with those seen in the GRAPE bulk-density data (see "Physical Properties" section, this chapter) and may be related to climatically controlled changes in Pleistocene sedimentation.

We interpret the remanent magnetization data from these intervals at Holes 902C and 902D as records of a thick Brunhes polarity interval (Chron C1n; Table 7), which is in agreement with the paleontological age of these sediments (≤474 k.y.; see "Biostratigraphy" section, this chapter). A short reversed polarity zone possibly is present at the base of Hole 902C (125–129 mbsf), which could be correlative to Chron C1r.1r = latest Matuyama Chron). However, the preliminary shipboard biostratigraphy suggests a Pleistocene/upper Miocene contact at 122.13 mbsf at Hole 902C (see "Biostratigraphy" section, this chapter). Therefore, the lower part of the normal polarity zone from 122.13 to 125 mbsf and the reversed polarity zone from 125 to 129 mbsf are records of the late Miocene geomagnetic field (BKV85, CK92).

At Hole 902D, reversed polarity magnetization begins at about 130 mbsf and continues down to about 400 mbsf, with possible thin normal intervals between about 280 and 290 mbsf (Fig. 16). This is a surprising result because the biostratigraphy indicates that these sediments are lower upper Miocene (see "Biostratigraphy" section, this chapter), an interval for which the GPTS predicts we should find several field reversals. With three candidate unconformities present over this stratigraphic interval correlating to reflectors (m0.5, Red; m0.7, blue; and m1, Tuscan), it is possible that the early late Miocene magnetic field at Site 902 is sporadically represented such that our thick reversed zone is actually a composite record of reversed polarity fields of the late Miocene (e.g., Chrons C4Ar and C5r). Such an interpretation requires that in Hole 902D the stratigraphic record of Chron C5n (an approximately 1-m.y.-long period of normal polarity in the early late Miocene) is absent (e.g., only being represented by possible normal zones between 280 and 290 mbsf).

The demagnetization behavior of the sediments changes in Hole 902D from about 420 mbsf to the bottom of the sampled interval (725 mbsf). Magnetization intensities (at 15 mT) are generally low throughout the interval (0.02–1.0 mA/m), with a notable peak of 90 mA/m occurring in silty clays at 430 mbsf (Figs. 17–18). The sediments demonstrate a remarkably low coercivity and in certain inter-

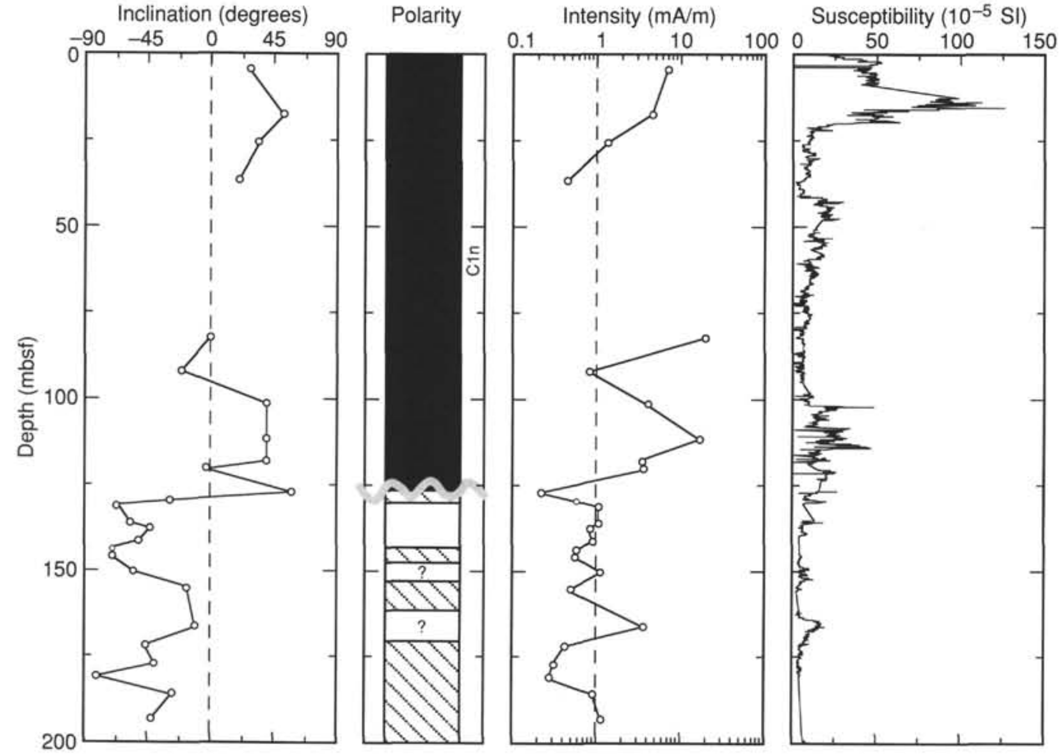

Figure 15. Inclination, magnetic polarity zones, magnetization intensity, and volume susceptibility for the interval from 0 to 200 mbsf in Hole 902D. Intensity cut-off value is 1 mA/m for discrete samples. In the polarity column, black = normal polarity, white = reversed polarity, and cross-hatched = uninterpretable.

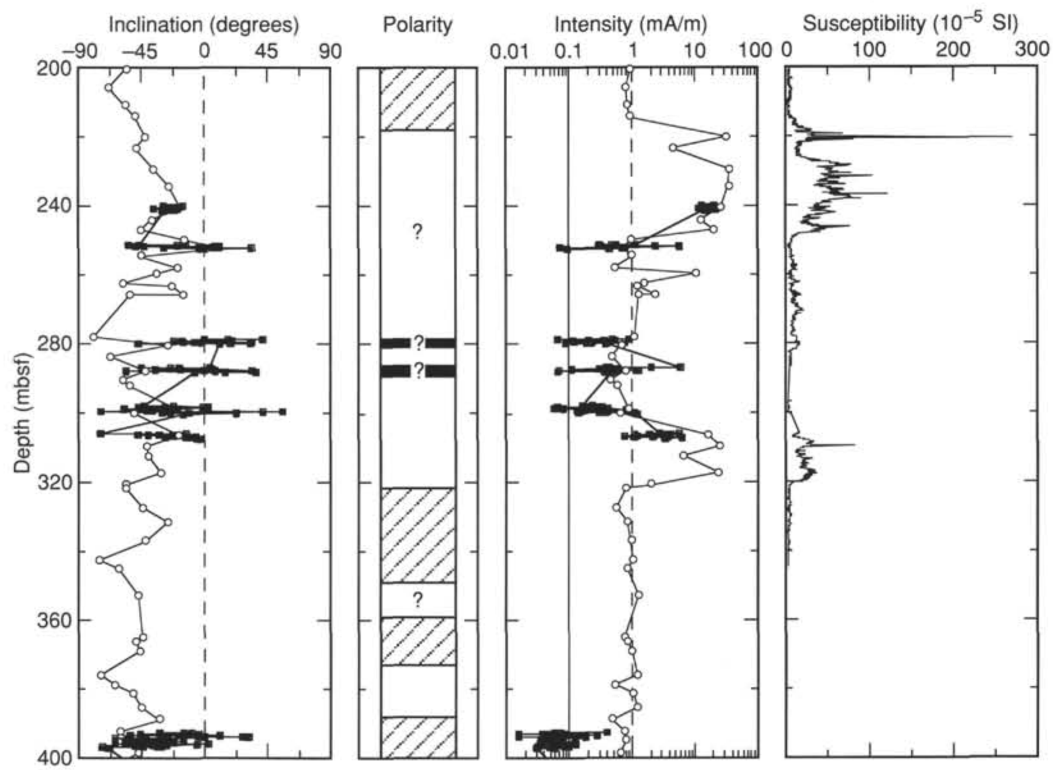

Figure 16. Inclination, magnetic polarity zones, magnetization intensity, and volume susceptibility for the interval from 200 to 400 mbsf in Hole 902D. Intensity cut-off value is 1 mA/m for discrete samples, and 0.1 mA/m for pass-through measurements. Open and closed symbols indicate discrete and pass-through data, respectively. In the polarity column, black = normal polarity, white = reversed polarity, and cross-hatched = uninterpretable.

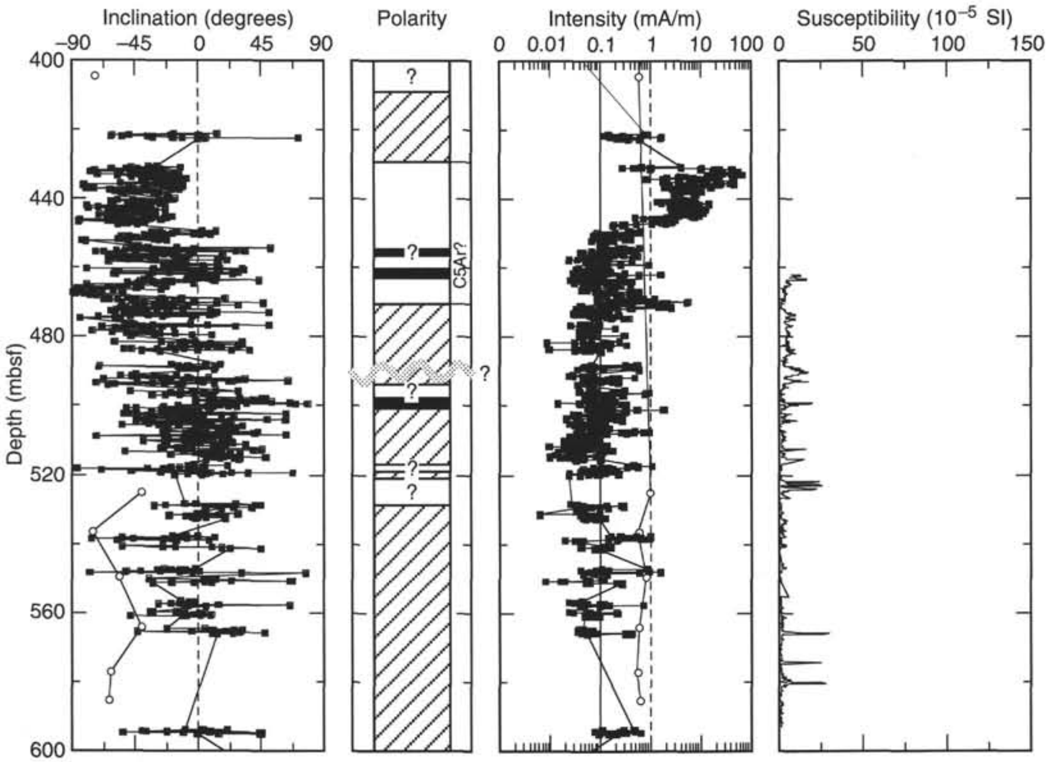

Figure 17. Inclination, magnetic polarity zones, magnetization intensity, and volume susceptibility for the interval from 400 to 600 mbsf in Hole 902D. Intensity cut-off value is 1 mA/m for discrete samples, and 0.1 mA/m for pass-through measurements. Open and closed symbols indicate discrete and pass-through data, respectively. In the polarity column, black = normal polarity, white = reversed polarity, and cross-hatched = uninterpretable.

vals are unstable to AF demagnetization. The median destructive AF field is generally 10 mT, and up to 70% of the magnetization is lost by 10-mT AF demagnetization in the interval from 520 to 590 mbsf. From 590 to 725 mbsf, magnetizations are weak, largely normal with a high degree of scatter (Fig. 18), and again readily demagnetized in fields less than 10 mT.

Based on these observations, it is very difficult to confidently construct a polarity stratigraphy for the bottom half of Hole 902D, and we judge polarity as generally uncertain over much of this stratigraphic interval. However, given the middle middle Miocene age estimate for the sediments (see "Biostratigraphy" section, this chapter) and the general trends of inclination in zones where magnetization intensity is sufficiently strong, we can attempt a correlation to the GPTS (Table 7). The predominantly reversed polarity interval between 429 and 470 mbsf with two short normal polarity zones near the base (Fig. 17) could correlate to Chron C5Ar. Based on the estimated age limits of the Oligocene section at Hole 902D (~26 and ~30.5 Ma, respectively) and suggested location of the boundary between nannofossil Zones NP24/NP25 (see "Biostratigraphy" section, this chapter), it is possible to correlate the interval from 630 to 670 mbsf to late Oligocene polarity chrons. The normal polarity zone between 632 and 653 mbsf and generally reversed zone between 653 and 670 mbsf may correlate to Chrons C8n and C8r, respectively, or, alternatively, to Chrons C9n and C9r (Fig. 18). Unfortunately, at this stage in the study, we lack the age resolution needed to distinguish between these two alternative correlations.

Our interpretations of the demagnetization data and correlations to the GPTS need to be confirmed with shore-based analyses of discrete samples. Our plan is to examine large-volume discrete samples from Hole 902D to increase the remanent magnetization signal for laboratory analyses including thermal demagnetization. In addition, we will conduct detailed rock magnetic studies to help us understand the origin of the different magnetizations we have encountered at Site 902.

SEDIMENTATION RATES

The upper Eocene to Miocene section recovered at Site 902 is discontinuous (see "Biostratigraphy" section, this chapter), and no Pliocene to lower middle Pleistocene strata were recovered. We describe problems with the chronology of Site 902, divide the section into unconformity-bounded (allostratigraphic) units, correlate the Pleistocene section to the SPECMAP time scale (Imbrie et al., 1984), and place upper limits on the sedimentation rates.

For a number of unrelated reasons, it is difficult to derive confidently a temporal interpretation of the Miocene section. First, calcareous microfossils that have been tied to the magnetochronology are absent from most of the upper and middle Miocene sections (between Cores 150-902D-13H and -61X; 123.92–551.25 mbsf). Second, although diatom and dinoflagellate distributions allow a zonal subdivision of the upper and middle Miocene interval, the number of species whose appearance and/or disappearance levels have been tied to the magnetochronology is very restricted. Third, polarity patterns observed may indicate a record dissected by unconformities (see "Paleomagnetism" section, this chapter). Thus, the greatest obstacle in estimating sedimentation rates for the upper Eocene to Miocene at Site 902 may be stratigraphic gaps. Note that in comparing Pleistocene sedimentation rates to older rates, we have not accounted for the effects of compaction on the older sections.

Six main allostratigraphic units were recognized at Hole 902D based on an integrated biostratigraphy (calcareous nannofossils, diatoms, dinoflagellates, and planktonic foraminifers): upper Eocene, upper lower to upper Oligocene, lower Miocene, middle Miocene, upper Miocene, and middle Pleistocene to Holocene. The contacts between these allostratigraphic units correlate with seismic reflections that can be traced from seismic sequence boundaries beneath the continental shelf (see "Seismic Stratigraphy" section, this chapter). Other seismic sequence boundaries, disconformities, and biostratigraphic

Table 7. Reversal boundary depths, Site 902.

Depth (mbsf)	Polarity	Interpreted polarity zone
150-902C:		
0.0–122.5	N	C1n
122.5–125.0	N	late Miocene chrons
125.0–129.0	R	late Miocene chrons
150-902D:		
0.0–125.0	N	C1n
125.0–130.0	?	No zonation
130.0–143.0	R	C4Ar–C5r composite?
143.0–147.0	?	C4Ar–C5r composite?
147.0–153.0	R	C4Ar–C5r composite?
153.0–161.0	?	C4Ar–C5r composite?
161.0–170.0	R	C4Ar–C5r composite?
170.0–218.0	?	C4Ar–C5r composite?
218.0–278.0	R?	C4Ar–C5r composite?
278.0–281.0	N?	C4Ar–C5r composite?
281.0–286.0	R?	C4Ar–C5r composite?
286.0–289.0	N?	C4Ar–C5r composite?
289.0–322.0	R	C4Ar–C5r composite?
322.0–349.0	?	C4Ar–C5r composite?
349.0–360.0	R?	C4Ar–C5r composite?
360.0–373.0	?	C4Ar–C5r composite?
373.0–388.0	R	C4Ar–C5r composite?
388.0–400.0	?	C4Ar–C5r composite?
400.0–408.0	R?	No zonation
408.0–429.0	?	No zonation
429.0–455.0	R	C5Ar?
455.0–457.0	N?	C5Ar?
457.0–460.0	R	C5Ar?
460.0–463.0	N	C5Ar?
463.0–470.0	R	C5Ar?
470.0–491.0	?	No zonation
491.0–497.0	R?	No zonation
497.0–501.0	N	No zonation
501.0–517.0	?	No zonation
517.0–518.0	R?	No zonation
518.0–521.0	?	No zonation
521.0–528.0	R?	No zonation
528.0–632.0	?	No zonation
632.0–638.0	N	C8n or C9n?
638.0–646.0	?	C8n or C9n?
646.0–649.0	N	C8n or C9n?
649.0–653.0	?	C8n or C9n?
653.0–655.0	R?	C8r or C9r?
655.0–661.0	N?	C8r or C9r?
661.0–670.0	R?	C8r or C9r?
670.0–676.0	?	No zonation
676.0–680.0	N	No zonation
680.0–722.0	?	No zonation
722.0–725.0	N	No zonation
725.0–736.0	?	No zonation

Note: N = normal, R = reversed, and ? = uncertain.

breaks occur in the section. Rigorous placement of most of the reflectors and determination of the age of the breaks require shore-based studies. We provide preliminary integration of the shipboard biostratigraphic, lithostratigraphic, magnetostratigraphic, and seismic stratigraphic data so that future studies can focus on the placement and ages of these breaks.

A precise chronology for the middle to upper Pleistocene sections (<474 ka) at Site 902 can be derived using GRAPE and gravimetric bulk-density measurements, and nannofossil datum levels (e.g., Shackleton and Shipboard Scientific Party, 1992). At Hole 902D, the Holocene–Pleistocene section extends from 0 to 121.1 mbsf (Core 150-902D-1H to Section 150-902D-13H-3, 110 cm); it corresponds to lithologic Unit I (see "Lithostratigraphy" section, this chapter). Nannofossils show that the section from 1 to 115 mbsf at Hole 902C lies between the last appearance datum (LAD) of *P. lacunosa* and the *E. huxleyi* abundance datum. This establishes that the section is younger than 474 ka and older than 80 ka, from oxygen isotope stage 12 to 5.1 (terminology of Imbrie et al., 1984).

GRAPE data provide a means of correlating among holes and to the Pleistocene time scale (e.g., Shackleton and Shipboard Scientific Party, 1992). Like any ordinal correlation tool, GRAPE data cannot be used alone to recognize stratigraphic breaks. Because mass-flow processes are typically common in slope settings, we anticipated many stratigraphic breaks and possible poor biostratigraphic control in the Pleistocene and therefore expected problems in using the GRAPE data to correlate to the time scale. However, the GRAPE data show clear patterns in the Pleistocene section at Hole 902C (Fig. 19), and biostratigraphic control proved to be sufficient for correlation. The high variability in the GRAPE data is a result, in part, of gas expansion effects that introduce low-density artifacts. Gas pycnometer bulk-density analyses (see "Physical Properties" section, this chapter) show similar patterns as GRAPE data without the low-density artifacts, and we use the pycnometer data to correlate to the SPECMAP time scale (Imbrie et al., 1984). Glacial stages yield high densities, whereas interglacials yield low values (Fig. 19); the glacial-interglacial interpretations were confirmed with foraminifer and nannoplankton data (see "Biostratigraphy" section, this chapter). Smear slides and biostratigraphic assemblages derived from core-catcher samples show that interglacial stages contain greater biogenic input and, hence, lower densities. An excellent match exists between the density data and the SPECMAP oxygen isotope time scale back to stage 10; however, unlike glacial stages 6, 8, and 12, stage 10 has only a minor density increase. Our correlations indicate that a hiatus may occur in stage 10. Mean sedimentation rates between stages 5.4 and 12.4 were 29 cm/k.y. (Fig. 20). Identification of the substages of the SPECMAP time scale are tentative (Fig. 19); therefore, we estimated sedimentation rates between the major glacial-interglacial stages: stage 6 = 27 cm/k.y.; stage 7 = 24 cm/k.y.; stage 8 = 51 cm/k.y.; stage 9 = 29 cm/k.y.; stage 10 = 11 cm/k.y. (a minimum estimate because of a possible hiatus), stage 11 = 29 cm/k.y.; and stage 12 = 22 cm/k.y.

An unconformity separates the middle Pleistocene from the upper Miocene. The age of the upper part of the Miocene at Site 902 is uncertain, although it is possible that the reversed magnetozone below the Brunhes Chronozone correlates with Chrons C3Ar or C4r.

As noted above, the chronology of the middle and upper Miocene section is difficult to determine. The middle/upper Miocene boundary is tentatively placed with the tentative base of dinoflagellate Zone G (267.59 mbsf). Dinoflagellates indicate a probable stratigraphic break between Zones F and E (between 449 and 450 mbsf; Samples 150-902D-49X-CC and -50X-1, 93–98 cm). The upper part of dinoflagellate Zone B is not represented, indicating a possible gap between cores 56 and 58 (515.98–536.64 mbsf). Diatom and dinoflagellate data indicate a possible biostratigraphic break within Core 150-902D-54X (see "Biostratigraphy" section, this chapter).

Integration of the magnetostratigraphic and diatom biostratigraphic data may provide clues to the ages of the middle to upper Miocene. The section between 130 and 400 mbsf contains magnetic field polarities predominantly reversed (see "Paleomagnetism" section, this chapter). If we assume that the field is represented, we can make preliminary and speculative correlations to the Geomagnetic Polarity Time Scale (BKV85, CK92).

1. A thick reversed magnetozone between 160 and 280 mbsf may correlate with Chron C4Ar (8.9–8.2 Ma); although this requires extremely high sedimentation rates (>18 cm/k.y.), this is supported by the highest occurrence of *D. hustedtii* at 156 mbsf (LAD within Chron 10 = C4r; Burckle et al., 1982). This also requires that the long normal polarity interval of Chron C5 (10.42–8.92 Ma) is represented by less than 9 m.

2. A thick reversed polarity magnetozone from 280 to 390 mbsf may correlate with Chron C5r; this is supported by the highest occurrence of *D. punctata* var. *hustedtii* (LAD Chron 12 = C5r; Burckle et al., 1982; ~11.5 Ma) at approximately 300 mbsf. This correlation would require high sedimentation rates (>11 cm/k.y.) during Chron C5r (11.55–10.54 Ma).

3. A reversed magnetozone from 429 to 455 mbsf may correlate with Chron C5Ar partim (~12.5–12.1 Ma).

The lower Miocene extends from at least 564.6 to 594.8 mbsf (between Samples 150-902D-61X-CC and -66X-5, 30 cm). No calcareous microfossils occur in the upper levels, but the dinoflagellate stratigraphy indicates that the lower Miocene may extend up to 536.0

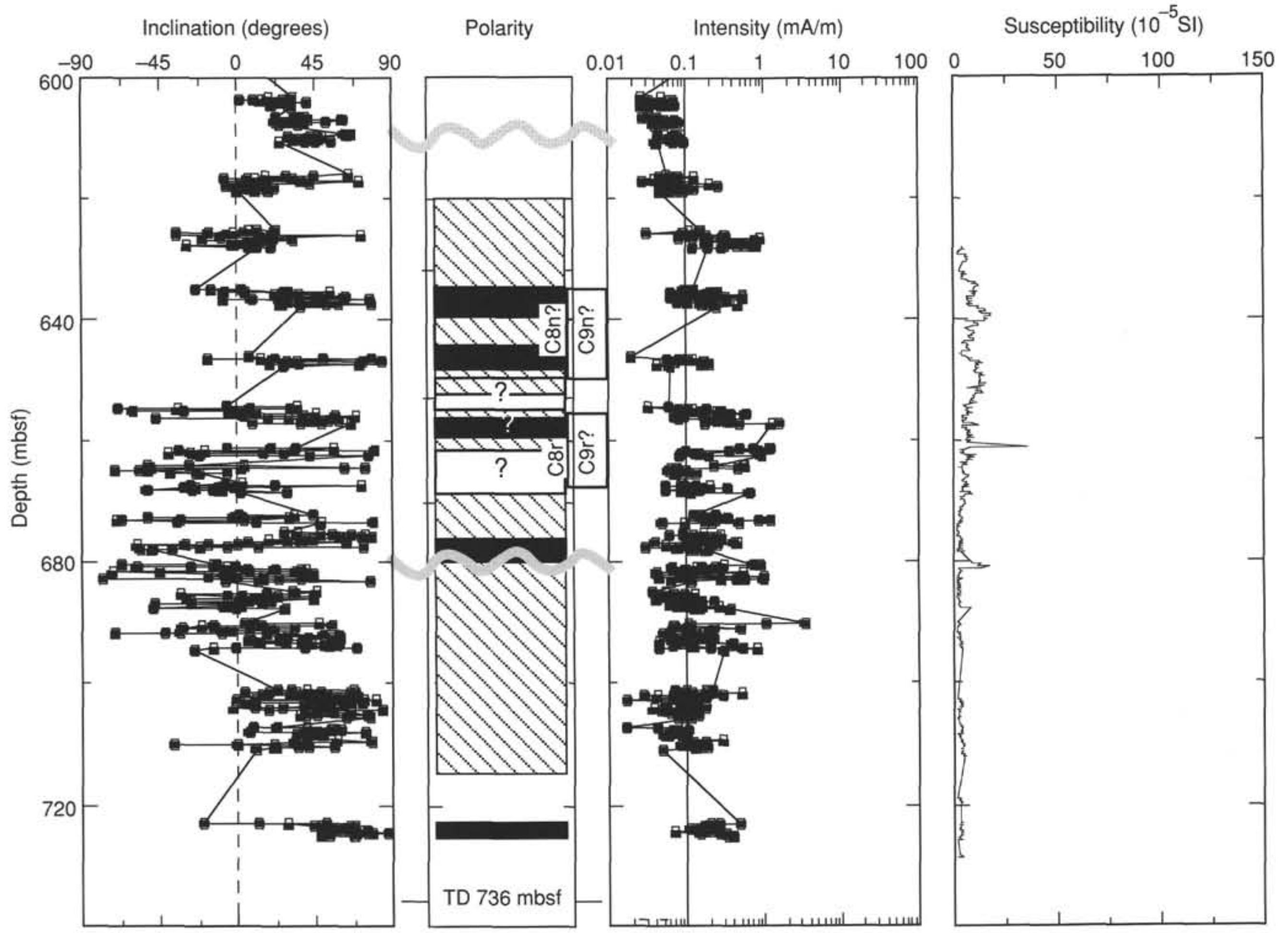

Figure 18. Inclination, magnetic polarity zones, magnetization intensity, and volume susceptibility for the interval from 600 to 725 mbsf in Hole 902D. Intensity cut-off value is 0.1 mA/m for discrete samples. Open and closed symbols indicate discrete and pass-through data, respectively. In the polarity column, black = normal polarity, white = reversed polarity, and cross-hatched = uninterpretable.

mbsf (Core 150-902D-58X). Diatoms place level 545.5 mbsf (Sample 150-902D-59X-CC) in the middle Miocene. It is not possible to determine the sedimentation rates for this unit, which is probably discontinuous (see "Biostratigraphy" section, this chapter). In support of this, a sharp lithologic break occurs at 594.8 mbsf (Sample 150-902D-65X-1, 108 cm; see "Lithostratigraphy" section, this chapter), within Zone NN2. The long Biochron NN2 (>4 m.y.) is represented by only about 30 m of sediment. The resulting substantially lower sedimentation rate than above or below (Fig. 21), may be in fact more apparent than real and may be the effect of a stratigraphic gap.

The upper and uppermost lower Oligocene extends from 613.0 to 680.9 mbsf (Sections 150-902D-66X-CC to -74X-1, 74 cm). An unconformity occurs between 609.6 and 613.0 mbsf (Sections 150-902D-66X-5, 30 cm, and -66X-CC) based on the absence of upper Zone NP25 and possibly Zone NN1. The upper part of Zone NP25 is truncated at Hole 902D, as indicated by the simultaneous highest occurrences of *Sphenolithus ciperoensis, Reticulofenestra bisecta,* and *Zygrhablithus bijugatus* in Sample 150-902D-66X-CC. The youngest Oligocene levels are correlative with Chron C7N or older (>25.6 Ma). The minimum extent of the hiatus at the Oligocene/Miocene boundary is from 25.6 to 23.2 Ma. Based on the estimated ages of 25.6 and 30.2 Ma, respectively, for the first appearance datum (FAD) and LAD of *Sphenolithus ciperoensis* (BKF85), the Oligocene section was deposited at a rate of about 1.1 cm/k.y.; alternatively, assuming that the 69 m of Oligocene sediments were deposited from 25.6 to 30.2 Ma, maximum sedimentation rates were 1.5 cm/k.y.

A sharp lithologic contact separates upper Eocene gray marls and Oligocene silty clays in Core 150-902D-74X, 74 cm (see "Lithostratigraphy" section, this chapter). The upper Eocene extends from total depth (736.40 mbsf; Core 150-902D-82X) to 680.9 mbsf. It corresponds to lithologic Unit VII (see "Lithostratigraphy" section, this chapter). Based on the calcareous nannofossil stratigraphy, it was deposited during the late Eocene (during Biochron NP19–20), at rates greater than 3.6 cm/k.y. This is based on the FAD of *Isthmolithus recurvus* estimated at 38.6 Ma (C.W. Poag and M.-P. Aubry, unpubl. data, 1993) and the LAD of *Discoaster saipanensis,* estimated at 36.8 Ma (BKF85).

ORGANIC GEOCHEMISTRY

Shipboard organic geochemical studies of sediments from Holes 902A, 902C, and 902D included volatile hydrocarbon and nonhydrocarbon gases, Rock-Eval, and elemental analyses. The instrumentation, operating conditions, and procedures are summarized in Chapter 3 (this volume).

Volatile Gases from Sediments

Volatile gases released from the sediments recovered at Site 902 were continuously measured as part of the shipboard safety and pollution monitoring program. Both headspace and vacutainer techniques were employed. Expansion voids at Site 902 were observed between

Table 8. Vacutainer gas composition from sediments at Site 902.

Core, section, interval (cm)	Depth (mbsf)	O_2	N_2	CO_2	H_2S	C_1	$C_{2=}$	C_2	$C_{3=}$	C_3	iC_4	C_4	iC_5	C_5	iC_6	C_6	C_1/C_2	C_1/C_{2+}
150-902C-																		
7H-3, 73–74	48.735	117336	385150	365254	0	364017	0	81	0	0	0	0	0	0	0	0	4494	4494
8H-5, 20–21	56.205	113649	391282	262086	0	357454	0	59	0	0	0	0	0	0	0	0	6059	6059
9H-3, 43–44	62.935	90356	292458	356124	0	490221	0	64	0	0	0	0	0	0	0	0	7660	7660
10H-4, 15–16	73.655	6891	50155	10246	0	821982	0	143	0	0	0	0	0	0	0	0	5748	5748
11H-5, 34–35	84.845	60624	202077	453087	0	666316	0	119	0	0	0	0	0	0	0	0	5599	5599
12H-4, 104–105	93.545	70762	230527	408730	0	567105	25	172	47	158	40	39	41	0	0	0	3297	1086
13H-3, 112–113	101.625	92581	301693	384655	0	555589	0	111	0	0	0	0	0	0	0	0	5005	5005
14H-4, 100–101	111.005	79887	260230	386199	0	545296	0	114	0	0	0	0	0	0	0	0	4783	4783
15H-4, 20–21	119.705	98904	329803	327374	0	457302	18	138	0	112	0	0	0	0	0	0	3314	1706
16H-6, 30–31	128.805	115697	378268	267141	0	370365	0	100	0	0	0	0	0	0	0	0	3704	3704
150-902D-																		
5H-2, 91–92	43.415	8188	43348	20730	0	815855	0	65	0	54	0	0	0	0	0	0	12552	6856
5H-2, 140–141	43.905	7937	42281	21203	0	821270	0	54	0	0	0	0	0	0	0	0	15209	15209
5H-3, 52–53	44.525	8630	48340	17330	0	812659	0	63	0	0	0	0	0	0	0	0	12899	12899
7H-4, 60–61	65.105	6494	16892	14951	0	841624	0	58	0	0	0	0	0	0	0	0	14511	14511
9H-1, 5–6	79.055	0	15861	228493	0	440198	0	70	0	0	0	0	0	0	0	0	6289	6289
10H-3, 4–5	91.545	132309	441047	495331	0	694394	0	116	0	0	0	0	0	0	0	0	5986	5986
11H-5, 18–19	104.185	62195	202077	460113	0	10372	0	69	0	69	0	0	0	0	0	0	150	75
12H-6, 53–54	115.535	37194	113567	274940	0	0	0	98	0	0	0	0	0	0	0	0	100000	0
14H-1, 107–108	132.075	7962	27308	602393	0	818910	0	206	0	0	0	0	0	0	0	0	3975	3975
16H-1, 101–102	136.015	138020	461198	186524	0	244216	0	85	0	0	0	0	0	0	0	0	2873	2873

Note: Volatile gas concentrations given in parts per million (ppm).

43 and 136 mbsf (Table 8), and gas pressures were high enough to push end caps off some of the core liners and to explode some of the vacutainers. The gas was sampled from voids using evacuated vacutainers. Sampled gas was then injected directly onto the Hewlett-Packard 5890a gas chromatograph (HP). The headspace method was routinely conducted on samples from every core. Gas was thermally desorbed from the sediment by placing a plug of sediment in a septum-sealed vial, then heating the sample to 70°C for 30 min, and finally injecting it onto either the Hach Carle gas chromatograph (HC) or the HP (Table 9). Initially, the HC gas chromatograph was not functioning properly at Site 902. This plus the very rapid recovery of cores lead to some headspace samples being stored for several hours in the oven before being injected onto the HP because of the relatively long (30 min) analysis time required for each sample. Samples that have nonhydrocarbon gas results included were run on the HP gas chromatograph. At Site 902, the flame-ionization detector (FID) on the HP did not detect trace levels of methane, even though trace levels of methane are ubiquitous in laboratory air. Consequently, the zero values obtained for methane are considered to be artifacts of data acquisition and should more realistically be regarded as trace levels (1–3 ppm).

Methane concentrations were extremely high at several depths in Site 902. The headspace values range from 0 (trace) to just over 620,000 ppm, whereas vacutainer methane levels are significantly higher and reach slightly more than 820,000 ppm. The discrepancy in the data obtained from these two methods apparently results because the amounts of methane that degassed naturally into expansion voids were greater than the amount of methane liberated by the thermal desorption technique used for headspace gas preparation. Headspace methane may also have been depleted by exposure of the sediment to air when the cores arrived on deck, or by leakage of vial septums during heating in the oven.

Methane-headspace concentrations increase significantly and are highly variable (trace to 40,000 ppm) below 30.5 mbsf in both Holes 902C and 902D. Methanogenesis is generally initiated after sulfate-reducing bacteria are no longer active (Claypool and Kvenvolden, 1983), and sulfate measurements on interstitial water indicate that sulfate disappears relatively rapidly with total depletion at 30 mbsf (see "Inorganic Geochemistry" section, this chapter). A subsurface methane maximum is present in Hole 902D at 380 mbsf. This maximum, together with the variability of concentrations at shallower levels, may have been caused by increased fluxes of organic matter from the continental shelf, which were then degraded in situ. Ethane and higher hydrocarbons (up to C_5), including ethene and propane, were detected in trace amounts in a few samples below 100 mbsf, but they followed no obvious trend with depth. A suite of heavier volatile hydrocarbons (including methane, ethane, propane, butane, ethene, propene, isobutane, and isopentane) occurred in one sample at Hole 902C at 94 mbsf. These heavier hydrocarbons (C_{3+}) may be an artifact of data integration; however, trace amounts of high-molecular-weight hydrocarbons have been found to accompany biogenically generated methane in other marine sediments (Whelan and Sato, 1980). Although C_1/C_2 ratios decrease with depth below 450 mbsf, the C_1/C_2 ratios remained above 1000 and the shapes of the C_2 and C_3 curves are similar (Fig. 22). Relative abundances of these volatile hydrocarbons, together with their trends with depth, are characteristic of biogenically produced gas in marine sediments and have been found previously at many DSDP sites (Whelan and Sato, 1980).

In summary, the high concentrations of methane throughout the sediment relative to high- molecular-weight, volatile hydrocarbons, together with correspondingly high interstitial water alkalinity values (see "Inorganic Geochemistry" section, this chapter), suggest that the methane was produced by bacterial degradation of organic matter in situ rather than generated thermogenically by a deeper source. The exceptionally high concentrations indicate that conditions for methanogenic bacteria were optimal, probably owing to high sedimentation rates and an abundant supply of fresh, terrestrially derived organic matter.

Elemental Analysis

Elemental analysis, inorganic carbon (IC), and total organic carbon (TOC) measurements were performed on 90 samples from Site 902 taken at a frequency of one per core (Table 10). The inorganic carbon concentrations were measured by coulometry, which determines the total amount of carbon (liberated as CO_2) from about 20 mg of sediment after treatment with 2M HCl. Most of this carbon probably exists as calcite within the sediment. $CaCO_3$ values were calculated as percentages of inorganic carbon by

$$CaCO_3 = IC\ (\%) \times 8.34.$$

Total carbon was measured using the Carlo Erba 1500 Elemental Analyzer, and TOC values were then calculated by the difference between total carbon and inorganic carbon.

Inorganic-carbon concentrations show four distinct trends at Site 902 (Fig. 9). The uppermost interval of Pleistocene siliciclastic sediments from 0 to 100 mbsf contains carbonate concentrations of 0.3%

Table 9. Headspace gas composition from sediments at Site 902.

Core, section, interval (cm)	Depth (mbsf)	C_1	$C_{2=}$	C_2	$C_{3=}$	C_3	iC_4	nC_4	iC_5	nC_5	iC_6	nC_6	CO_2	O_2	N_2	C_1/C_2	C_1/C_{2+}
150-902A-																	
3H-4, 0–5	17.03	229	0	0	0	0	0	0	0	0	0	0	32965	165085	60793		
4H-4, 0–5	26.50	0	0	0	0	0	0	0	0	0	0	0	45472	156480	606610		
150-902C-																	
1H-3, 0–5	3.03	0	0	0	0	0	0	0	0	0	0	0	15273	168854	618649		
2H-4, 0–5	10.03	0	0	0	0	0	0	0	0	0	0	0	19805	165388	619773		
3H-4, 0–5	19.53	0	0	0	0	0	0	0	0	0	0	0	30432	154266	6263662		
4H-5, 0–5	30.53	39984	0	44	0	0	0	0	0	0	0	0	74948	145303	574744	909	909
5H-3, 0–5	37.03	14646	0	71	0	0	0	0	0	0	0	0	83357	79166	347813	206	206
9H-4, 0–5	64.53	10130	2	1	0	1	0	0	0	0	0	0				10130	2533
10H-4, 0–5	73.53	17547	2	1	0	1	0	0	0	0	0	0				17547	4387
11H-5, 0–5	83.03	0	0	0	0	0	0	0	0	0	0	0					
12H-4, 0–5	92.53	3189	0	58	0	0	0	0	0	0	0	0				55	55
13H-4, 0–5	102.00	40363	2	2	0	2	0	0	0	0	0	0				20182	6727
14H-4, 0–5	110.53	9465	1	1	0	0	0	0	0	0	0	0				9465	4733
15H-4, 0–5	119.53	166	1	0	0	0	0	0	0	0	0	0					166
16H-4, 0–5	125.53	43854	2	3	0	3	0	0	0	0	0	0				14618	5482
150-902D-																	
1H-2, 0–5	1.53	65	0	0	0	0	0	0	0	0	0	0	9327	173835	620879		
2H-4, 0–5	17.03	0	0	0	0	0	0	0	0	0	0	0	97007	10081	481844		
3H-2, 0–5	23.53	0	0	0	0	0	0	0	0	0	0	0					
4H-4, 0–5	36.03	0	0	0	0	0	0	0	0	0	0	0					
5H-4, 0–5	45.53	5	1	0	0	0	0	0	0	0	0	0					5
6H-4, 0–5	55.03	4205	1	0	0	0	0	0	0	0	0	0					4205
7H-4, 0–5	64.53	9196	1	0	0	1	0	0	0	0	0	0					4598
8H-5, 0–5	75.53	9975	2	0	0	1	0	0	0	0	0	0					3325
9H-4, 0–5	83.53	2	0	0	0	0	0	0	0	0	0	0					
10H-4, 0–5	93.03	14	0	0	0	0	0	0	0	0	0	0					
11H-4, 0–5	102.53	44287	2	2	0	1	0	0	0	0	0	0				22144	8857
12H-5, 0–5	113.53	7559	1	1	0	0	0	0	0	0	0	0				7559	3780
13H-4, 0–5	131.03	3	0	0	0	0	0	0	0	0	0	0					
14H-2, 0–5	128.00	43	1	0	0	1	0	0	0	0	0	0					22
16H-2, 0–5	135.53	8148	0	0	0	0	0	0	0	0	0	0	101876	43636	572778		
17H-3, 0–5	142.23	192932	5	10	0	8	0	0	0	0	0	0				19293	8388
18X-3, 0–5	148.00	428640	7	23	0	12	0	0	0	0	0	0				18637	10206
19X-2, 0–5	153.31	3244	0	0	0	0	0	0	0	0	0	0	33771	157480	617978		
20X-4, 0–5	166.00	18079	0	0	0	0	0	0	0	0	0	0	87435	126059	595771		
21X-4, 0–5	174.53	43152	0	71	0	0	0	0	0	0	0	0	147891	73344	579456	608	608
22X-4, 0–5	184.80	120743	3	14	0	5	0	0	0	0	0	0				8625	5488
23X-4, 0–5	194.70	94610	3	13	0	4	0	0	0	0	0	0				7278	4731
24X-4, 0–5	204.30	40452	7	2	0	3	0	0	0	0	0	0				20226	3371
25X-5, 0–5	215.40	9840	3	5	0	2	0	0	0	0	0	0				1968	984
26X-4, 0–5	223.60	18234	0	0	0	0	0	0	0	0	0	0	45746	161776	593117		
27X-4, 0–5	233.30	18234	0	0	0	0	0	0	0	0	0	0	84061	143532	595950		
28X-4, 0–5	242.90	52086	2	7	0	2	0	0	0	0	0	0				7441	4735
29X-4, 0–5	252.60	79024	3	13	0	3	0	0	0	0	0	0				6079	4159
30X-4, 0–5	262.20	22757	0	55	0	0	0	0	0	0	0	0	82287	127231	595473	414	414
31X-4, 0–5	271.80	140520	2	12	0	2	0	0	0	0	0	0				11710	8783
32X-4, 0–5	281.50	27392	0	58	0	0	0	0	0	0	0	0	91180	116778	474010	472	472
33X-4, 0–5	291.10	8443	0	0	0	0	0	0	0	0	0	0	78093	122807	504400		
34X-2, 0–5	297.80	17837	1	3	0	0	0	0	0	0	0	0				5126	4459
35X-4, 0–5	310.40	11990	0	0	0	0	0	0	0	0	0	0	56144	156879	597988		
36X-5, 0–5	321.50	10972	0	0	0	0	0	0	0	0	0	0	66826	143114	604951		
37X-4, 0–5	329.60	63143	1	6	0	1	0	0	0	0	0	0				10524	7893
38X-4, 0–5	339.30	78380	1	5	0	1	0	0	0	0	0	0				15676	11197
39X-5, 0–5	350.40	48121	1	5	0	0	0	0	0	0	0	0				9624	8020
40X-4, 0–5	358.50	28976	0	4	0	0	0	0	0	0	0	0				7244	7244
41X-4, 0–5	368.10	74814	0	7	0	0	0	0	0	0	0	0				10986	10688
42X-4, 0–5	377.80	71250	1	8	0	0	0	0	0	0	0	0				8906	7917
43X-4, 0–5	387.40	223006	1	8	0	1	0	0	0	0	0	0				27876	22301
44X-4, 0–5	397.10	78336	1	6	0	1	0	0	0	0	0	0				13056	9792
45X-2, 0–5	403.70	620011	2	14	0	2	0	0	0	0	0	0				44287	34445
46X-4, 0–5	416.40	12	0	0	0	0	0	0	0	0	0	0					
47X-5, 0–5	427.20	210831	2	5	0	1	0	0	0	0	0	0				42166	26354
48X-4, 0–5	435.10	5871	0	1	0	0	0	0	0	0	0	0				5871	5871
49X-4, 0–5	444.50	28837	0	4	0	0	0	0	0	0	0	0				7209	7209
50X-4, 0–5	453.80	51878	1	5	0	0	0	0	0	0	0	0				10376	8646
51X-4, 0–5	463.40	36607	1	8	0	2	0	0	0	0	0	0				4576	3328
52X-4, 0–5	473.10	9211	3	5	0	2	0	0	0	0	0	0				1842	921
53X-4, 0–5	482.70	70957	0	9	0	1	0	0	0	0	0	0				7884	7096
54X-4, 0–5	492.40	62850	0	10	0	1	0	0	0	0	0	0				6285	5714
55X-4, 0–5	502.10	59370	1	12	0	2	0	0	0	0	0	0				4948	3958
56X-5, 0–5	513.20	74910	1	16	0	2	0	0	0	0	0	0				4682	3943
57X-5, 0–5	523.00	63228	0	9	0	1	0	0	0	0	0	0				7025	6323
58X-5, 0–5	532.70	90532	1	30	0	2	0	0	0	0	0	0				3018	2743
59X-2, 0–5	537.50	93875	0	15	0	1	0	0	0	0	0	0				6258	5867
60X-3, 0–5	548.50	7531	0	3	0	0	0	0	0	0	0	0				2510	2510
61X-2, 0–5	556.50	110058	0	39	0	2	0	0	0	0	0	0				2822	2684
62X-4, 0–5	569.10	85960	0	18	0	1	0	0	0	0	0	0				4776	4524
63X-4, 0–5	578.90	44237	0	9	0	1	0	0	0	0	0	0				4915	4424
64X-4, 0–5	588.50	40482	0	8	0	1	0	0	0	0	0	0				5060	4498
65X-1, 0–5	595.15	97891	1	30	0	4	0	0	0	0	0	0				3263	2797
66X-4, 0–5	607.80	76	0	1	0	0	0	0	0	0	0	0				76	76
67X-4, 0–5	617.50	63276	0	14	0	1	0	0	0	0	0	0				4520	4218
68X-4, 0–5	626.70	21295	1	13	0	2	0	0	0	0	0	0				1638	1331
69X-4, 0–5	636.40	9325	1	16	0	3	0	0	0	0	0	0				583	466
70X-5, 0–5	647.60	47931	1	17	0	2	0	0	0	0	0	0				2819	2397
71X-4, 0–5	655.70	55614	0	13	0	1	0	0	0	0	0	0				4278	3972
72X-4, 0–5	665.40	97808	0	40	0	2	0	0	0	0	0	0				2445	2329
73X-2, 0–5	673.45	91168	1	71	0	4	0	0	0	0	0	0				1284	1200
74X-4, 0–5	684.70	63300	0	16	0	1	0	0	0	0	0	0				3956	3724
75X-3, 0–5	692.90	117307	1	47	0	3	0	0	0	0	0	0				2496	2300
76X-5, 0–5	705.50	151563	1	66	0	3	0	0	0	0	0	0				2296	2165
77X-2, 0–5	710.70	48248	1	18	0	2	0	0	0	0	0	0				2680	2298
78X-1, 0–5	718.00	55346	1	19	0	1.4	0	0	0	0	0	0				2913	2586

Note: Volatile gas concentrations given in parts per million (ppm).

Table 10. Inorganic carbon, organic carbon, and elemental analysis data from sediments at Site 902.

Core, section, interval (cm)	Depth (mbsf)	Total carbon (wt%)	Inorganic carbon (wt%)	Total organic carbon (wt%)	$CaCO_3$ (wt%)	Nitrogen (wt%)	Sulfur (wt%)	C/N
150-902C-								
1H-1, 27–30	0.29	2.88	1.34	1.54	11.16	0.18	0.60	9
2H-3, 69–71	18.70	0.77	0.38	0.39	3.17	0.04	0.68	9
3H-3, 47–49	28.45	2.17	1.67	0.50	13.91	0.06	0.11	8
4H-3, 38–41	37.50	1.73	3.88	0.00	32.32	0.07	0.37	0
5H-3, 85–87	46.86	5.41	3.55	1.86	29.57	0.19	0.65	10
7H-1, 98–100	52.99	1.99	1.67	0.32	13.91	0.06	0.18	5
8H-3, 46–48	58.47	1.34	1.07	0.27	8.91	0.05	0.15	6
9H-3, 109–111	64.10	1.83	1.04	0.79	8.66	0.27	0.11	3
10H-6, 111–113	77.62	1.84	0.77	1.07	6.41	0.14	0.69	7
11H-4, 108–110	84.59	4.78	3.85	0.93	32.07	0.11	0.57	9
12H-5, 47–49	94.48	1.73	0.97	0.76	8.08	0.01	1.15	76
13H-1, 70–72	98.71	1.95	1.42	0.53	11.83	0.09	1.45	6
14H-1, 58–62	106.60	1.05	0.40	0.65	3.33	0.05	0.12	14
15H-3, 47–49	118.50	0.84	0.66	0.18	5.50	0.04	0.09	5
16H-3, 44–46	124.50	2.12	0.04	2.08	0.33	0.15	2.03	14
150-902D-								
1H-1, 30–32	0.30	0.77	0.33	0.44	2.70	0.03	0.18	15
2H-3, 45–48	15.95	2.17	1.78	0.39	14.80	0.06	0.16	7
3H-7, 24–26	31.24	1.92	1.26	0.66	10.50	0.07	0.58	9
4H-4, 121–124	37.26	6.01	3.67	2.34	30.60	0.22	0.72	11
9H-1, 31–33	79.31	2.14	0.83	1.31	6.90	0.16	0.68	8
15H-3, 46–48	134.20	2.09	0.21	1.88	1.70	0.16	2.07	12
16H-3, 36–38	137.40	2.27	0.06	2.21	0.50	0.17	2.19	13
17H-3, 36–38	142.60	2.86	0.05	2.81	0.40	0.19	2.19	15
18X-3, 79–81	148.80	1.69	0.02	1.67	0.20	0.14	1.81	12
19X-3, 62–64	155.40	2.42	0.01	2.41	0.10	1.31	1.68	2
20X-4, 99–101	167.00	1.86	0.39	1.47	3.20	0.16	1.22	9
22X-1, 39–41	180.70	2.43	0.19	2.24	1.60	0.17	1.69	13
21X-CC, 27–29	180.80	2.71	0.25	2.46	2.10	0.19	1.76	13
23X-1, 26–28	190.50	1.92	0.40	1.52	3.30	0.15	0.36	10
24X-1, 110–112	200.90	1.67	0.03	1.64	0.20	0.11	1.52	15
25X-1, 125–128	210.70	3.04	0.06	2.98	0.50	0.20	2.67	15
27X-2, 90–93	231.20	0.87	0.19	0.68	1.60	0.09	0.13	8
28X-4, 99–101	243.90	1.45	0.71	0.74	5.90	0.11	0.18	7
29X-4, 79–81	253.40	2.67	0.25	2.42	2.10	0.18	1.58	13
29X-5, 7–9	254.20	5.71	0.35	5.36	2.90	0.27	5.65	20
30X-6, 123–125	266.40	0.89	0.28	0.61	2.30	0.11	1.56	6
31X-3, 133–135	271.60	1.21	0.74	0.47	6.20	0.84	0.18	1
32X-2, 74–76	279.20	1.94	0.18	1.76	1.50	0.13	2.04	14
33X-2, 53–55	288.60	1.98	0.10	1.88	0.80	0.14	2.02	13
34X-3, 43–45	299.70	0.94	0.21	0.73	1.70	0.11	3.15	7
35X-3, 80–82	309.70	1.18	0.44	0.74	3.70	0.12	0.18	6
36X-4, 60–62	320.60	2.87	0.39	2.48	3.20	0.19	1.03	13
37X-3, 20–22	328.30	2.77	0.35	2.42	2.90	0.22	3.07	11
38X-2, 31–32	336.60	2.26	0.27	1.99	2.20	0.17	1.99	12
39X-4, 42–44	349.30	1.8	—	0.00	0.00	0.15	2.19	0
40X-3, 106–107	358.10	2.51	0.41	2.10	3.40	0.17	1.30	12
41X-2, 102–104	366.10	2.53	0.36	2.17	3.00	0.16	1.60	14
42X-2, 74–76	375.50	1.91	0.42	1.49	3.50	0.16	1.46	9
43X-4, 52–54	387.90	2.42	0.35	2.07	2.90	0.19	2.03	11
44X-4, 52–54	397.60	1.44	0.22	1.22	1.80	0.13	2.41	9
45X-2, 77–79	404.50	1.79	0.36	1.43	3.00	0.15	0.54	10
46X-3, 80–81	415.70	1.96	0.51	1.45	4.20	0.12	0.37	12
47X-2, 56–58	423.30	1.89	0.45	1.44	3.70	0.16	1.00	9
48X-2, 59–61	432.70	1.24	0.19	1.05	1.60	0.05	0.60	21
49X-1, 74–77	440.70	1.62	0.91	0.71	7.60	0.14	3.37	5
50X-3, 54–56	452.80	1.96	0.36	1.60	3.00	0.17	4.47	9
51X-6, 103–104	467.40	2.44	0.00	2.44	0.00	0.18	1.81	14
52X-3, 57–59	472.20	3.25	0.25	3.00	2.10	0.23	2.28	13
52X-6, 56–58	476.70	2.8	0.06	2.74	0.50	0.19	2.40	14
53X-3, 25–27	481.50	2.64	0.14	2.50	1.20	0.18	1.79	14
54X-6, 56–59	496.00	3.28	0.04	3.24	0.30	0.18	1.40	18
55X-3, 77–79	501.40	3.01	0.06	2.95	0.50	0.18	1.52	16
56X-6, 70–72	515.40	1.75	0.04	1.71	0.30	0.13	2.02	13
57X-3, 60–62	520.60	3.09	0.09	3.00	0.70	0.16	1.45	19
58X-3, 72–74	530.40	3.97	0.07	3.90	0.60	0.22	1.99	18
59X-3, 49–51	539.50	3.59	0.18	3.41	1.50	0.19	2.10	18
60X-3, 82–84	549.30	3.06	0.06	3.00	0.50	0.18	2.26	17
61X-3, 31–32	558.30	3.21	0.01	3.20	0.10	0.16	1.75	20
62X-3, 76–78	568.40	3.99	1.20	2.79	10.00	0.18	1.84	16
63X-3, 80–81	578.20	3.84	1.82	2.02	15.20	0.12	1.67	17
64X-1, 137–139	585.40	3.92	1.01	2.91	8.40	0.18	1.78	16
65X-2, 69–71	595.90	6.28	4.73	1.55	39.40	0.12	0.13	13
66X-3, 56–58	606.90	5.05	2.95	2.10	24.60	0.15	1.05	14
67X-3, 74–75	616.70	4.42	2.86	1.56	23.80	0.12	0.97	13
68X-4, 39–40	627.10	3.46	1.75	1.71	14.60	0.13	0.86	13
69X-4, 56–57	637.00	3.98	2.36	1.62	19.70	0.12	0.96	14
70X-5, 28–30	647.90	2.96	1.05	1.91	8.70	0.11	1.01	17
71X-3, 58–60	654.80	3.95	2.96	1.99	16.30	0.13	1.04	15
72X-5, 24–26	667.10	4.04	1.85	2.19	15.40	0.13	1.05	17
73X-3, 107–108	674.60	5.47	2.57	2.90	21.40	0.17	1.07	17
74X-3, 85–86	684.10	6.55	6.01	0.54	50.10	0.05	0.05	11
75X-1, 71–73	690.60	5.86	5.56	0.30	46.30	0.04	0.00	8
76X-3, 54–56	703.00	5.77	5.08	0.69	42.30	0.06	0.01	12
77X-2, 70–72	711.40	5.53	5.03	0.50	41.90	0.06	0.38	8
78X-1, 17–19	719.00	5.62	5.14	0.48	42.80	0.53	0.36	1
79X-3, 39–41	725.70	4.37	3.83	0.54	31.90	0.07	0.85	8
80X-CC, 16–18	728.90	4.57	3.73	0.84	31.10	0.07	0.52	12
81X-CC, 5–7	733.50	4.44	3.85	0.59	32.10	0.06	0.46	10
82X-CC, 21–23	736.30	7.81	7.53	0.28	62.70	0.03	0.19	9

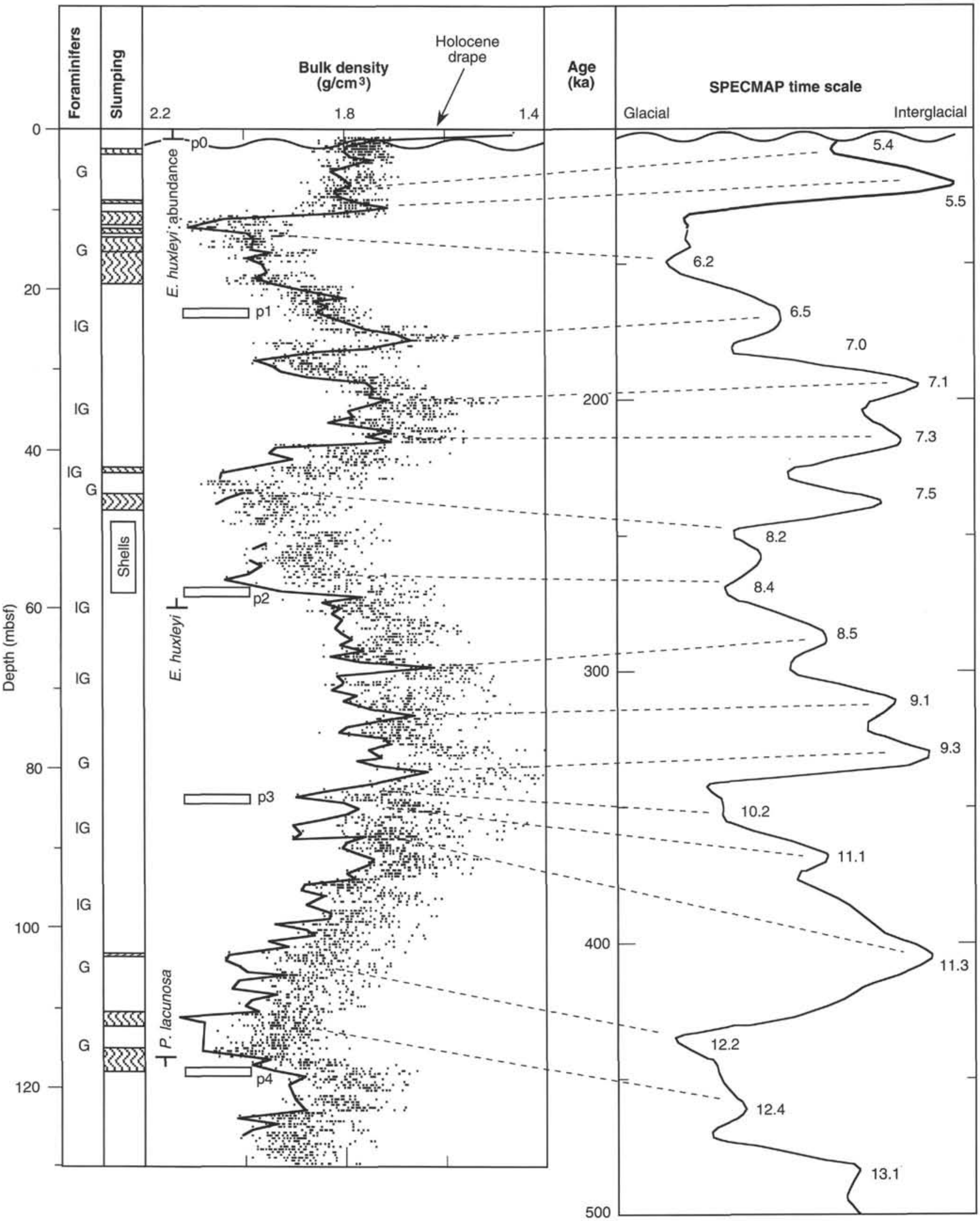

Figure 19. Correlations in Hole 902C between foraminiferal assemblages (G = glacial, IG = interglacial), GRAPE (points) and pycnometer (solid line) bulk density data, and the SPECMAP time scale (from Imbrie et al., 1984). Oxygen isotopic substages are noted along the latter. The density scale has been inverted to match trends in the SPECMAP curve.

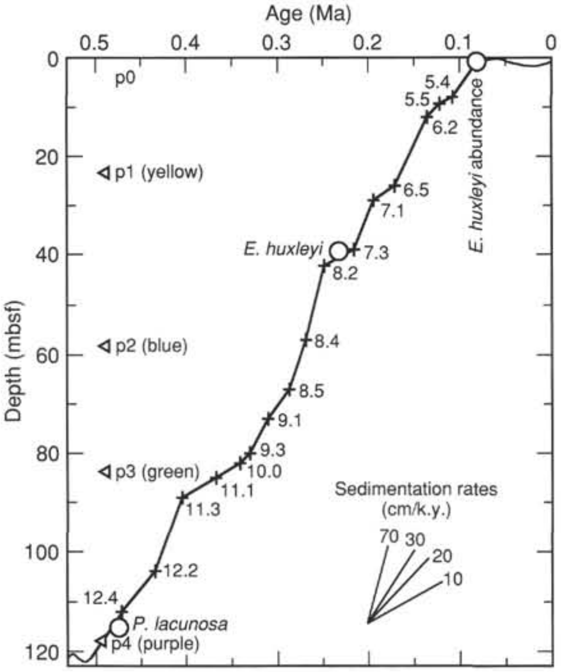

Figure 20. Age-depth diagram for the Pleistocene of Hole 902C based on the oxygen isotope substage correlations established using density data (Fig. 19). p0 through p4 correlate to seismic reflectors.

to 3.9% (2.7% and 32.3% $CaCO_3$). The interval of predominantly Miocene strata between 100 and 555 mbsf has carbonate concentrations that range from 0% to 0.7% (0%–6.2% $CaCO_3$). In the interval from 555 to 680 mbsf, carbonate values vary from 1.01% to 4.73% (8.4%–39% $CaCO_3$), and in the deepest interval from 680 to 736 mbsf carbonate increases dramatically (6.0%–7.5%; 50.1%–62.7% $CaCO_3$).

The very low $CaCO_3$ values in the Miocene sediments generally coincide with an absence of calcareous fossils (see "Biostratigraphy" section, this chapter), a decrease in pH values (possibly associated with the remineralization of organic matter; see "Inorganic Geochemistry" section, this chapter) and high TOC and methane concentrations. These observations suggest that carbonate has been removed by dissolution during diagenesis. The carbonate-enriched sediments at the base of Hole 902D reflect the penetration of Eocene chalks (see "Lithostratigraphy" section, this chapter).

Organic-carbon concentrations vary from 0.1% to 3.9% (Table 10) and average 1.6%; these concentrations are more than three times higher than the content usually observed in siliciclastic, open-marine environments (McIver, 1975). Two principal types of organic matter are delivered to ocean sediments: (1) algal organic material derived from marine organisms is relatively labile and tends to be poorly preserved in the marine environment, whereas (2) terrestrial organic matter tends to contain more complex, polymeric compounds (e.g., cellulose), has a refractory nature and is less prone to degradation. The character of the organic matter (see below) and the nature of the depositional setting suggest that the elevated TOC values at Site 902 are produced by a combination of abundant, terrestrially derived material, high sedimentation rates caused by mass-flow events, and periods of high marine productivity. Woody fragments were observed in sediments at Hole 902D throughout lithologic Unit IV (152–404 mbsf; see "Lithostratigraphy" section, this chapter). Because of their resilient molecular makeup and rapid accumulation rates, these materials survived the transport from their point of origin. However, the highest TOC values at Site 902 were found between 467 and 585 mbsf and are all greater than 1.5%. The sediments and fossil organisms within this interval are predominantly marine in character, and diatoms are particularly abundant (see "Lithostratigraphy" and "Biostratigraphy" sections, this chapter). Marginally higher hydrogen indexes shown by the Rock-Eval data (see below and Fig. 23) also indicate a change to a more marine-influenced environment in the lower Miocene. The integration of data collected from sediment in the lower Miocene interval at Site 902, together with similar findings in lower Miocene sediment at the COST B-3 well (Poag, 1980), suggest that the highest TOC values may have resulted from the upwelling of nutrient-laden bottom water along the shelf edge.

Organic Matter Characterization

Organic matter was characterized at Site 902 by Rock-Eval and organic C/N ratios. Rock-Eval data were obtained from 15 samples from Hole 902D (Table 11). The two Rock-Eval parameters used to determine the source of the organic matter are the hydrogen index (mg HC/g TOC) and the oxygen index (mg CO_2/g TOC). The hydrogen index (HI) is the quantity of hydrocarbons generated by pyrolysis of the organic matter (S_2), and the oxygen index (OI) is the quantity of CO_2 that is generated (S_3). Typically, terrestrially derived organic matter has high OI and low HI, whereas the reverse is generally true for marine algal remains (Espitalié et al., 1977). On the van Krevelen-type diagram (Fig. 23), most of the samples plot in the field of immature marine organic matter. Although this type of diagram was actually designed to establish the origin of mature kerogens (Tissot and Welte, 1984), parameters calculated by Rock-Eval are useful for the characterization of immature, lipid-rich sedimentary organic matter (Shipboard Scientific Party, 1989). The sample from 433 mbsf in Hole 902D (Table 11) has an extremely high oxygen index and may have contained organic matter low in hydrogen components (e.g., woody fragments). The C/N ratio of this sample is relatively high and corroborates this hypothesis (Table 10). However, for sediments containing less than 0.5% TOC, these Rock-Eval parameters should be viewed with caution. Pyrolysis products may adhere to clay minerals and produce anomalously low HI values; thus, indices may be miscalculated because of large errors in the Rock-Eval TOC values (see Chapter 3, this volume). The HI values are commonly greater than 300 in the lower Miocene, possibly reflecting an increased marine algal influence. These data corroborate the observation of increased amorphous algal organic matter in kerogen isolations (see "Biostratigraphy" section, this chapter) from sediments of this period. All T_{max} values are less than 435°C and thus indicate the immaturity of the sediment organic matter at all depths. In addition, the petroleum index (the ratio of the S_1 to the S_2 peak; see "Organic Geochemistry" section, Chapter 3, this volume) is between 0.1 and 0.2, indicating that thermal evolution of organic matter has occurred. The majority of the samples have total hydrocarbon values (S_1 + S_2) of greater than 3500 ppm, indicating that these sediments would have moderate-to-good source-rock potential if buried to sufficient depth (Espitalié et al., 1977).

Algal organic matter generally has C/N ratios between 5 and 10, whereas values for terrestrially derived organic matter vary between 20 and 100 (Emerson and Hedges, 1988). The C/N values at Hole 902D (Table 10 and Fig. 9) commonly fall between these discrete limits, indicating a mixture of marine and terrestrially derived organic matter. The variability of Pleistocene values suggests that some samples contain predominantly algal, marine organic matter whereas others are dominantly terrestrial material. Very low values (<5) occur where TOC is particularly low, which causes the nitrogen in ammonium, associated with clay mineral lattices, to interfere with the organic signature. These samples cannot be used to indicate the source of the organic matter. Even in the lower Miocene, where more pelagic facies are present, C/N values are commonly 15. This is probably an artifact of organic matter diagenesis in which nitrogen is preferentially remineralized over carbon because of its association with more labile compounds such as proteins.

Bitumen was extracted from four samples using organic solvents (see Chapter 3, this volume) to investigate the molecular nature of the

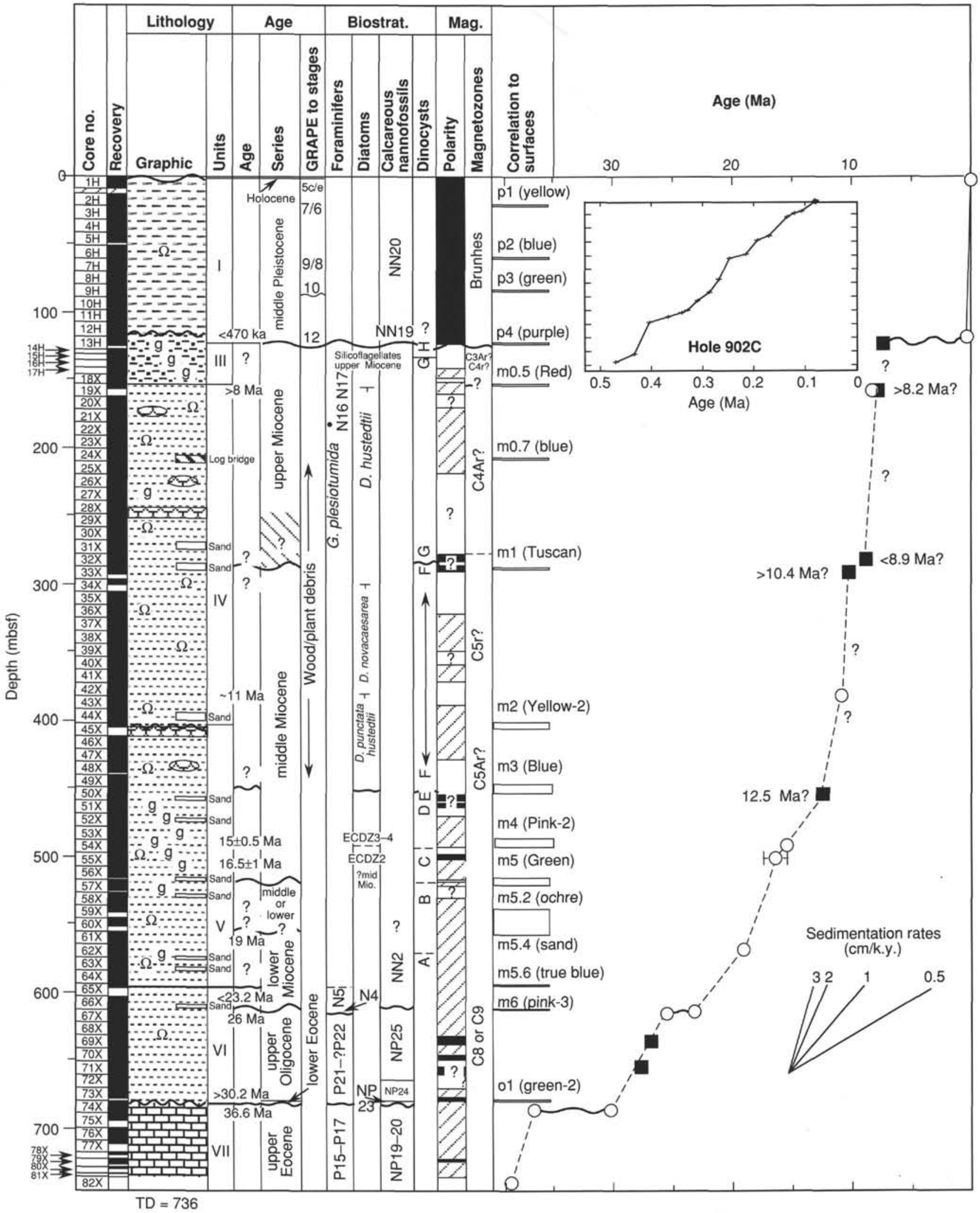

Figure 21. Age-depth diagram for Hole 902D showing lithostratigraphic units, age interpretations (including the correlations of GRAPE data to oxygen isotope stages derived from Hole 902C), biostratigraphy, magnetostratigraphy (black = normal polarities, white = reversed, and cross-hatched = uncertain), and seismic reflectors. Inset shows age-depth diagram for the Pleistocene of Hole 902C (Fig. 20). Wavy lines indicate hiatuses and/or unconformities noted in the borehole. TD = total depth.

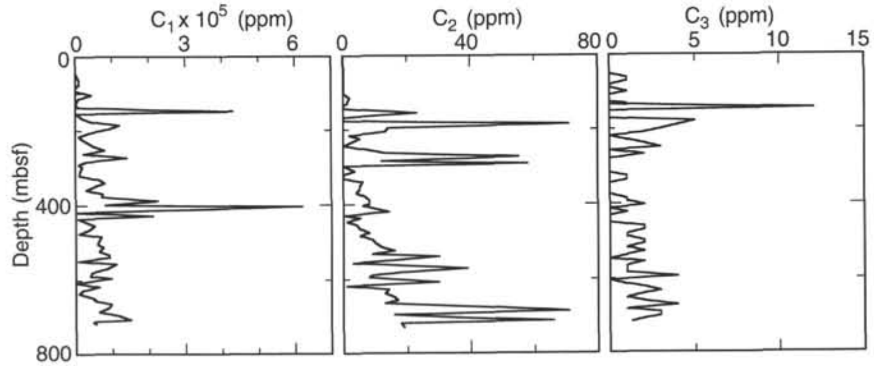

Figure 22. Headspace volatile hydrocarbon composition vs. depth for sediment samples from Hole 902D.

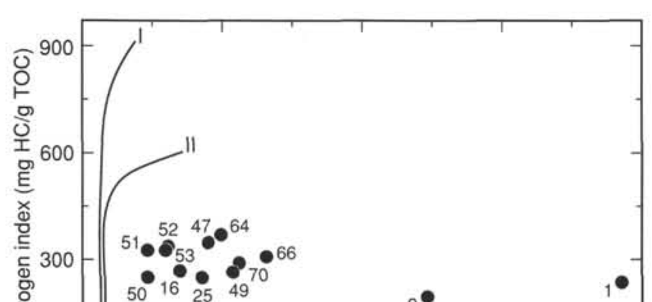

Figure 23. Van Krevelen-type diagram of sediment samples from Hole 902D. Black dots identify samples; adjacent number identifiers are the core from which the sample was derived. All samples plot in the section for immature marine organic matter; however, samples at shallow levels (1 and 9) are enriched in relatively labile oxygen-rich functional groups.

organic matter. Lipid studies from various Miocene sediments at Hole 902D (Fig. 24) complement sedimentological (see "Lithostratigraphy" section, this chapter) and faunal (see "Biostratigraphy" section, this chapter) observations. All three studies show that the lower Miocene had more marine-influenced facies than the rest of the section; studies of the lipids also indicate that some terrestrial contribution continued throughout this same period. *N*-alkanes have shorter chain lengths (n-C_{15} through n-C_{23}) and are usually associated with a marine algal origin; in contrast, those with 25–35 carbon atoms are derived from continental organic matter. The lipid fractions analyzed at Site 902 from Samples 150-902D-43X-4, 52–54 cm, and -49X-1, 54–56 cm, contain (1) a homologous series of n-alkanes from n-C_{17} through n-C_{31}, (2) long-chain n-alkanes with an odd-over-even carbon-number predominance from n-C_{25} to n-C_{31}, and (3) a carbon maximum at n-C_{29} (Fig. 24). In contrast, Sample 150-902D-58X-3, 72–74 cm, appears to have a larger component of short-chain-length n-alkanes, indicating more marine-influenced organic matter (Fig. 24). The marked odd-over-even n-alkane carbon-number predominance is a trend observed in many Holocene detrital sediments that receive an important contribution from continental runoff (Bray and Evans, 1961) because high-molecular-weight, odd-numbered carbon n-alkanes are present in the cuticular material of continental plants. The terrestrial organic-matter contribution usually controls the n-alkane signature of the sediment lipids because a higher proportion of these compounds are present in land-derived organic matter than in marine planktonic matter (Tissot and Welte, 1984). In addition, high abundances of high-molecular weight compounds that elute at a late stage in the chromatograms are tentatively identified as cuticular-derived (higher plant) wax esters. The unresolved complex mixture evidenced by the sharp rise in the base line is typical of sediment bitumen that has been degraded by bacteria. In Figure 25, the marine signature, in addition to n-alkanes lower than C_{23}, is particularly well represented by the C_{37} and C_{38} alkenones, which are the group of compounds that elutes at around 43 min in the chromatogram (Fig. 24). These long-chain di- and tri-unsaturated ketones are specific biomarkers for *Coccolithophoridae* such as *Emiliania huxleyi* (Volkman et al., 1980); furthermore, these ketones are produced in variable ratios to ensure cell membrane fluidity at the ambient seawater temperature they inhabit. These compounds have been identified previously in sediments drilled by ODP (e.g., Ruddiman, Sarnthein, Baldauf, et al., 1988; Behrmann, Lewis, Musgrave, et al., 1992) and have been used to try to intercalibrate different methods of sea-surface-temperature reconstructions (Behrmann, Lewis, Musgrave, et al., 1992). The U^k37 index (the ratio of the di- to tri-unsaturated ketone) has a linear relationship with ambient sea-surface temperature and is calculated by the formula:

$$C_{37:2}/(C_{37:2} + C_{37:3}).$$

This index is then translated to paleotemperatures according to the calibration of Prahl et al. (1988). In the sample analyzed from Hole 902C, the chromatography of these compounds looked good (Fig. 25); thus, at future sites, higher resolution sampling may produce good records of Pleistocene paleo-sea-surface temperatures from these biomarkers.

INORGANIC GEOCHEMISTRY

Forty-one interstitial water samples were collected at Site 902: 2 from Hole 902A, 6 from Hole 902C, and 33 from Hole 902D. Sampled depths range from 0.5 to 724 mbsf. Analytical results (Table 12 and Fig. 26) were determined on samples from approximately every third core, except in Hole 902D, where every core to 100 mbsf was sampled. Samples from Holes 902A, 902C, and 902D are plotted together on all graphs in this report.

The sulfate-ion concentration decreases rapidly to a trace at 36 mbsf and remains low at greater depths (Fig. 27). The rapid removal of sulfate results from the activity of sulfate-reducing bacteria in these rapidly deposited, organic-rich sediments. The decrease in sulfate ion corresponds to a rapid increase in phosphate ion, ammonium ion, and titration alkalinity (Fig. 26). Phosphate increases to several sharp maxima of 253 μM at 36 mbsf and 331 μM at 55 mbsf, then rapidly decreases to 6 μM downcore. Ammonium concentration increases to a maximum of 15.3 mM at 83.5 mbsf, then fluctuates between values of 6 and 10 mM downcore. Alkalinity increases to 35 mM at 36 mbsf and continues to increase to a maximum of 44 mM at 75.5 mbsf. Alkalinity then decreases to 31 mM at 125 mbsf, slightly increases to a broad local maximum of 37 mM at 223 mbsf, then gradually decreases

Table 11. Results of Rock-Eval pyrolysis, Site 902.

Core, section, interval (cm)	Depth (mbsf)	T_{max} (°C)	S_1 (mg/g)	S_2 (mg/g)	S_3 (mg/g)	TOC (wt%)	HI	OI	PI	S_2/S_3
150-902D-										
1H-1, 30–32	0.3	—	0.10	0.80	1.26	0.33	242	381	0.11	0.63
9H-1, 31–33	79.3	423	0.63	2.24	2.92	1.17	191	249	0.22	0.76
16H-3, 36–38	138.4	424	1.07	6.09	1.47	2.15	283	68	0.15	4.14
25X-1, 125–128	210.7	421	1.15	6.44	2.06	2.57	250	80	0.15	3.12
47X-2, 56–58	423.3	422	1.12	6.63	1.66	1.85	358	89	0.14	3.99
48X-2, 59–61	432.7	582	0.06	1.27	3.34	0.33	384	1012	0.05	0.38
49X-1, 74–77	440.8	426	0.44	3.13	1.26	1.15	272	109	0.12	2.48
50X-3, 54–56	452.9	418	0.83	4.72	0.87	1.83	257	47	0.15	5.42
51X-6, 103–104	468.0	420	1.24	7.81	1.16	2.44	320	47	0.14	6.73
52X-6, 56–58	477.1	419	0.99	8.29	1.57	2.58	321	60	0.11	5.28
53X-3, 25–27	481.3	418	1.12	8.52	1.56	2.63	323	59	0.12	5.46
64X-1, 137–139	585.4	411	1.50	10.60	2.75	2.75	385	100	0.12	3.85
66X-3, 56–58	606.9	423	0.55	6.48	2.76	2.13	304	129	0.08	2.34
70X-5, 28–30	647.9	423	0.50	5.10	1.98	1.71	298	115	0.09	2.57
75X-1, 71–73	690.6	424	0.04	0.62	1.77	0.34	182	520	0.06	0.35

Note: TOC = total organic carbon, HI = hydrogen index, OI = oxygen index, and PI = production index.

to 18 mM at 724 mbsf. The high values of phosphate, ammonium, and alkalinity in the uppermost 100 mbsf correspond to the high organic-carbon contents (0.3–4.0 wt%) and high methane contents (up to 80 vol% of total gas from 40 to 123 mbsf; see "Organic Geochemistry" section, this chapter) and represent the by-products of organic-matter degradation by sulfate-reducing bacteria above 36 mbsf and by methanogens below 36 mbsf. The relatively high concentrations of ammonium and alkalinity downcore are probably derived from the bacterial degradation of organic matter. In addition to the diffusion of sulfate from overlying seawater, sulfate may also be supplied to sediments below 300 mbsf from the upward migration of high-salinity pore waters (see below). Sulfate migration from below is suggested by the slight increase in sulfate observed within the interval of high salinity. The broad alkalinity and ammonium maxima below 200 mbsf suggest that these concentrations were derived from methanogenesis and sulfate reduction, rather than migration within the brine, because these concentrations occur in sediments having significantly higher organic-carbon contents. (Sulfate reduction and methanogenesis appear to be mutually exclusive.)

Salinity initially decreases from 35.5‰ to 34.5‰ from 0.5 and 55 mbsf, which reflects the loss of sulfate, calcium, magnesium, and potassium ions. Salinity then increases rapidly to 49‰ at 281 mbsf (Fig. 26). Between 281 and 724 mbsf, salinity increases more gradually to a maximum of 54‰ at 665 mbsf. The chloride profile is similar to the salinity profile (Fig. 26). The chloride concentration is close to the seawater value to 36 mbsf, then increases rapidly between 45.5 and 281 mbsf to 842 mM chloride. Chloride then increases gradually downhole to a maximum of 942 mM by 665 mbsf. The steep chloride gradient occurs between two major unconformities at the middle/upper Miocene boundary (m1 = Tuscan reflector) and the upper Miocene/upper Pleistocene boundary (p4 = purple reflector; see "Seismic Stratigraphic" section, this chapter). A similar steep salinity gradient was observed across the Pleistocene/Pliocene boundary from 55 to 105 mbsf at DSDP Site 612, located 7 km south in 1400 m of water depth (Poag, Watts, et al., 1987). The high salinity and chloride values indicate the migration or diffusion of a salt brine from greater depths. Maximum salinity values of around 53‰ were found in Upper Cretaceous rocks recovered at DSDP Site 612, approximately the same as the maximum salinity of 54‰ found at this site. The origin of the brine may be associated with the dissolution of deeply buried Jurassic salt. Diapirs have been observed in seismic profiles (Grow et al., 1988).

The steep increase in salinity and chloride corresponds to a sharp drop in pH from around 7.6 at 195 mbsf to 6.8 at 224 mbsf (Fig. 26). Thereafter, pH continues to decrease with depth to a minimum value of 6.5 at 609 mbsf; this trend parallels a more gradual increase in chloride and salinity. The slightly acidic pH values correspond to sediments at depths of 200–550 mbsf and which contain only rare occurrences and ghosts of calcareous microfossils (see "Biostratigraphy" section, this chapter). Below 640 mbsf, samples have pH values of ~7.5 and correspond to the Oligocene/Miocene boundary and an increase in calcareous fossils.

Calcium decreases from 10.2 to 2.0 mM between 1.5 and 46.5 mbsf and then increases to a near-seawater value by 195 mbsf (Fig. 26). Calcium increases very gradually from 195 to 454 mbsf and then increases to a maximum of 27 mM by 724 mbsf. Strontium is high near the surface (185 µM at 1.5 mbsf) and decreases to a value of 83 µM by 46 mbsf (Fig. 26). Strontium increases to 199 µM at 310 mbsf and then increases rapidly to a maximum of 453 µM at 724 mbsf. The strontium profile is similar to the calcium profile and suggests Sr uptake during the precipitation of diagenetic carbonates (Ca uptake) and Sr release during recrystallization or dissolution of relatively Sr-rich biogenic carbonate. The increase in Sr below 550 mbsf corresponds to an increase in calcareous fossils and the occurrence of chalk. Magnesium ion also decreases to a minimum concentration of 35.2 mM by 46.5 mbsf (Fig. 26). Magnesium then progressively increases to a maximum value of 53 mM by 427 mbsf. Magnesium decreases to 40.6 mM by 609 mbsf and then decreases more rapidly to a minimum of 25.4 mM at 724 mbsf. The decrease in Ca, Mg, and Sr at 46.5 mbsf (the depth of the sulfate minimum) suggests precipitation of diagenetic carbonate promoted by the rapid increase in alkalinity during sulfate reduction. Dolomite was found in upper Pleistocene sediments between 10 and 120 mbsf and in the Eocene chalks (see "Lithostratigraphy" section, this chapter).

Potassium concentration remains fairly close to that of seawater, except for generally higher values between 45.5 and 125.5 mbsf, with a maximum value of 12.8 mM at 83.5 mbsf (Fig. 26). Potassium decreases to a minimum of 8.6 mM below 680 mbsf, which corresponds to the disconformable Eocene/Oligocene contact. The K maximum at 83.5 mbsf corresponds to the ammonium maximum and suggests that some cation exchange may occur between the pore water and such exchangeable clay minerals as smectite. Potassium normally decreases with increasing burial depth at deep-sea sites because of its uptake in the alteration of volcanic sediment and underlying basalt (Gieskes, 1981). The increase in K may also be explained by the temperature-of-squeezing effect, which has been observed to cause an increase in K concentration (Waterman, 1973).

Iron increases to maxima of 40–50 µM at depths of 136–368 mbsf (Fig. 26). The high Fe values correspond to the sediment interval containing abundant pyrite, glauconite, and siderite (see "Lithostratigraphy" section, this chapter). Manganese is greatest (6 µM) near the sediment/seawater interface, decreases rapidly to 1 µM by 20 mbsf, and then increases to around 3 µM between 125 and 368 mbsf (Fig. 26). Trends in the Mn and Fe profiles are similar. Silica increases rapidly in the first 200 mbsf to 1217 µM and then more gradually to

Table 12. Interstitial water data, Site 902.

Core, section, interval (cm)	Depth (mbsf)	IW (mL)	pH	Alkalinity (mM)	Salinity (‰)	Cl^- (tit) (mM)	SO_4^{2-} (mM)	NH_4^+ (mM)	PO_4^{3-} (µM)	SiO_2 (µM)	Sr (µM)	Mn (µM)	Fe (µM)	Na^+ (calc) (mM)	Na^+ (chr) (mM)	K^+ (AA) (mM)	K^+ (chr) (mM)	Mg^{2+} (tit) (mM)	Mg^{2+} (chr) (mM)	Ca^{2+} (tit) (mM)	Ca^{2+} (chr) (mM)
150-902D-1H-1, 50–55	0.5	56	7.65	5.64	35.5	555	29.3	1.2	36	778	154	5.3	6.5	475	452	10.0	11.05	52.82	53.33	10.16	10.65
150-902A-1H-1, 145–150	1.5	56	7.60	6.45	36.0	558	30.3	0.9	8	460	185	6.6	10.3	485	484	11.9	11.41	50.74	51.16	9.76	9.72
150-902C-1H-2, 145–150	3.0	44	7.58	9.77	36.0	550	24.9	2.0	16	469	162	4.9	21.1	469	443	11.6	10.87	49.95	50.37	8.27	8.99
150-902D-2H-3, 145–150	17.0	26	7.58	19.14	34.5	550	14.7	3.2	119	763	120	2.2	3.3	472	450	10.1	9.80	43.65	43.09	3.58	3.77
150-902A-3H-3, 145–150	17.0	40	7.58	25.53	34.2	546	6.8	4.5	30	730	134	2.0	4.9	442	475	10.3	9.95	46.43	46.26	4.95	4.91
150-902C-3H-3, 145–150	19.5	32	7.55	24.50	35.0	552	8.8	4.7	166	642	125	2.0	5.7	456	474	11.4	10.17	44.85	43.58	3.83	3.81
150-902D-3H-1, 145–150	23.5	40	7.58	29.60	34.0	553	2.1	4.4	253	814	100	1.3	12.2	454	457	8.4	9.98	42.77	42.60	2.81	2.90
150-902D-4H-3, 145–150	36.0	42	7.74	34.84	34.5	546	1.6	7.3	217	811	88	2.1	3.3	445	454	10.4	10.30	41.02	41.20	2.70	2.56
150-902D-5H-3, 150–155	45.5	45	7.77	30.43	34.5	567	1.3	10.0	138	584	83	1.6	3.4	469	490	12.3	11.81	37.37	36.91	1.99	4.40
150-902C-7H-1, 145–150	46.5	23	7.70	29.46	34.5	566	1.3	10.1	235	548	108	1.6	6.5	473	462	11.6	10.98	34.83	34.56	2.26	2.31
150-902D-6H-3, 145–150	55.0	29	7.49	31.74	34.5	568	1.5	11.9	331	656	86	1.8	8.2	470	467	14.0	10.68	35.07	35.22	2.64	2.64
150-902D-7H-3, 145–150	63.7	36	7.37	39.17	35.5	576	1.6	12.8	310	787	91	2.3	22.2	475	470	10.8	10.84	37.44	37.10	3.38	3.26
150-902C-10H-3, 145–150	73.5	33	7.69	42.41	36.5	579	2.0	14.0	285	909	123	2.4	6.2	469	473	11.7	11.27	40.61	38.72	3.93	3.62
150-902D-8H-4, 145–150	75.5	44	7.50	44.45	36.5	572	1.6	13.4	254	974	94	2.4	26.5	465	481	11.5	11.58	39.27	38.58	3.83	3.49
150-902D-9H-3, 150–155	83.5	36	7.52	41.76	37.0	594	1.5	15.3	171	761	88	1.9	9.8	484	514	12.9	12.80	39.03	38.23	3.44	3.20
150-902D-10H-3, 135–140	92.9	42	7.69	39.95	37.0	591	1.5	14.3	195	1033	100	2.7	29.5	483	492	11.5	11.22	38.92	39.53	3.97	3.63
150-902C-13H-3, 150–155	102.0	57	7.68	31.69	37.0	620	1.9	12.0	109	854	145	1.7	10.5	513	532	12.6	11.34	39.47	37.22	3.83	4.75
150-902D-11H-3, 145–150	102.5	56	7.50	33.84	38.0	619	1.4	12.5	98	833	105	1.8	14.6	512	500	11.7	11.00	39.16	38.46	3.73	3.45
150-902D-13H-3, 145–150	121.5	42	7.44	31.27	39.5	654	1.3	8.9	42	885	117	2.9	51.4	541	546	11.2	10.87	42.32	42.04	5.33	4.92
150-902C-16H-2, 150–155	125.5	29	7.29	30.59	39.5	669	1.3	9.1	70	668	165	3.2	4.4	555	528	10.9	11.18	42.30	42.84	5.76	5.48
150-902D-16H-1, 145–150	137.0	20	7.61	31.02	39.0	672	1.9	7.3	63	854	131	2.8	4.3	555	536	10.4	9.74	44.78	44.33	6.60	6.45
150-902D-20X-3, 145–150	166.0	26	7.03	34.37	42.5	726	1.9	7.6	53	1129	151	2.6	22.7	597	564	10.7	10.24	48.76	47.04	8.21	7.79
150-902D-23X-3, 145–150	194.7	26	7.67	35.98	45.2	761	NM	7.2	53	1143	171	2.9	33.0	628	637	10.1	10.99	48.73	48.00	9.07	7.98
150-902D-26X-3, 145–150	223.5	44	6.80	36.74	46.5	790	1.3	8.1	39	1217	182	2.9	42.2	653	653	10.9	10.45	51.20	48.88	9.09	8.80
150-902D-29X-3, 140–150	252.5	44	6.80	35.48	48.0	822	1.4	8.7	35	1146	191	2.7	47.0	686	670	10.9	10.34	50.39	49.99	9.28	9.07
150-902D-32X-3, 140–150	281.4	30	6.82	35.64	49.0	836	1.3	9.7	30	1124	191	3.2	34.8	696	673	11.8	10.40	50.63	49.97	9.66	9.47
150-902D-35X-3, 140–150	310.3	42	6.76	36.10	49.0	848	1.8	9.5	16	1215	199	3.1	50.8	707	688	10.4	10.24	52.13	50.27	9.82	8.79
150-902D-38X-3, 140–150	339.2	43	6.77	35.81	49.0	845	2.0	8.9	22	NM	185	3.1	44.4	705	686	10.5	10.36	52.49	50.43	9.87	9.32
150-902D-41X-3, 140–150	368.0	52	6.72	35.33	49.0	852	1.0	9.9	26	1296	185	3.0	47.2	708	684	10.4	10.12	52.85	51.77	9.92	9.04
150-902D-44X-3, 140–150	397.4	38	6.73	34.09	50.0	861	1.7	9.7	22	1258	177	2.4	45.6	720	685	10.4	9.69	52.46	52.58	9.49	9.73
150-902D-47X-4, 140–150	427.1	36	6.69	33.14	50.5	866	1.3	9.4	14	1275	174	2.3	43.3	723	702	9.9	10.00	52.97	51.84	10.02	10.37
150-902D-50X-3, 140–150	453.7	32	6.68	31.68	51.5	882	1.5	8.9	NM	1313	180	2.6	43.8	743	696	10.2	9.75	50.76	50.74	10.57	8.05
150-902D-53X-3, 140–150	482.4	52	6.69	27.24	50.0	869	3.1	9.5	6	1373	188	2.1	27.4	744	700	10.1	9.70	47.63	48.25	8.10	6.58
150-902D-56X-4, 140–150	513.1	60	6.62	27.44	52.0	897	1.7	9.7	8	1475	208	1.6	16.5	757	718	10.6	10.17	46.89	46.71	14.44	11.29
150-902D-59X-1, 140–150	537.4	53	6.59	27.97	52.0	900	1.5	10.2	8	1547	231	1.8	34.6	757	733	9.8	10.30	45.24	43.60	17.33	14.57
150-902D-62X-3, 140–150	569.0	46	6.57	27.22	52.0	916	1.7	10.0	6	1394	265	1.9	14.4	782	730	10.1	10.13	42.82	42.34	15.40	13.95
150-902D-66X-4, 140–150	609.2	29	6.53	23.05	52.0	894	2.7	8.5	NM	1456	299	1.6	11.4	758	707	10.2	9.95	40.64	40.28	20.48	16.25
150-902D-69X-4, 140–150	637.8	30	7.49	26.19	53.5	936	1.9	9.3	NM	NM	368	2.2	31.1	795	747	10.0	9.85	40.23	39.59	22.33	21.78
150-902D-72X-3, 140–150	665.3	36	6.59	25.10	54.0	942	1.9	9.0	NM	NM	453	2.3	30.9	804	752	10.4	10.42	41.33	39.39	19.58	17.99
150-902D-75X-2, 140–150	692.8	3	7.61	17.75	NM	NM	1.9	NM	NM	NM	NM	NM	NM	NM	735	9.2	8.59	35.69	39.94	20.67	20.47
150-902D-79X-2, 0–10	724.3	5	7.53	17.75	50.5	873	3.6	6.1	NM	NM	NM	NM	NM	760	700	9.3	8.61	25.41	23.93	27.00	32.12

Note: IW = interstitial water, NM = not measured, AA = atomic absorption, chr = chromatography, tit = titration, and calc = calculated.

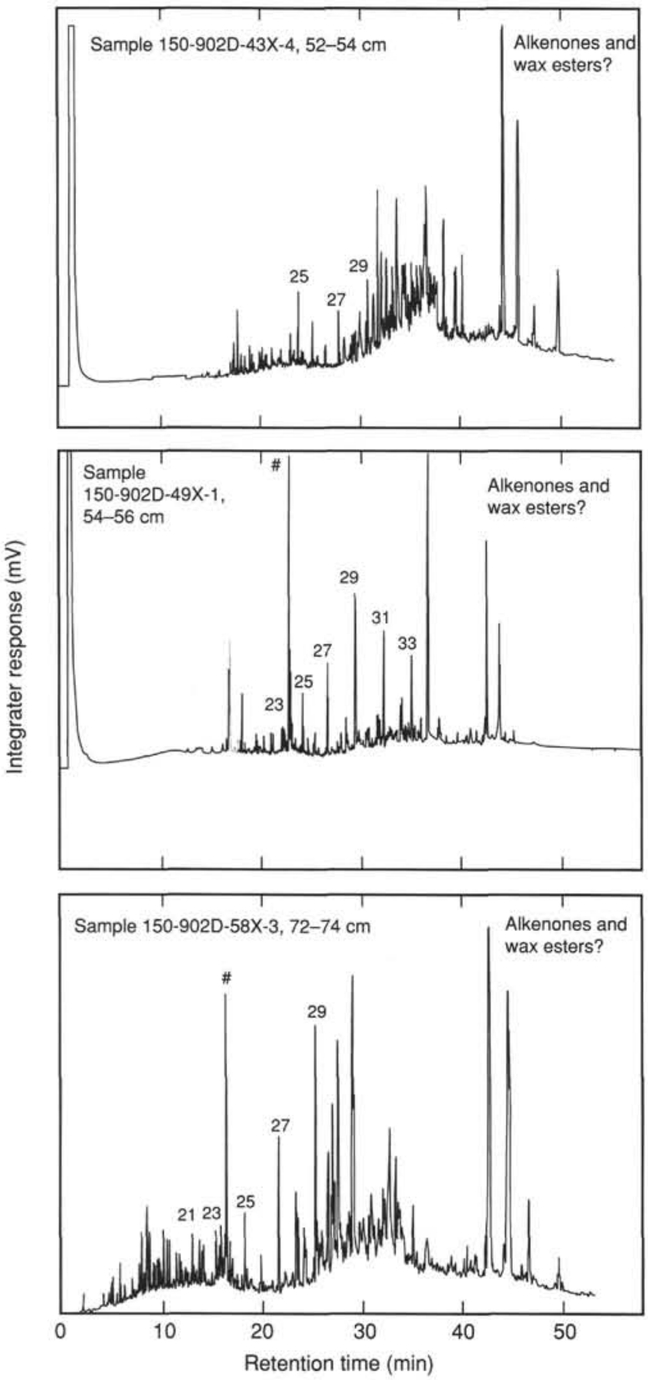

Figure 24. *N*-hexane extracts from Miocene sediment samples at Site 902. Numbers refer to carbon numbers of *n*-alkanes. Number sign (#) = a contamination peak, probably a plasticizer from the core liner.

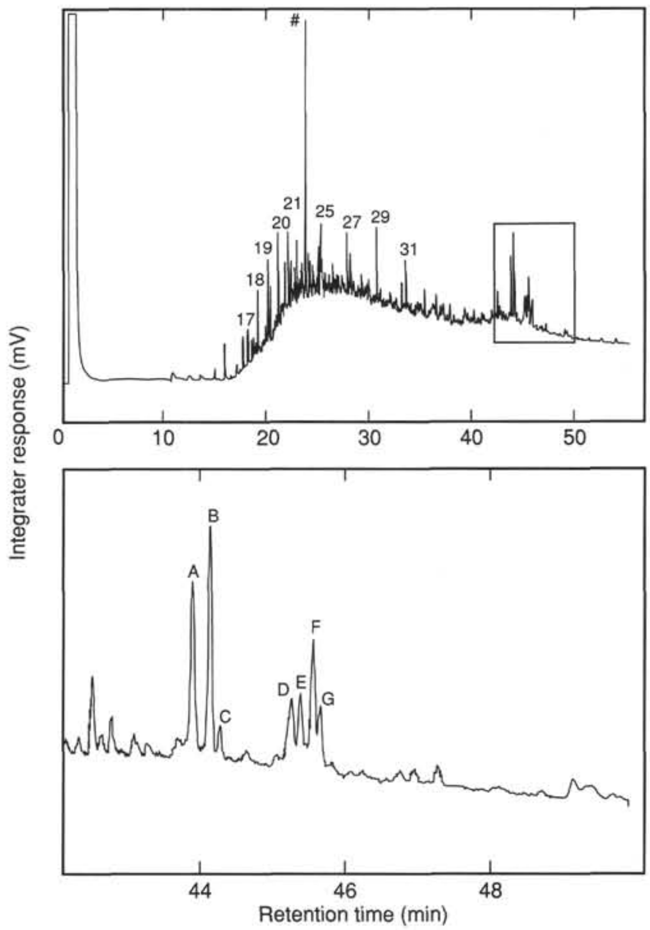

Figure 25. *N*-hexane extract from Sample 150-902C-1H-1. Numbers refer to carbon numbers of *n*-alkanes. Number sign (#) = a contamination peak, probably a plasticizer from the core liner. A = $C_{37:3}$ alkenone, B = $C_{37:2}$ alkenone, C = $C_{37:2}$ methylalkenoate, D = $C_{38:3}$ ethyl alkenone, E = $C_{38:3}$ methylalkenone, F = $C_{38:2}$ ethylalkenoate, and G = $C_{38:2}$ methylalkenoate.

a maximum value of 1547 µM at 537 mbsf (Fig. 26). The high silica values result from the high diatom content of the sediment and the high solubility of amorphous, biogenic silica (opal-A).

PHYSICAL PROPERTIES

GRAPE and Index Properties

Bulk densities measured using the GRAPE closely follow the trend of bulk-density values calculated from index properties samples using the mass-volume (MV) method (Figs. 28–31). In the upper 30 mbsf, GRAPE bulk densities are approximately equal to MV bulk densities. GRAPE bulk densities are generally lower than MV values below 30 mbsf; below 680 mbsf, however, they again approach the MV values.

Two samples for measurement of index properties (bulk density, water content, porosity, and grain density) were taken per section in Holes 902A to 902C. Hole 902D was sampled at a reduced rate of three to four samples per core for cores with full recovery, with fewer samples from shorter cores.

Downhole variations in bulk density are cyclic, with little indication of a general trend of increasing bulk density with depth in the upper 500 mbsf (Figs. 28–31). Ten units were defined on the basis of changes in bulk-density values (Table 13 and Figs. 28–31). With the exception of Units I and II, each represents a single cycle. The uppermost units (I to VI) are best defined by data from Holes 902A, 902B, and 902C (Figs. 28–30), where closer sampling provided enhanced resolution. The depths to unit boundaries differ from hole to hole and are summarized in Table 13. Depths quoted below are from Hole 902D.

The steep downhole rise in bulk density from 1.47 to 1.85 g/cm^3 within Holocene sediment just beneath the seafloor defines Unit I (0–1 mbsf). Unit II (1–12 mbsf) is characterized by constant bulk densities on the order of 1.85 g/cm^3 in Holes 902C and 902D, but this unit contains peaks in Holes 902A and 902B (up to 2.1 g/cm^3 in Hole 902A). An abrupt downhole rise in bulk density at the top of Unit III (12–26 mbsf), to a peak of 2.2 g/cm^3 in Hole 902C, is followed by a more gentle decline to 1.8 g/cm^3. Unit IV (26–41 mbsf) includes an

Table 13. Depth intervals for bulk density units, Site 902.

Bulk density units	Depth intervals (mbsf) Hole 902A	Hole 902B	Hole 902C	Hole 902D
I	0–1	0–1	0–1	0–1
II	1–7	1–9	1–11	1–12
III	7–22	9–TD	11–27	12–26
IVA	22–TD		27–34	26–35
IVB			34–39	35–41
VA			39–67	41–69
VB			67–91	69–91
VIA			91–TD	91–164
VIB				164–197
VIIA				197–298
VIIB				298–393
VIIIA				393–463
VIIIB				463–595
IXA				595–626
IXB				626–680
X				680–TD

Note: TD = total depth.

upper bulk-density cycle, Subunit IVA (26–35 mbsf), with a sharp downhole increase in bulk density from 1.8 to 2.05 g/cm^3 at its top, subsequently decreasing downhole to 1.75 g/cm^3. This is followed downhole by a second minor cycle with a lower peak of 1.89 g/cm^3 (Subunit IVB, 35–41 mbsf). Unit V (41–91 mbsf) is also divided into subunits. The abrupt downhole rise in bulk density from 1.69 g/cm^3 to a peak of 2.1 g/cm^3 at the top of Subunit VA (41–69 mbsf) is followed by a slightly less steep decline to values of approximately 1.87 g/cm^3. The downhole decrease in bulk density continues through Subunit VB (69–91 mbsf), but with a greatly reduced gradient.

Units VI to VIII follow the pattern of Unit V in comprising peaks of varying amplitude. They commonly begin with a steep downhole rise in bulk density followed by a generally less steep downhole decline ("A" subunits). "A" subunits are followed in turn by intervals of gently declining or near-constant bulk density ("B" subunits). Bulk density in Subunit VIA (91–164 mbsf) rises downhole to a peak of 2.22 g/cm^3 at 114.2 mbsf, a value not matched until the top of Unit X. The pronounced peak at ~152 mbsf represents a lithified nodule and correlates with seismic reflector m0.5 (Red) (see "Seismic Stratigraphy" section, this chapter). Subunit VIB (164–197 mbsf) exhibits relatively constant bulk-density values around 1.75–1.84 g/cm^3. Subunit VIIA (197–298 mbsf) has a broad peak across which bulk density fluctuates about a value of approximately 1.9 g/cm^3, with individual values between 1.76 and 2.02 g/cm^3. A thin, but pronounced, interval of lower density (1.65 g/cm^3) lies at the boundary of Subunits VIIA and VIIB (298–393 mbsf) and correlates with seismic reflector m1 (Tuscan) (see "Seismic Stratigraphy" section, this chapter). Subunit VIIB displays a gentle downhole decrease in bulk-density values from 1.89 to 1.64 g/cm^3. Steeply increasing bulk density marks the top of Unit VIII (393–595 mbsf) and may be related to seismic reflector m2 (Yellow-2) (see "Seismic Stratigraphy" section, this chapter). Bulk density rises downhole to a peak of 1.96 g/cm^3 just below the top of Subunit VIIIA (393–463 mbsf), then decreases downhole to 1.60 g/cm^3 at the bottom of the subunit. Subunit VIIIB (463–595 mbsf) is characterized by variable but gradually increasing bulk density, to a peak value of 1.71 g/cm^3. Bulk density increases rapidly to a peak of 2.03 g/cm^3 at the top of Unit IX (595–680 mbsf), subsequently decreasing downhole to 1.71 g/cm^3 at the base of Subunit IXA (595–626 mbsf). The top of Unit IX is marked by a sharp downhole rise in bulk density to a peak value of 2.03 g/cm^3 in Subunit IXA, before declining to 1.71 g/cm^3 at the base of Subunit IXA. A second bulk-density cycle, with a slightly lower peak of 1.93 g/cm^3, constitutes Subunit IXB (626–680 mbsf). Bulk density falls to 1.72 g/cm^3 at the base of Unit IX. The top of Unit X (680 mbsf to total depth [TD]) is marked by a rapid downhole increase in bulk density to 2.18 g/cm^3. The subsequent downhole trend in Unit X is of gently decreasing bulk density. The tops of Units IX and X correlate with seismic reflectors m5 (true blue) and m6 (green-2), respectively (see "Seismic Stratigraphy" section, this chapter).

The tops of Units IX and X correspond approximately to the tops of lithologic Units VI and VII, respectively. Bulk-density Unit X correlates with Eocene chalk. Other bulk-density units correlate less well with lithologic unit boundaries, but the top of bulk-density Subunit VIB is only 12 m below the top of lithologic Unit IV, and the top of bulk-density Subunit VIIB is 5 m below that of lithologic Subunit IVB and the top of bulk-density Unit VIII is 10 m above the top of lithologic Unit V (see Figs. 28–31 for the relationship between bulk-density and lithologic units).

Isolated peaks in the bulk-density record correspond to measurements from thin (generally <10 cm) lithified zones. At least two lithified zones, at 463 mbsf (thickness 1.3 m) and 565 mbsf (thickness approximately 2 m and correlating with seismic reflector m5.4 [sand]), could confidently be termed "beds," as opposed to "nodules" or "clasts."

Porosity and wet water content vary inversely with bulk density, but these two components closely mirror the trends of the bulk-density plot. This suggests that most of the variations in bulk density are the result of variations in porosity (Figs. 28–31).

Grain densities are fairly constant at 2.9 g/cm^3 in the upper 280 mbsf and below 630 mbsf. In the uppermost 40 mbsf (Figs. 28–30), grain density values tend to follow the trend of water content and porosity and vary inversely with bulk density. Below 150 mbsf, however, they follow the general downhole trend of bulk density. Grain densities fall to a low of 2.6 g/cm^3 in the vicinity of 500 mbsf (Fig. 31).

An anomalous downhole trend of decreasing bulk density characterizes the upper 500 mbsf. Furthermore, measured values of grain density are higher than expected for common minerals. These issues are addressed further in physical properties reports for subsequent sites. Measurements of dry volumes were made at those sites as a second method of calculating grain densities. One concern is that the sediment may not be fully saturated, as is assumed in the calculation of index properties. Expansion of gas in pores could account for partial saturation (see discussion of compressional-wave velocity below). If helium did not penetrate all gas-filled pore space during volume measurement with the pycnometer (e.g., in impermeable clays), measured bulk volumes would be too high, resulting in lower bulk-density values. A second potential problem is the possible retention of some water after oven drying, also associated with clayey sediment, which could potentially result in dry weights that were too high.

Compressional-wave Velocity

Reasonable *P*-wave logger (PWL) and digital sonic velocimeter (DSV) results were obtained only from the upper 28 mbsf in Holes 902A to 902D (Figs. 28–31). In that interval, DSV measurements were made at the same depth interval as index properties samples. No significant change occurred in PWL and DSV velocities in the upper 11 mbsf from Hole 902C (bulk-density Unit II; Fig. 30). Velocities increase from around 1550 to 1750 m/s at 12 mbsf, corresponding to the base of Unit II. From 12 mbsf to around 25 mbsf, PWL and DSV indicate a trend of decreasing velocity to about 1570 m/s, paralleling the trend of decreasing density in Unit III. The PWL and DSV velocities from Holes 902A and 902B also parallel the trends of bulk density in those holes, with prominent velocity peaks present in Unit II in Hole 902A (Fig. 28). Velocities from the upper 12 mbsf from Hole 902D increase from 1550 to 1680 m/s, decreasing to 1580 m/s at 24 mbsf (Fig. 31; only DSV data are shown). Anomalously low velocities (<water velocity) were measured by both the PWL and DSV data sets from Hole 902D between 9 and 12 mbsf.

No velocity data were obtained from 30 to 300 mbsf. The signal passing through the sediment between transducers of both PWL and DSV was too attenuated to yield a measurable velocity, possibly because of microfractures genetically related to visible fractures in the sediment. Fracturing may have been related to degassing, which

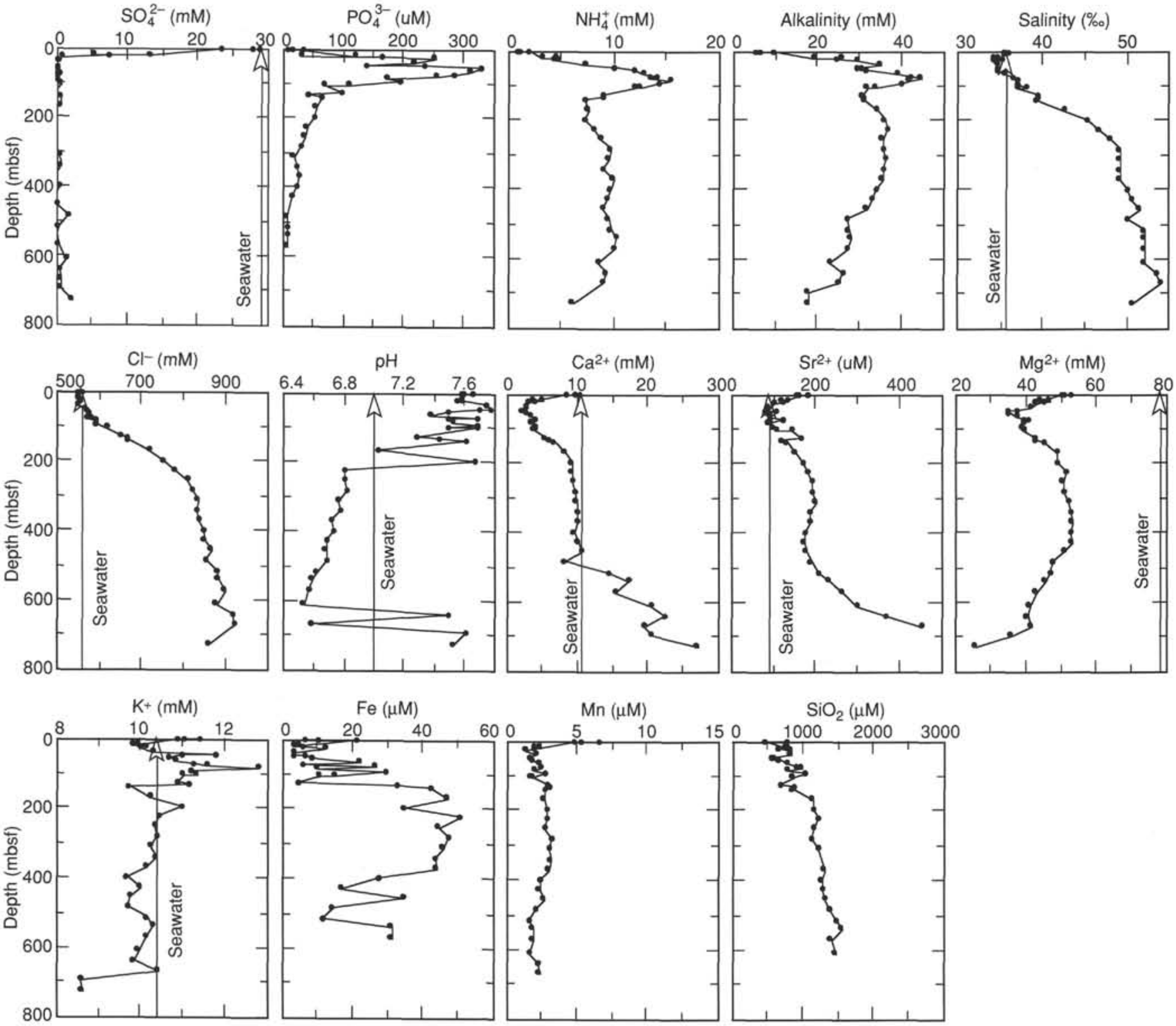

Figure 26. Interstitial water geochemical data vs. depth, Site 902.

was observed in all APC cores beginning with Core 150-902D-4H (32 mbsf). Degassing of some XCB cores is also likely to have occurred but was more difficult to detect.

In the interval from 317 mbsf to TD, the DSV transducers were inserted into unconsolidated sandy intervals without achieving results. Compressional-wave velocity measurements were obtained at irregular intervals in this interval, however, using the Hamilton Frame. Some Hamilton Frame measurements were made on sediments in the liner (perpendicular to the core axis). This approach was found to be ineffective in most cases, probably because of gaps between core and liner and poor sediment-to-liner contact. The best results were obtained when the sediment had sufficient strength to permit a sample to be cut and placed directly between the transducers of the Hamilton Frame. Compressional-wave velocity measurements were attempted both parallel and perpendicular to the core axis on trimmed samples. In some instances, recordable data could be obtained in only one direction. From 317 mbsf to TD, this technique enabled measurement of compressional-wave velocity both parallel and perpendicular to the core axis (Fig. 31). Measured velocities generally increase from around 1440 to 1590 m/s in the upper part of this interval to between 1580 and

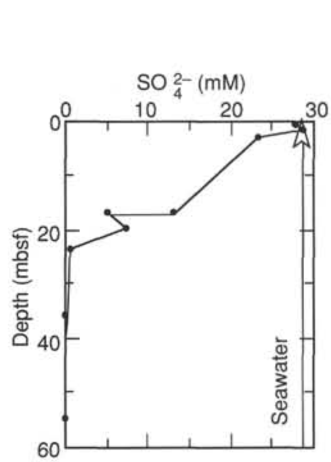

Figure 27. Detail of sulfate ion data vs. depth (0–60 mbsf), Site 902.

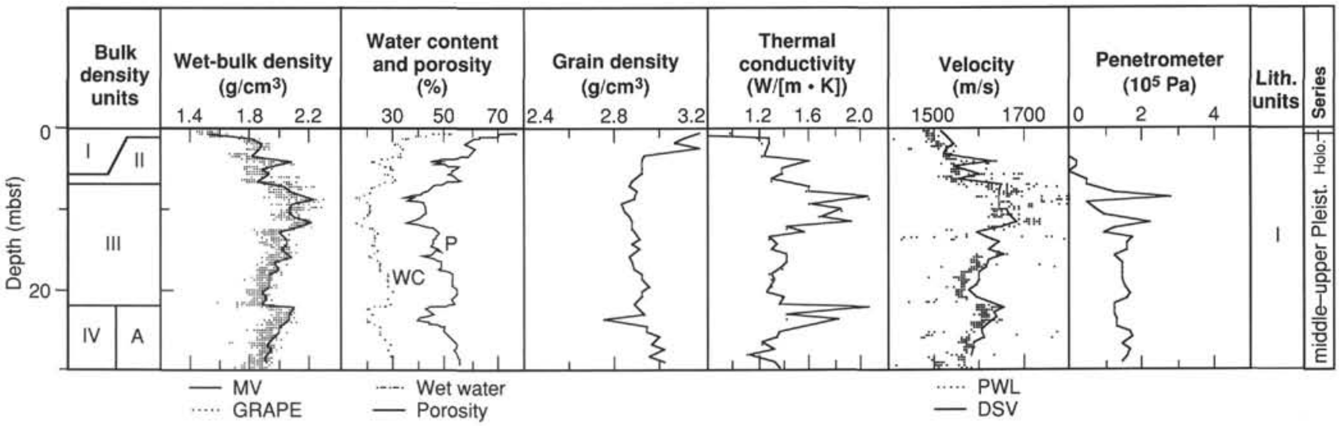

Figure 28. Physical properties results (wet-bulk density, water content and porosity, grain density, thermal conductivity, compressional velocity, and penetrometer readings), Hole 902A. MV = mass-volume method.

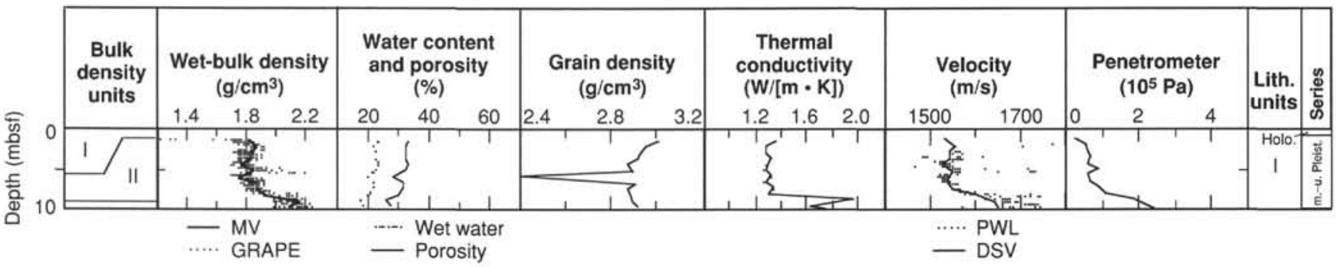

Figure 29. Physical properties results (wet-bulk density, water content and porosity, grain density, thermal conductivity, compressional velocity, and penetrometer readings), Hole 902B. MV = mass-volume method.

1870 m/s at 673 mbsf. Values of approximately 2200 m/s were measured in silts to fine sands with indurated nodules. A compressional-wave velocity value of approximately 3100 m/s was measured for the 1.3-m-thick lithified bed at 463 mbsf, and another value of 4200 m/s measured for the 2-m-thick lithified bed at 565 mbsf. Once again, many anomalously low velocities (<water velocity) were also measured, most of which have been removed from the data shown in Figure 29. At 681 mbsf, corresponding to the change from siliciclastic-dominated lithology to siliceous chalk, velocities increase to between 1900 and 2270 m/s and remain at that level until TD. Compressional-wave velocities measured parallel to the core axis are often significantly different from those measured perpendicular to the core axis, but no systematic relative offset is apparent.

Thermal Conductivity

Eight thermal conductivity measurements were made per core in Holes 902A, 902B, and 902C (Figs. 28–30). The number of measurements was reduced to four per core for most of Hole 902D, but eight measurements per core were made between 30 and 120 mbsf (Fig. 31).

Thermal conductivities varied between 0.5 and 2.25 W/(m · K). Results confirmed that thermal conductivity is inversely related to water content and, consequently, in saturated sediments, to porosity (Lovell, 1984). Thermal conductivity measurements, therefore, follow the trend of bulk density, as almost all of the bulk-density units can be identified on the thermal conductivity profiles. A notable exception is the boundary between Units IX and X (the siliciclastic/chalk boundary).

Penetrometer

Two penetrometer measurements per section were made in Holes 902A to 902D (Figs. 28–31). The general trend is that of a downhole increase in sediment strength. Except in the uppermost 30 mbsf, penetrometer readings tend to be inversely related to bulk density. For example, low bulk densities in Subunits VB and VIA correspond to high penetrometer values, particularly in Hole 902D. In addition, the downhole increase in penetrometer readings beginning at the boundary between bulk-density Subunits VIIA and VIIB corresponds to the start of a downhole decrease in density. Low penetrometer readings were also obtained at the same depth as the bulk-density peak in bulk-density Subunit VIIIA.

APC DOWNHOLE TEMPERATURE MEASUREMENTS

A total of 18 APC downhole temperature measurements were taken at Site 902: one at the first hole, which was abandoned because of inadvertent failure of the shear pins during reaming for Core 150-902A-4H; six at the third hole, which was left after Core 150-902C-10H because of liner failures and decreasing penetration; and eleven at the fourth hole, from Cores 150-902D-6H to -16H, the last APC core. Depths of measurements, depth error estimate, averaged thermal conductivity values, the temperature tool probe used for each station, and tentative, calculated temperature estimates are listed in Table 14. General information on tool calibration, deployment, processing, and error estimates is given in Chapter 3 (this volume).

Data from Cores 150-902C-3H, -4H, -6H, and -7H, and from Cores 150-902D-8H, -9H, -13H, -14H, -15H, and -16H (10 out of 18 cores at this site) display "classic" smooth decay curves, with single spikes at insertion and removal of the tool (Fig. 32). Records from Core 150-902A-3H, Core 150-902C-10H, and Cores 150-902D-6H, -10H, -11H, and -12H display one or two "shoulders" or kinks in the cooling curves, which are probably related to the geometry of the experiment. Why these occur for some stations and not for others is

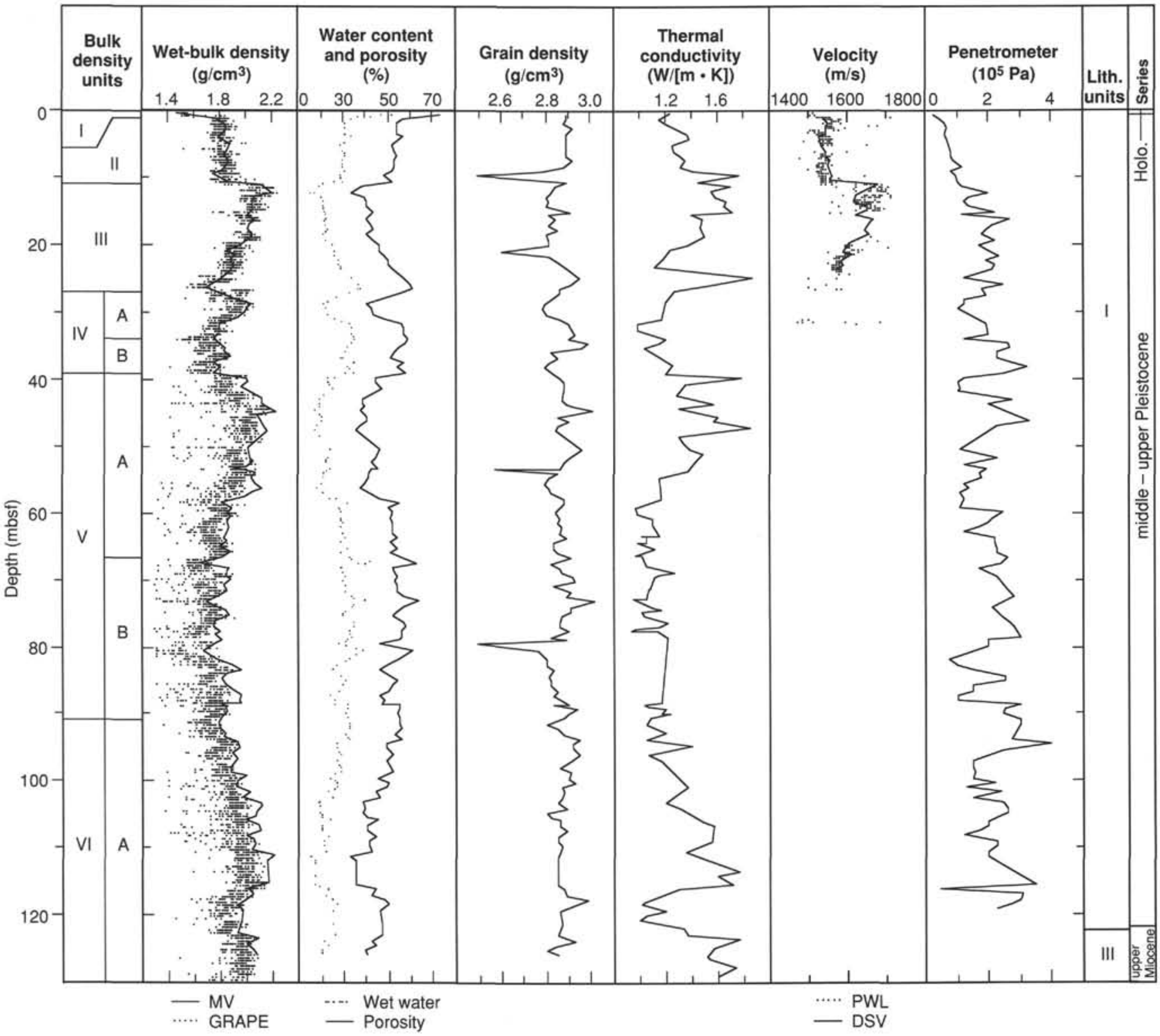

Figure 30. Physical properties results (wet-bulk density, water content and porosity, grain density, thermal conductivity, compressional velocity, and penetrometer readings), Hole 902C. MV = mass-volume method.

unclear. The later section of the curve is usually used for temperature estimates. Of the remaining stations, Core 150-902C-5H and Cores 150-902D-7H and -10H display noisy curves, possibly caused by multiple penetrations or significant movement during deployment; estimated errors are the largest here because only relatively small curve sections can be matched with theoretical decay curves.

The temperature vs. depth plot based on this preliminary analysis shows a relatively linear trend of 4.0°C per 100 m (Fig. 33). Minor fluctuations are mostly within the tentative error of approximately 0.2° to 0.4°C.

DOWNHOLE LOGGING

Introduction

Logging was conducted on two occasions for a total of four logging runs at Hole 902D (Table 15). Three tool strings were used: the sonic-induction, the porosity, and the Formation MicroScanner (FMS) (see Chapter 3, this volume, for a description of these tools). Below we describe the acquisition and preliminary interpretation of log data completed at sea. Additional processing and display were conducted onshore by the Borehole Research Group, and their results are presented at the end of this chapter and on the CD-ROM disk in the back pocket of this volume. The FMS data are found only on the CD-ROM disk.

The first run was made after the hole was drilled with the APC and XCB to 507 mbsf. A wiper trip was made to the bottom, and the hole was prepared for logging. The sonic-induction tool string was used on this run. Logging was only successful above 216 mbsf as a bridge was encountered on the way down into the hole. Several unsuccessful attempts were made to break through the bridge before it was decided that the borehole should be drilled to total depth (TD) before any additional logging runs were attempted.

The second run was made when the borehole had been drilled to a TD of 740 mbsf. Another wiper trip was made to TD, and the hole was prepared for logging. The side-entry sub (SES) was used to clear the passage for the logging tools (for details of SES operations, see Chapter 3, this volume). We attempted to log without running pipe to

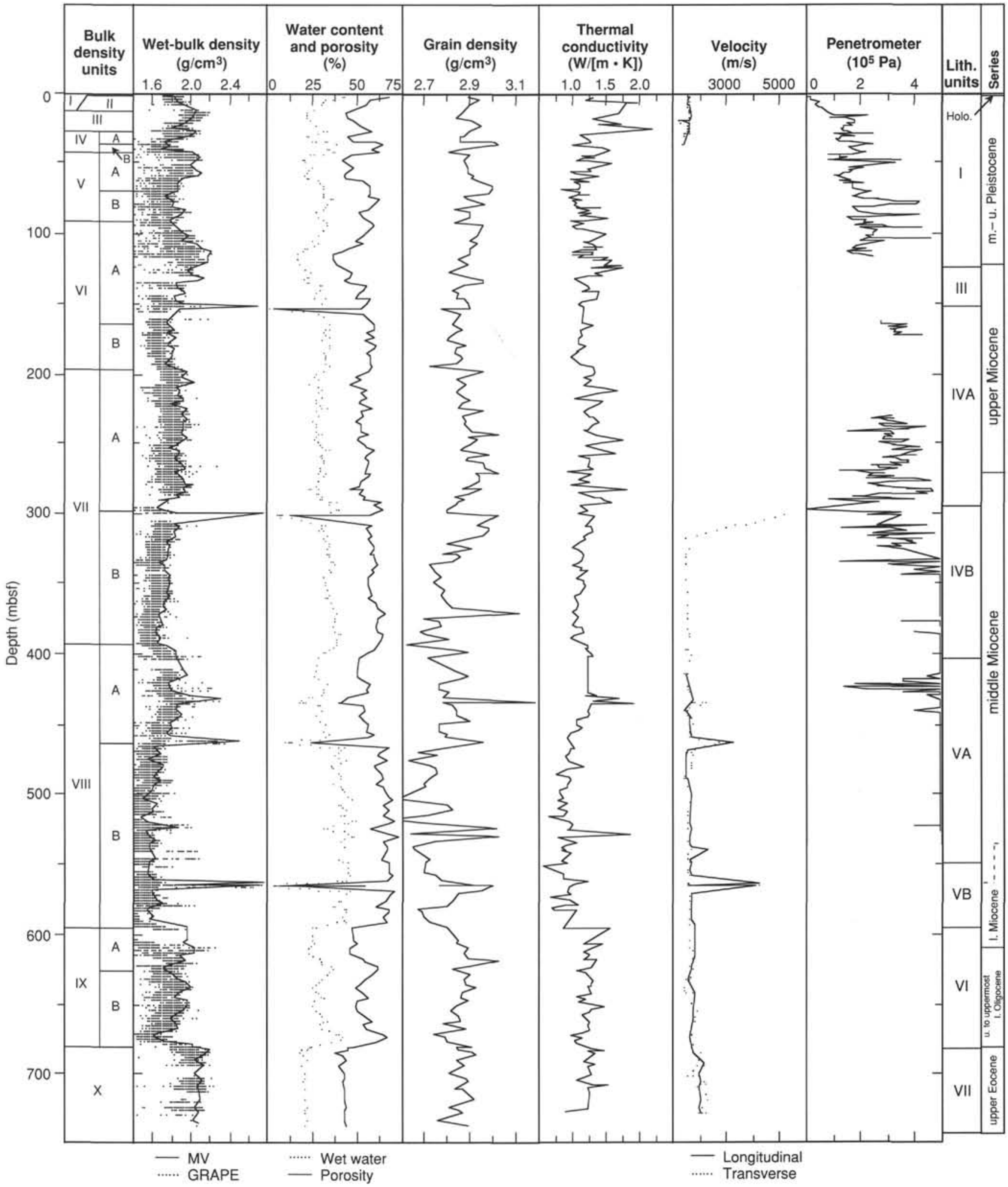

Figure 31. Physical properties results (wet-bulk density, water content and porosity, grain density, thermal conductivity, compressional velocity, and penetrometer readings), Hole 902D. Compressional wave measurements above 30 mbsf were made using the digital sound velocimeter (DSV), whereas those below 300 mbsf were made using the Hamilton Frame. Transverse compressional-wave values are parallel to the core axis (i.e., vertical), and longitudinal compressional-wave values are perpendicular to the core axis (i.e., horizontal). Penetrometer readings exceeding the instrument scale of 4.5×10^5 Pa are plotted at 5×10^5 Pa. MV = mass-volume method.

Table 14. APC downhole temperature measurements, Holes 902A, 902C, and 902D, using the ADARA tool.

Core no.	Depth (mbsf)	Depth error (m)	Thermal conductivity (W/[m · K])	Probe no.	Calculated temperature (C°)
150-902A-					
3H	22.0	2.0	1.4	12	5.4 ± 0.1
150-902C-					
3H	24.5	0.5	1.3	12	5.5 ± 0.1
4H	34.0	0.5	1.1	18	5.9 ± 0.1
5H	43.5	1.0	1.4	12	6.3 ± 1.0
6H	45.0	0.5	1.4	18	6.3 ± 0.2
7H	50.0	4.0	1.5	12	6.3 ± 0.1
150-902D-					
6H	60.0	4.0	1.1	18	6.7 ± 0.2
7H	69.5	0.5	1.2	12	6.9 ± 0.2
150-902C-					
10H	78.5	0.5	1.1	12	7.6 ± 0.3
150-902D-					
8H	79.0	0.5	1.1	18	7.8 ± 0.2
9H	88.5	0.5	1.2	12	8.0 ± 0.2
10H	98.0	0.5	1.2	18	7.9 ± 0.5
11H	107.5	0.5	1.4	12	8.6 ± 0.3
12H	117.0	0.5	1.3	18	9.4 ± 0.5
13H	126.5	0.5	1.6	12	8.9 ± 0.3
14H	131.0	0.4	1.6	18	9.9 ± 0.3
15H	135.0	0.4	1.2	12	9.9 ± 0.3
16H	140.0	0.4	1.2	18	10.3 ± 0.2

Notes: The bottom of the drilled interval of a core is used as the measurement depth and is given in meters below seafloor (mbsf). Thermal conductivity values are based on a 4-m box car average (±2 m from depth measurements). See Chapter 3 (this volume) for information regarding the probe numbers.

TD by pulling the drill string to 171 mbsf and lowering the tool. At 236 mbsf a bridge was encountered that could not be passed. The tool string was drawn back into the drill pipe and then lowered with the drill pipe to the bottom of the borehole. The pipe was then gradually raised and logging started at 676 mbsf with the tool string following the drill pipe up the hole. The drill pipe was kept about a hundred meters ahead of the tool string to avoid disturbing the logging measurements. During the second run, the logging measurements were continued within the drill pipe to get natural gamma ray readings above the seafloor. This enabled logging depths to be correlated with depths recorded during the drilling operations.

The third run was made with the porosity tool string and was performed in more or less the same way as the second run. This time, however, the pipe was lowered directly to the bottom of the hole. Logging started from 710 mbsf and ended below the drill pipe at 155 mbsf.

Caliper measurements from the previous run confirmed poor conditions in the upper part of the borehole. Consequently, only one pass of the FMS was made, and it was restricted to the lowermost 200 m of the borehole.

Log Quality

During logging runs 1, 3, and 4, the logging heave compensator was used even though sea conditions were very calm with almost no swell. After each logging run, part of the borehole was lost because of material filling the bottom of the hole, thus shortening the maximum logging depth.

Because of poor hole conditions in the upper part of the borehole, most of the logging data above 500 mbsf are of very low quality. In the lower part, where the diameter of the borehole varies much less (Fig. 34), the readings are normally of good quality.

In an attempt to break through the bridges on the way down, mud was forced into the shield surrounding the thermistors and the pressure sensor of the LDEO temperature tool. Also, during some of the logging runs, seawater or mud was used to flush out bridges that the tool string encountered as it descended. These disturbances in the borehole and to the tool have made it impossible to record a good temperature profile.

Table 15. Total drilling depth, SES, tool configuration, logging interval, and logging speed at Hole 902D.

Total depth (mbsf)	SES	Tools (string and combination)	Logging interval (mbsf)	Logging speed (m/hr)
507	No	Sonic-induction tool string NGT/SDT/MCD/DIT/LDEO temperature	31 to 215	275
740	Yes	Sonic-induction tool string NGT/SDT/MCD/DIT/LDEO temperature	–30 to 676	275
740	Yes	Porosity tool string NGT/CNT/HLDT/LDEO temperature	155 to 710	275
740	Yes	Formation MicroScanner tool string NGT/MEST/LDEO temperature	502 to 689	275

Note: SES = side-entry sub.

Depth Shifting

Total gamma-ray data were recorded on every run, and this log was used for depth shifting. All logs are displayed in adjusted depth (Fig. 34).

Logging Results

In the upper part of the hole, several tight spots are present, and many intervals are present in which the caliper read the maximum diameter of 19 in., indicating caved intervals. These conditions characterized approximately the upper 500 m. It is difficult to detect distinct "log units" within this section, even though good correlations exist between the different logs in certain parts of the logging run.

In the lower good part of the borehole, several log units can be detected and correlation between the various logs is very good. Major changes in the character of the log curves have been used to define the units. Changes in log-curve character are normally caused by changes in the lithology and agreement can, therefore, be expected between log units and the units described through paleontologic and lithologic analyses.

By using data from the sonic-induction, porosity, and FMS tool string, four discrete log units were identified in the logged interval. These units are defined primarily on the basis of the resistivity, density, sonic velocity, and gamma-ray logs and the FMS images. Within the log units, smaller variations occur. The FMS readings (see CD-ROM, this volume) yield especially detailed information. Hole deviations increase from below 1° at 504 mbsf to ~3° at 690 mbsf.

Log Unit 1

Depth: Base of pipe at 66/120 mbsf down to 465 mbsf

Log Unit 1 extends from the bottom of the pipe down to approximately 465 mbsf. This lower boundary was also noted during the logging operations as a bridge. The upper 200 m are characterized by resistivity readings of approximately 1 Ωm, though layers with higher resistivity readings (of approximately 1.5 Ωm) are present within this unit. Velocity in this log unit varies from 1620 to 1650 m/s, with the higher readings in the lower part of the unit.

A change in several logs can be noted above 129 mbsf. As not all the logs were run in this upper interval, the significance of these variations is unclear.

Log Unit 2

Depth: 465–604 mbsf

Log Unit 2 is characterized by decreasing resistivity with depth. The resistivity varies from 0.6 Ωm in the upper part to 0.45 Ωm in the lower part, with several intervals of higher resistivity. Gamma radia-

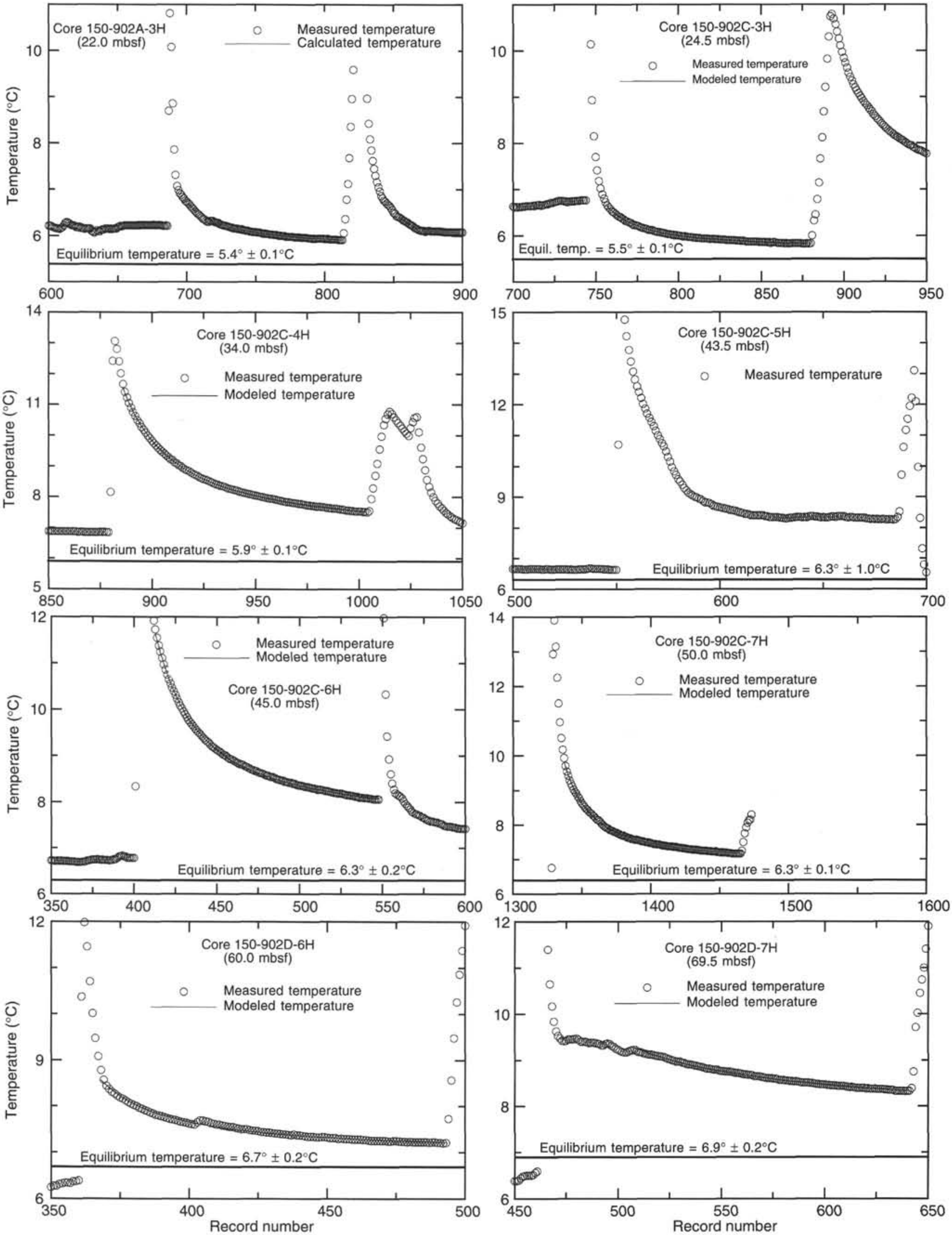

Figure 32. Plots of measured temperatures, modeled temperature equilibrium curves, and calculated equilibrium temperatures for 18 APC cores from Holes 902A, 902C, and 902D. Data based on measurements with the ADARA tool.

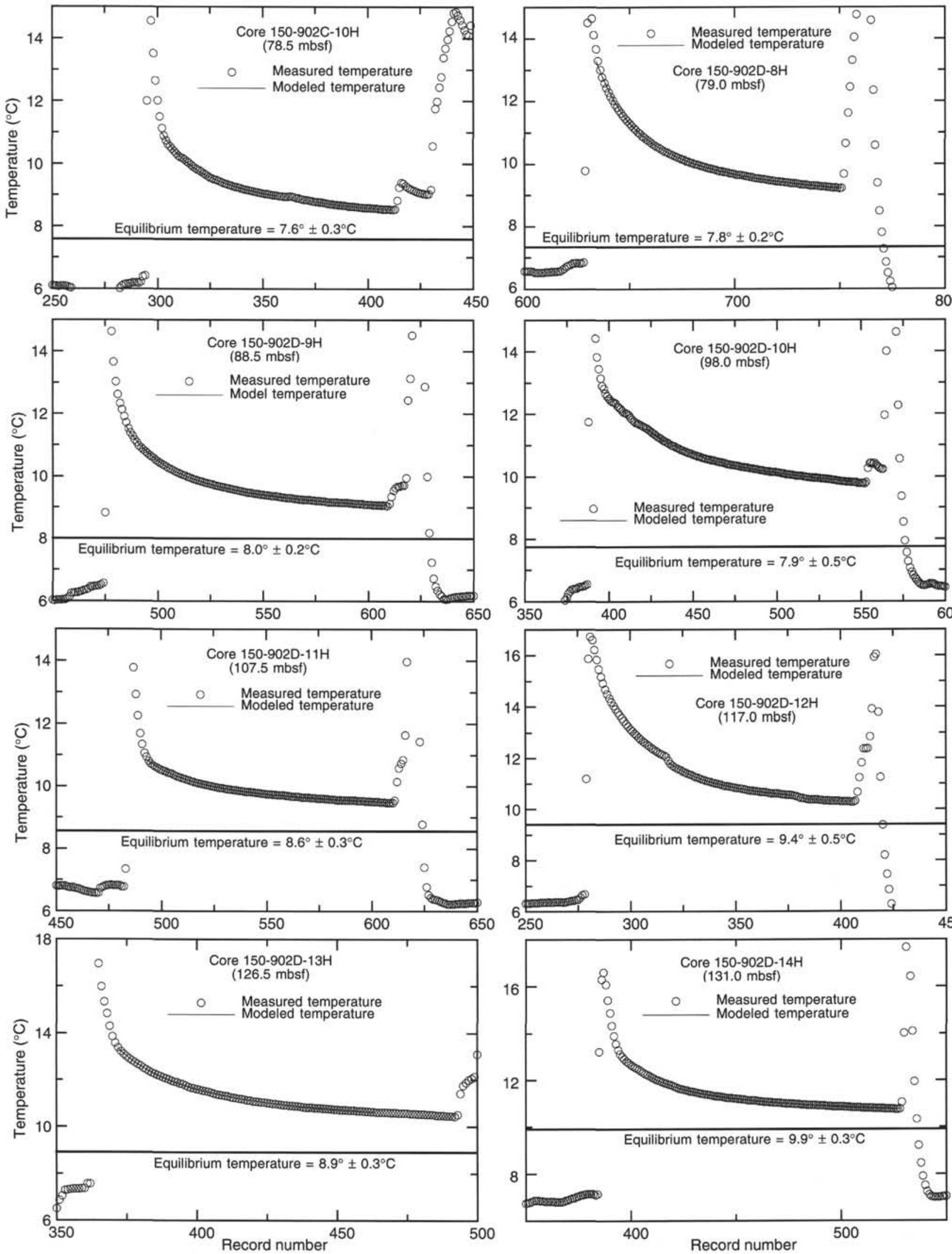

Figure 32 (continued).

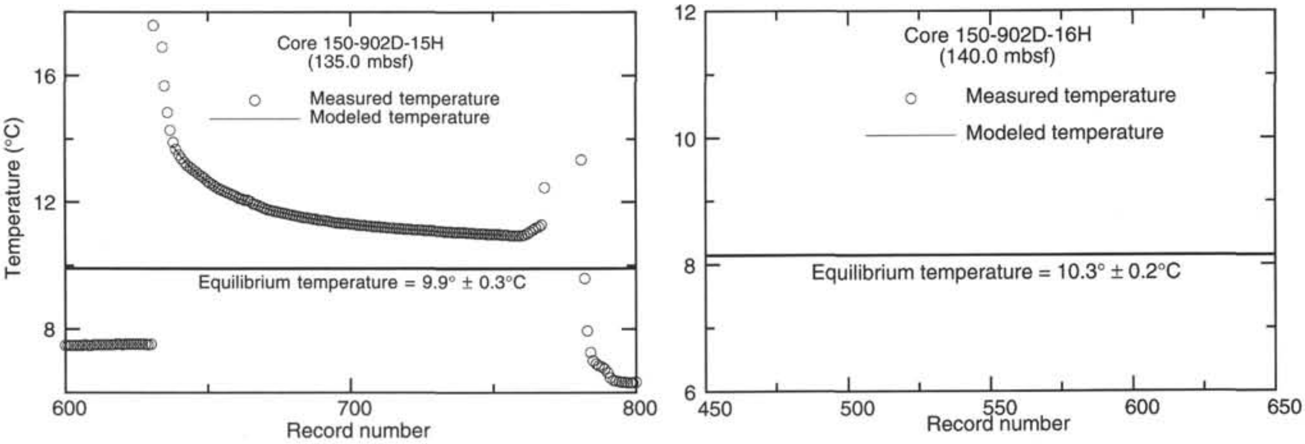

Figure 32 (continued).

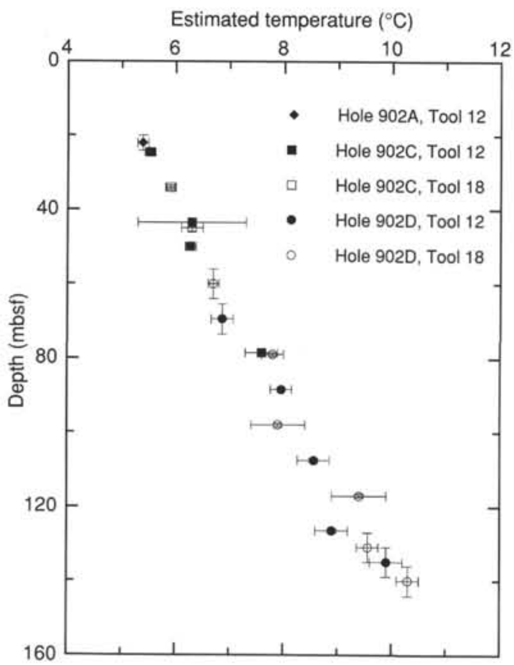

Figure 33. Depth vs. calculated equilibrium temperature curves for 18 APC cores at Holes 902A, 902C, and 902D. Data based on measurements with the ADARA tool.

tion is higher than in log unit 1 because of an increase in the uranium content. A small decrease in thorium content is also noted. Uranium content abruptly increases in several places (e.g., 529.5 and 584.5 mbsf), creating high gamma readings. Sonic velocity increases slightly with depth. The upper part has a velocity of 1733 m/s, which increases downhole to 1783 m/s. Sonic peaks correlate with peaks in the other logs.

The lower boundary at 604 mbsf can be seen clearly on the FMS images. All the peaks mentioned on the other logs correlate extremely well with changes in the FMS images.

Log Unit 3

Depth: 604–681 mbsf

Log Unit 3 is defined by changes in density and velocity values. Resistivity is higher than in log unit 2, approximately 0.7 Ωm, although the resistivity curve is less smooth particularly in the lower part. It especially fluctuates in the lower part. In comparison with log unit 2, no significant change occurs in the gamma-ray readings. In the upper part, the velocity increases to 1943 m/s. A distinct velocity increase up to 2905 m/s occurs at 616.5 mbsf.

Log Unit 4

Depth: 681 mbsf and below

The only logging tools that went deep enough to record log unit 4 are the gamma-ray and FMS tool. The contact between log units 3 and 4 corresponds to the contact between lithologic Units VI and VII (between siliciclastic sediments and clayey chalks; see "Lithostratigraphy" section, this chapter).

In the upper part, between 681 and 685 mbsf, the potassium content is higher. Below 685 mbsf, both potassium and uranium contents decrease, causing the total gamma-ray curve to decrease.

Downhole Temperature Measurements

Temperature measurements with the Lamont-Doherty temperature tool were made during runs 1, 3, and 4. The temperature tool was also attached to the tool string during the second run, but the instrument failed and no temperature data were recovered. Because of various disturbances, it was impossible to get a temperature profile showing the thermal regime of the formation. The bottom-hole temperatures (BHT) measured were 10.7°C during run 1 (TD = 507 mbsf) and 25.8°C during run 4 (TD = 689 mbsf).

From the recorded temperatures and a first estimate of the temperature disturbances induced by the operations, the average thermal gradient can be estimated to be about 35°C/km, decreasing toward depth. A better profile has to be processed onshore, based on the drilling and logging operations history. Nonetheless, this compares favorably with a gradient of 40°C/km derived from Adara temperature measurements (see "Physical Properties" section, this chapter).

Synthetic Seismogram

The poor condition of the upper part of the hole made the density measurements in this section questionable, and it is impossible to produce a synthetic seismogram for the entire logged interval. Nevertheless, the density and sonic traveltime logged in the lower 250 m of the hole have provided a reflection coefficient series for this section. Convolved with an appropriate wavelet, this series resulted in the seismogram in Figure 35. When compared with the original seismic survey results (Cruise Ew9009 MCS Line 1027), it is possible to correlate the synthetic seismogram with the major seismic reflectors

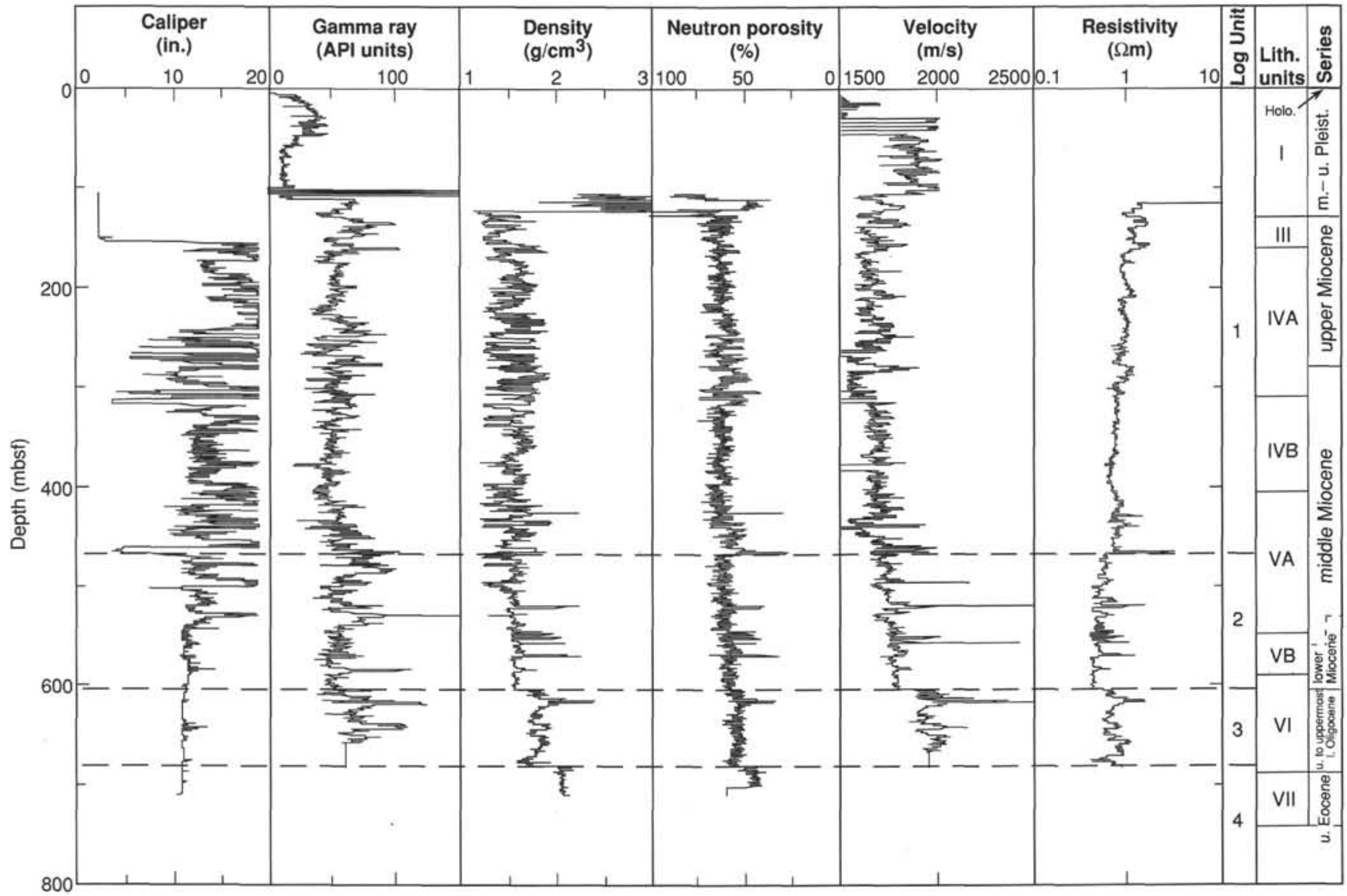

Figure 34. Log units in Hole 902D based on observations of density, caliper, gamma ray, deep resistivity, neutron porosity, and velocity. More detailed plots of log data processed post-cruise by the Borehole Research Group are found at the end of this chapter and on the CD-ROM disk in the back pocket of this volume.

from this section: m5 (Green) (605–620 ms TWT), m5.2/m5.4 (ochre/ sand) (645–675 ms TWT), m6 (pink-3) (700 ms TWT), and o1 (green-2) (780 ms TWT).

SEISMIC STRATIGRAPHY

Introduction

Seismic stratigraphic studies of the Miocene and older section is based on analysis of the Cruise Ew9009 and Exxon seismic grids on the shelf that provide direct ties to the slope (see Chapter 2, this volume). Seismic stratigraphic studies of the Pleistocene section rely primarily on analyses of slope profiles collected during Leg 150 (see Chapter 4, this volume). Seismic profiles used to locate and interpret results at Site 902 are Cruise Ew9009 MCS Lines 1027 (Fig. 2) and 1005 (see Fig. 2 in Chapter 7, this volume).

Most reflectors that we identified within the Pleistocene section at Site 902 are associated with slump/mass flow deposits, consistent with their typically irregular and occasionally downcutting seismic character. These can be traced with available seismic profiles to the outer shelf where the geometric relationships used to define sequence boundaries (see Chapter 3, this volume) indicate these reflectors at Site 902 are likely correlatives to sequence boundaries.

In contrast, pre-Pleistocene reflectors that we identified at Site 902 are generally higher amplitude and more nearly smooth and continuous. Erosional relationships are apparent, but less common than in the Pleistocene section. Acoustic character between these major reflectors is typically useful for inferring depositional processes in those cases where reflectors are more than 40 ms apart. Several Oligocene-Miocene reflectors identified as sequence boundaries by Greenlee et al. (1992) were traced from the continental shelf using the Cruise Ew9009 seismic grid (see Chapter 2, this volume). These included the following: Red, Tuscan, Yellow-2, Blue, Pink-2, and Green. Additional reflectors identified as potential sequence boundaries (G.S. Mountain, K.G. Miller, and N. Christie-Blick, unpubl. data, 1990) have been traced to Site 902 using these same data, and include the Eocene-Miocene reflectors ochre, sand, true blue, pink-3, and green-2. However, uncertainties are present in some correlations to the shelf reflectors because of problems with downlapping, erosion, and masking of reflectors. Therefore, we established a local alphanumeric scheme (Fig. 36 and Table 16) that is tentatively correlated with the shelf reflections.

Time-depth relationships for correlation of seismic profiles to the boreholes were initially derived from three sources (Fig. 10 in Chapter 3, this volume): (1) a velocity log from the COST B-3 well (Scholle, 1980); (2) shelf semblance velocities obtained from an analysis of Cruise Ew9009 CDP stacks on the adjacent shelf (G.S. Mountain, unpubl. data, 1991); and (3) sonobuoy data from the continental rise (Houtz, 1980; Mountain and Tucholke, 1985). In general, the COST B-3 sonic velocities provided the most reasonable correlations between seismic profiles and cores, although they are not applicable above the first sonic velocity measurement made at the COST B-3 well (~329 mbsf). None of the time-depth functions yielded realistic velocities for the section within 40 ms of the seafloor.

The time-depth function derived from the COST B-3 well (Table 16) was used initially to estimate the depth in meters below seafloor (mbsf) of major reflectors crossing the drill site. These estimates were the basis for preliminary ties to the lithologic column, and they provided reasonably good fits between reflectors m1 to m3 and prom-

Table 16. Seismic reflectors identified at Site 902.

Name	Color	Two-way traveltime (ms)	Depth (mbsf)	Calculated velocities (m/s) Interval	Average	Correlation to borehole
p0	—	1.3	1	1500	1500	
p1	yellow	30	23	1533	1533	Slump.
p2	blue	75	58	1556	1547	Inflection in GRAPE density.
p3	green	107	84	1625	1570	Probable hiatus stage 10; minor density change.
p4	purple	150	118	1581	1573	Density change at *P. lacunosa*; near lithologic Unit I/III contact.
m0.5	Red*	195	152.5	1533	1564	Lithologic Unit III/IV.
m0.7	blue	265	208	1586	1570	Bridge in borehole.
m1	Tuscan*	350	289	1906	1651	Major sand bed; possible hiatus; dinoflagellate F/G boundary.
m2	Yellow-2*	500	407	1573	1628	Thin sand; boundary lithologic Units IV/V contact.
m3	Blue*	550	450	1720	1636	Glauconite bed?; dinoflagellate E/F boundary.
m4	Pink-2*	597	492	1753	1648	Large negative reflection coefficient; glauconite sand; dinoflagellate; ECDZ2/ECDZ4.
m5	Green*	620	519	2348	1674	Large negative reflection coefficient.
m5.2	ochre**	645	540	1680	1674	Large negative reflection coefficient.
m5.4	sand**	675	570	2000	1689	Large negative reflection coefficient; major sand bed.
m5.6	true blue**	***	595			Lithologic Unit V/IV contact.
m6	pink-3**	710	612	2400	1724	Large negative reflection coefficient; thin sand unconformity NN2/NP25.
o1	green-2**	780	681	1971	1746	Unconformity NP23/NP19–20; boundary lithologic Unit VI/VII contact.
e1	yellow	870	NP			
e2	red-3**	900	NP			

Notes: Single asterisk (*) = possibly equivalent to the shelf reflectors of this color (Greenlee et al., 1992); double asterisk (**) = possibly equivalent to the shelf reflectors of this color (G.S. Mountain, K.G. Miller, and N. Christie-Blick, unpubl. data, 1990); triple asterisk (***) = not resolvable.

inent surfaces in the borehole. However, this function predicted that reflector o1 (green-2) should occur at 654 mbsf, a depth we think is too shallow. We are confident that this high-amplitude reflector correlates with the distinct disconformity and large impedance contrast (see below) that separates upper Eocene chalks from upper lower Oligocene siliciclastic sediments at 680.9 mbsf. In addition, the COST B-3 time-depth function predicts lower Miocene reflectors m5–m6 at depths that are consistently offset from the levels of reasonably corresponding impedance contrasts (Fig. 36), lithologic changes, or possible hiatuses in the borehole.

Aware of these core-seismic discrepancies, we examined alternative log-seismic correlations for Hole 902D. Borehole conditions were excellent below ~525 mbsf, and the density and velocity logs provided distinct impedance contrasts (Fig. 36) that we used to evaluate seismic correlations both qualitatively and with synthetic seismograms (Fig. 35). Though hole conditions were poor above 525 mbsf, most log signatures show sharp changes at identical levels, suggesting that these data can still be used to guide the placement of seismic ties to the geologic record. The resulting core-seismic correlations and the average and interval velocities they imply are shown in Table 16.

Pleistocene Sequences

We identified five intra-Pleistocene seismic reflections on profiles crossing or passing near Site 902. These reflections were informally named p0, p1, p2, p3, and p4. Site 902 cannot be located relative to the *Ewing* seismic grid more precisely than ±100 m because of minor uncertainties in the navigation of the latter profiles (see Chapter 4, this volume). The pipe felt bottom at 815, 811, and 808 m at Holes 902A, 902C, and 902D, respectively. This differs slightly from the onsite PDR depth of 792 m (corrected) because of the sloping topography adjacent to Site 902 (Berkeley Canyon is 1 nmi northwest and unnamed "middle Berkeley" canyon thalweg is 0.4 nmi northwest; see Fig. 1 and Chapter 4, this volume, for details of the bathymetric survey). Because the thicknesses of the uppermost sequences vary greatly across short distances, the sub-bottom depths of Pleistocene reflectors at Site 902 change with minor (<0.2 nmi) changes in position. Despite these uncertainties, we were able to estimate the depth of Pleistocene sequences at Site 902 by using the water depth and the depth to other, deeper reflectors. The following discussion is based on locating Site 902 on *JOIDES Resolution* SCS Survey number 2 (see Fig. 2 in Chapter 4, this volume) and Cruise Ew9009 MCS Line 1027 using the water depth of 811 m.

The 3.5-kHz echogram profiles show that reflector p0 approaches seafloor near Site 902. This reflector apparently represents a disconformity that separates Holocene dark green pelagic mud from lighter green, stiffer, middle Pleistocene muds (older than *Pseudoemiliania huxleyi* abundance datum; >74–85 ka; >stage 5a).

Reflector p1 (yellow) occurs at 30 ms TWT below seafloor at the beacon drop. Assuming an interval velocity of 1533 m/s from seafloor to this level (Table 16), this reflector occurs at 23 mbsf. This is the depth of a lithologic contact at Section 150-902C-3H-5, 99 cm, with slumps above. This interval lies immediately above a unit of sharply lower bulk-density values than surrounding sediments (see Figs. 19 and 30) that we interpret constitutes reflector p1. Based on the patterns shown in the bulk-density measurements, this reflector correlates to the transition from interglacial stage 7 to glacial stage 6 (see Fig. 20).

Reflector p2 (blue) occurs at about 75 ms TWT below seafloor near Site 902. The best depth estimate for this reflector is that it correlates with 58 mbsf, assuming an interval velocity of 1556 m/s and association with a sharp upsection increase in density. This level correlates with the general transition from oxygen isotope stage 9 to stage 8 (see Figs. 19–20).

Reflector p3 (green) is at 107 ms below seafloor with a predicted depth of 84 mbsf (using rise sonobuoy time-depth) or 95 mbsf (using shelf semblance time-depth). There is broad peak in density at ~83–89 mbsf (see Fig. 19). Assuming an interval velocity of 1570 m/s correlates this reflector with a density change at 84 mbsf (see Fig. 19). This level is associated with a probable hiatus indicated by low sedimentation rates during oxygen isotope stage 10 (see Fig. 20).

Reflector p4 (purple) lies at 140–150 ms at Site 902, corresponding to a depth of 115–125 mbsf (using rise sonobuoy and shelf semblance time-depth, respectively). This correlates either with (1) a downhole decrease in density increase at 118 mbsf associated with the highest occurrence of *Pseudoemiliania lacunosa,* or (2) a disconformity noted at Section 150-902C-16H-1, 116 cm (122.16 mbsf) that separates the middle Pleistocene (stage 12.4) from the upper Miocene (see Fig. 20). Several slumps also occur immediately above this disconformity. Examination of interval velocities shows that this reflector best fits with a traveltime of 150 ms and a depth of 118 mbsf. Placing the reflector either lower in the borehole or higher on the seismic profile yields unrealistic interval velocities (>2000 vs. the value of 1800 m/s indicated on the velocity log). However, the placement of reflectors based on interval velocities is sensitive to minor uncertainties in the identification of overlying and underlying reflectors, and our correlations require evaluation of the impedance contrasts based on the density measurement (see "Physical Properties" section, this chapter).

In summary, we can identify one Holocene and four middle Pleistocene (< ~500 ka) depositional sequences at Site 902. We did not identify lower Pleistocene or Pliocene strata. We correlate the four reflectors that mark the upper Pleistocene sequence boundaries with the transitions into glacial stages 12, 10, 8, and 6 (i.e., during the glacioeustatic lowerings). Mass-transport deposits are associated with the lower parts of stages 12, 8, and 6, and correlate with reflectors p4, p2, and p1, respectively. Reduced sedimentation and/or a hiatus is associated with stage 10 and matches reflector p3.

Miocene Sequences

A major disconformity at 122.1 mbsf corresponds with reflector p4 (see above) and separates the middle Pleistocene section from the upper Miocene section at Site 902. This also marks the contact between lithologic Units I and III. Another contact occurs between lithologic Units III and IV at 152.5 mbsf (see "Lithostratigraphy" section, this chapter). We correlate reflector m0.5 (= Red of Greenlee et al., 1992) at 195 ms with this contact. Although this traveltime corresponds to 169 mbsf (Core 150-902D-20X) using the COST B-3 velocity log, we prefer the correlation to a sonic velocity peak at 152 mbsf (Fig. 34). This correlation yields a reasonable interval velocity of 1533 m/s (Table 16) and places reflector m0.5 immediately above the last occurrence of *D. hustedtii* (Sample 150-902D-19X-CC, LO Chron 10 = C4Ar; Burckle et al., 1982); thus reflector m0.5 is an intra-upper Miocene surface younger than ~8.0–8.3 Ma (Fig. 36). This is consistent with the speculation of Greenlee and Moore (1988) that this is the 8.2-Ma sequence boundary on the global sea-level curve of Haq et al. (1987).

An especially distinct and continuous reflector at 265 ms (m0.7, blue) has a predicted depth of 219 m. No clear lithologic contact was observed near this level, although a bridge formed in the borehole at 208 mbsf (Fig. 36). The velocity log shows a kick at 208–210 mbsf; that suggests a likely correlation, and yields the reasonable interval velocity of 1586 m/s. The precise age of this level is uncertain, although it is lower upper Miocene based on diatom and dinoflagellate correlations at Hole 902D (Fig. 36). Assuming that this reflector correlates with mid-chron C4Ar (Fig. 21, "Sedimentation Rates" section, this chapter), it would have an age of ~8 Ma (i.e., it is very close in age to reflector m0.5).

We identified reflector m1 (Tuscan of Greenlee et al., 1992) at 350 ms; this corresponds to a depth of 278 mbsf using the COST B-3 time-depth profile. This reflector is also reflector M1 of Miller et al. (1987) who traced this reflector between the COST B-3 well and DSDP Site 612. At Site 902, a broad velocity peak occurs at 275–285 mbsf and a series of sand layers occurs at 289 mbsf immediately below the predicted depth (Fig. 36). Assuming placement at 289 mbsf, interval velocity for the section between reflectors m0.7 and m1 is 1906 m/s (Table 16). The section below reflector m1 is remarkably barren of calcareous plankton, which is surprising because at COST B-3 (2 km south) the section contains planktonic foraminifers. If the magnetozones noted above and below m1 are interpreted as a record of polarity history, then this reflector matches a surface where most of Chronozone C5n (8.92–10.42 Ma; Fig. 36) has been removed and this may date reflector m1 as 9.7 ± 0.7 Ma. This is consistent with the age estimate for Tuscan of 9–11 Ma (Greenlee et al., 1992) and with the prediction that m1 correlates to the 10.5-Ma sequence boundary on the Haq et al. (1987) global curve. This is still poorly constrained, and more detailed shore-based analyses are planned.

Reflector m2 (= Yellow-2 of Greenlee et al., 1992) crosses Site 902 at 500 ms and corresponds to a depth of 397 m using the COST B-3 time-depth profile. Hole 902D penetrated sands at 403–412 mbsf, although recovery was poor for this interval. This level marks the contact between lithologic Units IV and V (see "Lithostratigraphy" section, this chapter). Two log-velocity peaks are present between 407 and 411. Assuming that reflector m2 lies at 407 mbsf at Hole 902D, interval velocities are 1573 m/s (Table 16); the slightly lower interval velocities of this section vs. the upper Miocene section are supported by velocity-log data (see "Downhole Measurements" section, this chapter). Reflector m2 occurs below the last occurrence of diatom *D. punctata* var. *hustedtii* at ~382 mbsf; this event has been linked with Chron 12 (= C5r) by Burckle et al. (1982) and has an age estimate of ~11 Ma using the time scale of BKV85. Reflector m2 occurs below a reversed magnetozone that may correlate with lower Chronozone C5r; this position suggests a maximum age of ~11.5 Ma for the level above reflector m2. The older limit on the age is constrained only by a speculative correlation to part of Chronozone C5Ar below (~12.1–12.5 Ma; Fig. 36).

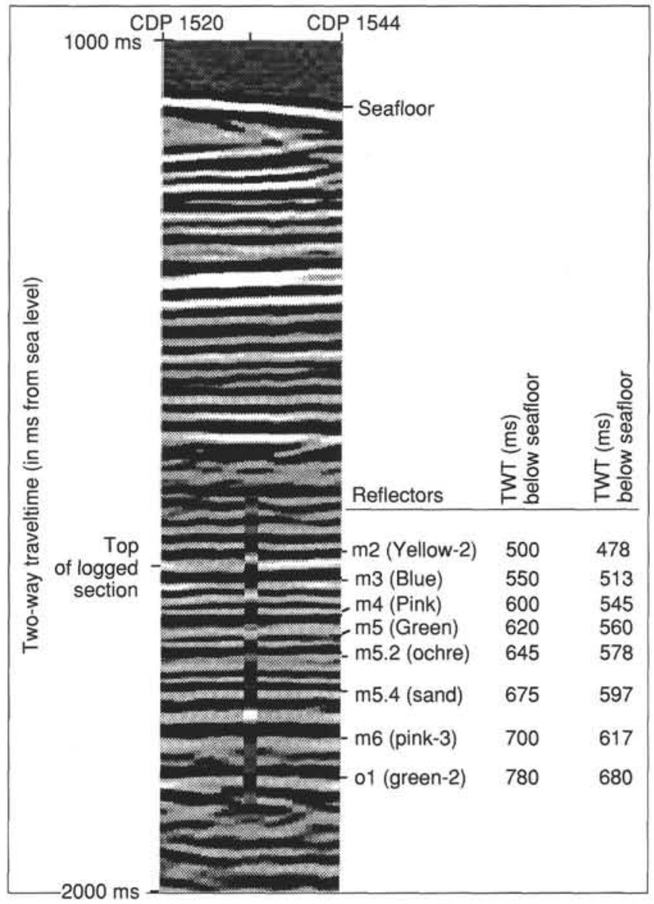

Figure 35. Synthetic seismogram from the lower 250 m of Hole 902D. The seismogram is inserted for comparison into Cruise Ew9009 MCS Line 1027 between CDP 1520 and CDP 1544.

Reflector m3 (= Blue of Greenlee et al., 1992) occurs at 550 ms with a predicted depth of 439 mbsf using the COST B-3 time-depth profile. A glauconite bed at 449–459 mbsf may correlate with this reflector. A velocity increase occurs at 449–451 mbsf, although a series of higher amplitude increases also occurs at 460–465 mbsf. Placing reflector m3 at 450 mbsf yields an interval velocity of 1720 m/s (Table 16), a value that is supported by similar log velocities for this interval. Dinoflagellates indicate a possible break between Zones E and F from 449.3 to 458.9 mbsf; the extreme thinness of Zone E is consistent with a disconformity near this level. The age of reflector m3 cannot be precisely estimated, although it is clearly middle middle Miocene. If the normal magnetozone at 429–455 mbsf correlates with part of Chron C5Ar (Fig. 36), then this reflector may be about 12.5 Ma.

Reflector m4 (= Pink-2 of Greenlee et al., 1992) lies at 597 ms with a predicted depth of 474 mbsf using the COST B-3 time-depth

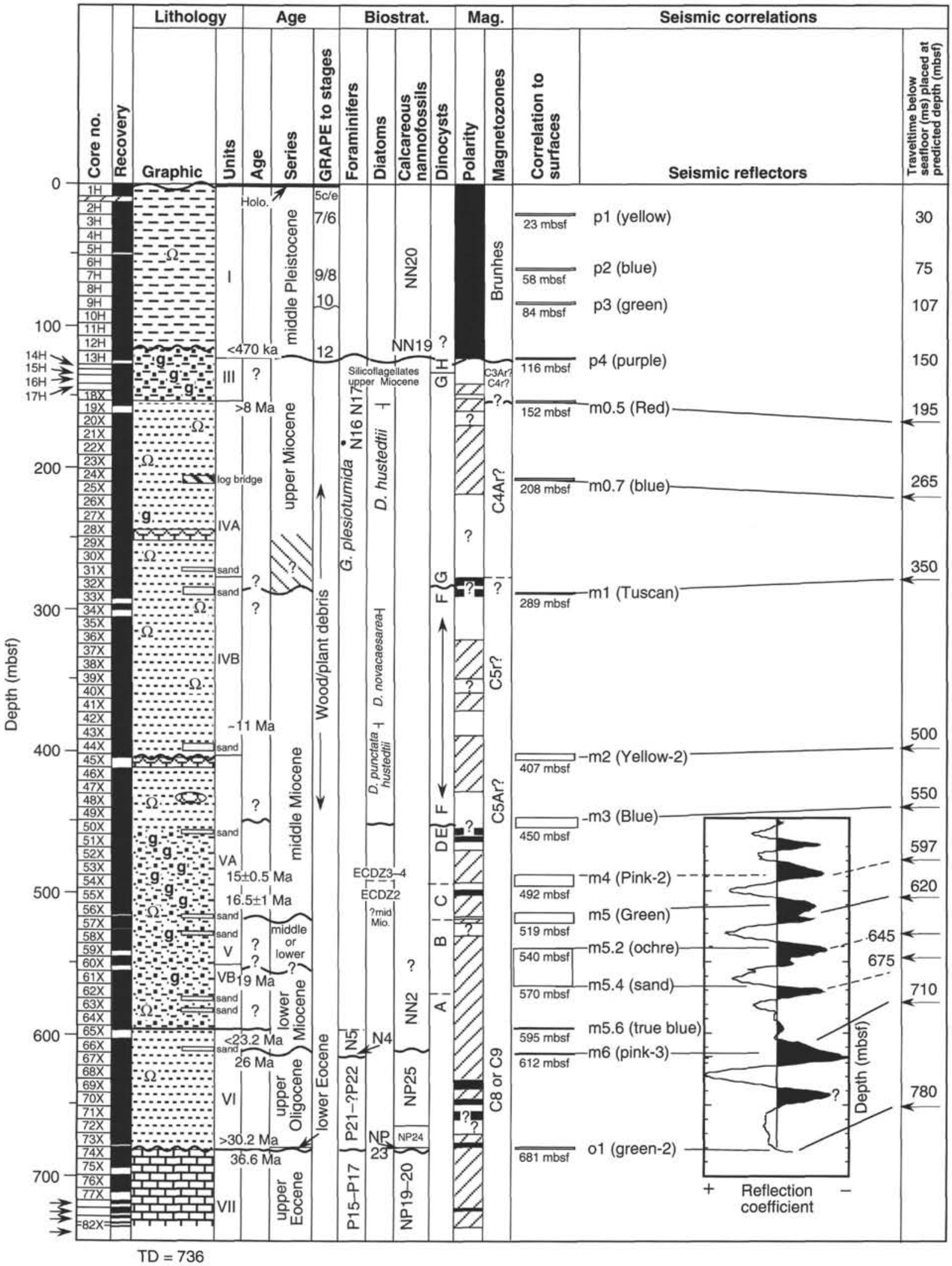

Figure 36. Seismic-core correlations for Hole 902D showing lithology, age, biostratigraphic zones, magnetozones, and seismic reflections discussed in text. TD = total depth.

profile. No obvious lithologic or biostratigraphic discontinuity is observable in the borehole at this depth. A velocity kick occurs at 492 mbsf along with a density decrease; this yields an interval velocity of 1753 m/s plus a large negative reflection coefficient and impedance contrast (Fig. 36). East Coast Diatom Zone (ECDZ) 3–4 and dinoflagellate Zone D lie above this level; ECDZ2 and Zone C lie below. The diatom zones roughly constrain the age to about 15.5 ± 0.5 Ma (Sugarman et al., 1993).

The position of reflector m5 (Green of Greenlee et al., 1992) is uncertain; it lies either at 605 or 620 ms with a predicted depth of 489 or 501 mbsf using B-3 velocities. We correlate reflector m5 with high-amplitude kicks in both velocity and density logs that build to maxima at 519 mbsf (Fig. 34); these peaks yield a very large reflection coefficient (Fig. 36). Correlation to 519 mbsf yields an interval velocity between reflectors m4 and m5 of 2000 m/s (Table 16). The age of this surface is not clear because diatoms indicate middle Miocene below whereas dinoflagellates indicate lower Miocene. Reflector m5 is older than East Coast Diatom Zone (ECDZ) 3–4 and lies just below a sample correlated to ECDZ2. This zone straddles the early/middle Miocene boundary and has an age estimate of 16.5 ± 1 Ma (Sugarman et al., 1993). This dates reflector m5 as older than 15.5 Ma, with a rough estimate of 16 Ma based on interpolation of sedimentation rates (see Fig. 21).

Three lower Miocene reflectors occur at Site 902: m5.2 (ochre), m5.4 (sand), and m6 (pink-3) (Fig. 36). They are identified at 645, 675, and 710 ms, with predicted depths of 524, 552, and 586 mbsf, respectively (using B-3 velocities). A series of sharp velocity and density peaks occur in this section. These changes are shown as three major impedance contrasts at 540, 570, and 612 mbsf (Fig. 36). These correlations yield high interval velocities (Table 16), although these estimates are very sensitive to minor changes in the placement of such closely spaced reflectors. In fact, the average interval velocity for the lower Miocene section from reflector m5 to m6 is 1958 m/s, consistent with high sonic log velocities (1800–1900 m/s with peaks approaching 2400 m/s).

Reflector m5.2 can be dated no more precisely than uppermost lower or lowermost middle Miocene. Reflector m5.4 correlates with the downhole return of calcareous nannofossils; it is underlain by the upper part of Zone NN2. This only establishes that reflector m5.4 is younger than about 19–20 Ma and older than ~16 Ma. Reflector m6 correlates with a paraconformity inferred from nannofossil data at 611 mbsf, where Zone NN2 overlies upper Oligocene Zone NP25, and dates the reflector as ~23–26 Ma.

Another break apparently occurs at 595 mbsf with a change from lithologic Unit V to VI and corresponds to a possible gap from upper Zone NN2 to lower NN2. This surface is younger than reflector m6 and may be the sedimentary expression of a reflection (m5.6, true blue) that merges with reflector m6 at Site 902.

Reflector o1 (green-2) occurs at 780 ms with a predicted depth of 650 mbsf. We correlate this reflector with the contact between upper Eocene chalks and Oligocene siliciclastics at 681 mbsf, the contact between lithologic Units VI and VII. No velocity log is available for this section, although the density log shows a sharp increase at 681 mbsf. Reflector o1 is associated with a disconformity separating the uppermost lower Oligocene (Zone NP23) from uppermost Eocene (Zone NP19–20), with the hiatus spanning 30.2–36.6 Ma.

Summary

We identify five Pleistocene reflectors that are matched to the SPECMAP time scale and correlated with glacioeustatic lowerings, mass-transport events, and at least one paraconformity. Correlations of the Miocene and older reflectors are based on depths predicted by interval velocities. These correlations are adjusted up- or down-section no more than several percent of their depth below seafloor to match reasonable surfaces in the hole based on lithologic, log, or physical properties character. Reflectors m1, m2, m4, m5.4, m6, and o1 are all associated with mass transported sediments that are typically rich in quartz and/or glauconite. Impedance contrasts derived from log data predict significant reflections at several of these surfaces and correlate to seismic profiles across Site 902; several match contacts between lithologic units. Though tentative at present, ages of reflectors traced from the shelf are: m1 (Tuscan) = ?10 Ma, m2 (Yellow-2) = 11–12 Ma, m4 (Pink-2) = ~12–13 Ma , m5 (Green) = 16 Ma, m6 (pink-3) = 23–26 Ma, and o1 (green-2) = 30.2–36.6 Ma. These ages are generally consistent with dates of these same reflectors traced and correlated to Site 903.

SUMMARY AND CONCLUSIONS

Before drilling Site 902, Oligocene to middle Miocene strata from the New Jersey slope were represented only in discontinuously cored or rotary sampled sections. At Site 902 we continuously cored and logged a thick upper Eocene to Holocene section punctuated by disconformities. Site 902 provides a chronology for middle-slope (811 m water depth) deposition, as well as down-dip portions of depositional sequences traced from the shelf.

In general, carbonates characterized Eocene deposition on the slope; however, the middle slope at Site 902 was more strongly influenced by terrigenous muds in the Eocene than was the lower slope (e.g., DSDP Site 612 and outcrops on the lower slope). There is an early Oligocene hiatus (36.6 to slightly older than 30.2 Ma) at this site. By the latest early Oligocene, there was a switch to siliciclastic deposition of silty clays. The early Oligocene hiatus encompassed two glacioeustatic lowerings at around 35.8 and 32.5 Ma that have been inferred previously from the marine oxygen isotopic record. A hiatus also occurred 25.6 to 23.2 Ma across the Oligocene/Miocene boundary. It encompasses another inferred glacioeustatic lowering at 23.5 Ma.

Early Miocene sedimentation was dominated by glauconite silty clays with occasional quartz sand interbeds. Abundant diatoms, together with common marine organic matter, indicate high surface-water productivity beginning in the early Miocene. The correlation of four seismic sequence boundaries to the lower Miocene section at Site 902 suggests that deposition was probably discontinuous, although shipboard magnetobiostratigraphic control was not sufficient to document possible stratigraphic gaps. However, sandy layers occur at the base of each seismic sequence. The main lower Miocene clinoforms associated with these sequences were deposited nearly 100 km landward, beneath the modern inner shelf (Greenlee et al., 1992). Shallowing occurred from the late Eocene (middle bathyal; 600–1000 m) to early Miocene (upper bathyal; 200–600 m).

Terrigenous silty clays and clayey silts containing abundant plant and wood fragments accumulated at rates greater than 8 cm/k.y. in the late middle to early late Miocene (~12–8 Ma). Organic-carbon accumulation rates were very high, resulting in syn- or postdepositional lowering of pore-water pH, dissolution of calcareous microfossils, cementation into siderite nodules, and formation of pyrite. Four middle-upper Miocene seismic reflections were drilled at Site 902; sandy units appear to correlate with each reflection. Again this suggests discontinuous deposition, although biostratigraphic control is not sufficient to determine the extent of the stratigraphic gaps (if any) associated with the reflections. During the late Miocene, layers of glauconite sand were deposited along with mass-flow deposits. This transition to increased sedimentation rate and downslope transport in the middle to late Miocene probably reflects the seaward progradation of clinoforms from a position beneath the modern middle shelf to the outer shelf.

A late Miocene to middle Pleistocene hiatus (~7–8 to 0.5 Ma) at this site is associated with erosional truncation that is now marked by seismic reflector p4. Middle Pleistocene to Holocene deposition was primarily hemipelagic silty clays to clayey silts. Rare mass-transport events occurred during glacial stages 12, 8, and 6. A probable hiatus is associated with glacial stage 10, and seismic reflectors correlate with the transitions from interglacial to glacial stages. Although downslope transport apparently occurred throughout the Pleistocene (as evidenced by the transport of benthic fauna), mass-transport deposits were apparently emplaced during glacial stages.

The principal result from Site 902 is that apparent sequence boundaries traced from beneath the shelf to the slope on seismic data can be recognized as stratal surfaces and dated at Site 902. Reflectors observed on Cruise Ew9009 MCS Line 1027 and their stratigraphic positions are as follows:

reflector p1 (yellow), stage 7/6 transition;
reflector p2 (blue), stage 9/8 transition;
reflector p3 (green), stage 11/10 boundary;
reflector p4 (purple), stratigraphic gap between the middle Pleistocene and upper Miocene;
reflector m0.5 (= Red of Greenlee et al., 1992), intra-upper Miocene;
reflector m0.7 (blue), within lower upper Miocene;
reflector m1 (= Tuscan of Greenlee et al., 1992), near the middle/upper Miocene boundary;
reflector m2 (= Yellow-2 of Greenlee et al., 1992), within the middle middle Miocene;
reflector m3 (= Blue of Greenlee et al., 1992), within the middle middle Miocene;
reflector m4 (= Pink-2 of Greenlee et al., 1992), lower middle Miocene;
reflector m5 (= Green of Greenlee et al., 1992), approximately the lower/middle Miocene boundary (16 Ma);
reflector m5.2 (ochre), lower Miocene;
reflector m5.4 (sand), lower Miocene;
reflector m6 (pink-3), a stratigraphic gap spanning the Miocene/Oligocene boundary (hiatus ~23–26 Ma); and
reflector o1 (green-2), a hiatus spanning most of the early Oligocene.

Ms 150IR-106

NOTE: For all sites drilled, core-description forms ("barrel sheets") and core photographs can be found in Section 4, beginning on page 369. Forms containing smear-slide data can be found in Section 5, beginning on page 833. Thin-section data are given in Section 6, beginning on page 875.

SHORE-BASED LOG PROCESSING
Hole 902D

Bottom felt: 819 mbrf (used for depth shift to seafloor)
Total penetration: 740.1 mbsf
Total core recovered: 676.96 m (91.9%)

Logging Runs

Logging string 1: DIT/SDT/NGT
Logging string 2: HLDT/CNTG/NGT (upper and lower sections)
Logging string 3: FMS/GPIT/NGT (1 pass)

Drill Pipe

The following drill-pipe depths are as they appear on the logs after differential depth shift (see **Depth shift** section) and depth shift to the seafloor. As such, there might be a discrepancy with the original depths given by the drillers on board. Possible reasons for depth discrepancies are ship heave and drill-string and/or wireline stretch.
DIT/SDT/NGT: Bottom of drill pipe at ~107 mbsf
HLDT/CNTG/NGT: Bottom of drill pipe at ~121.5 mbsf
FMS/GPIT/NGT: Did not reach the bottom of the drill pipe owing to bad hole conditions. Only the lower part of the hole was logged.

Processing

Depth shift: All logs have been interactively depth shifted with reference to NGT from HLDT/CNTG/NGT runs, and to the seafloor (– 819 m).
Gamma-ray processing: NGT data were processed to correct for borehole size and type of drilling fluid.
Acoustic data processing: Because of the extremely poor quality of the sonic logs in the interval above 523 mbsf, shore-based processing has been performed only in the lower part of the hole.

Quality Control

Hole diameter was recorded by the hydraulic caliper on the HLDT tool (CALI), and by the caliper on the FMS string (C1 and C2).
Invalid gamma-ray data were detected at 98–102 mbsf (DIT/SDT/NGT run). Invalid density + density-related data (PEF, DRHO) were detected at 586, 596, and 676 mbsf.

Hole 902D: Resistivity-Velocity-Natural Gamma Ray Log Summary

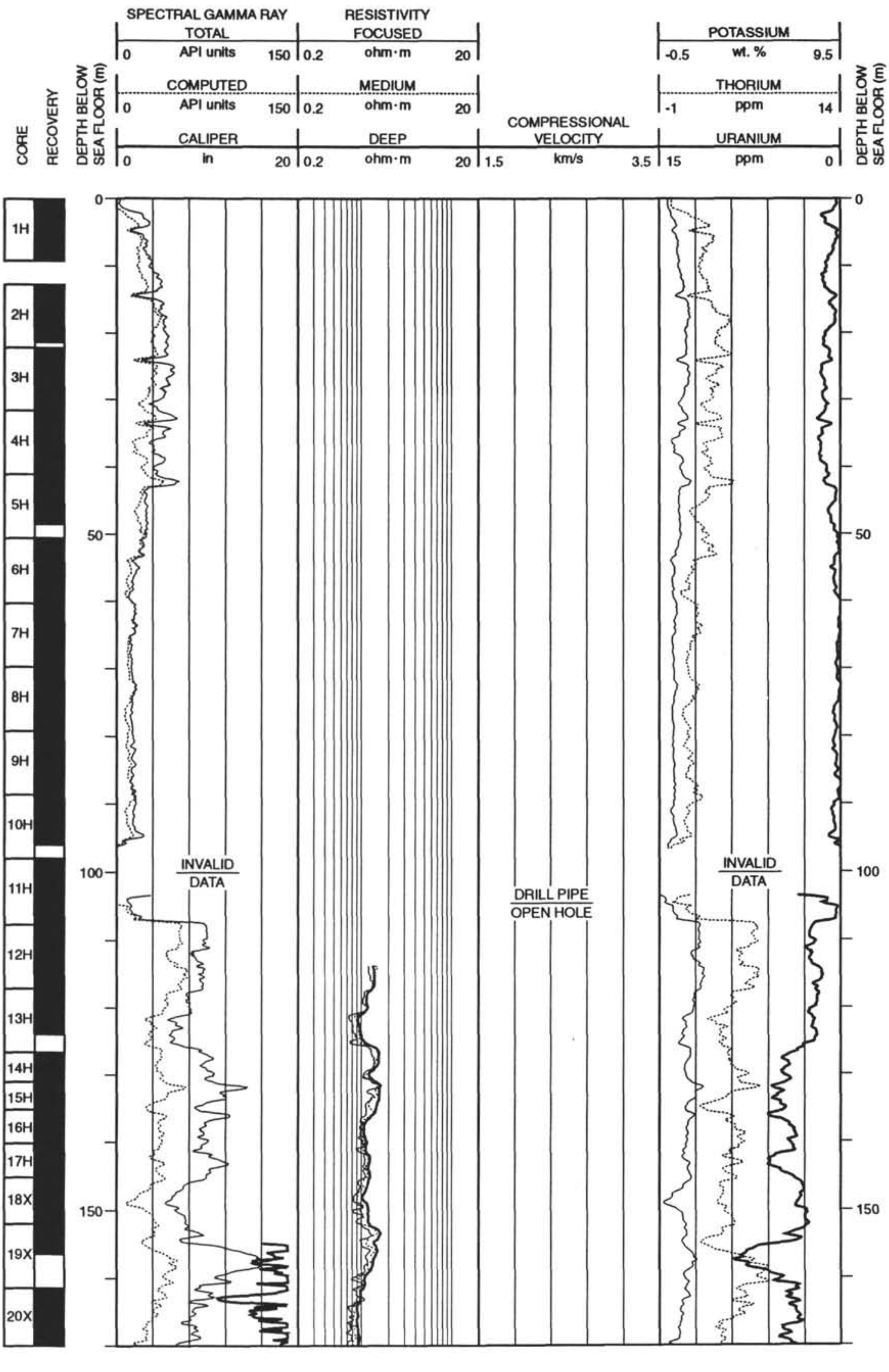

Hole 902D: Resistivity-Velocity-Natural Gamma Ray Log Summary (continued)

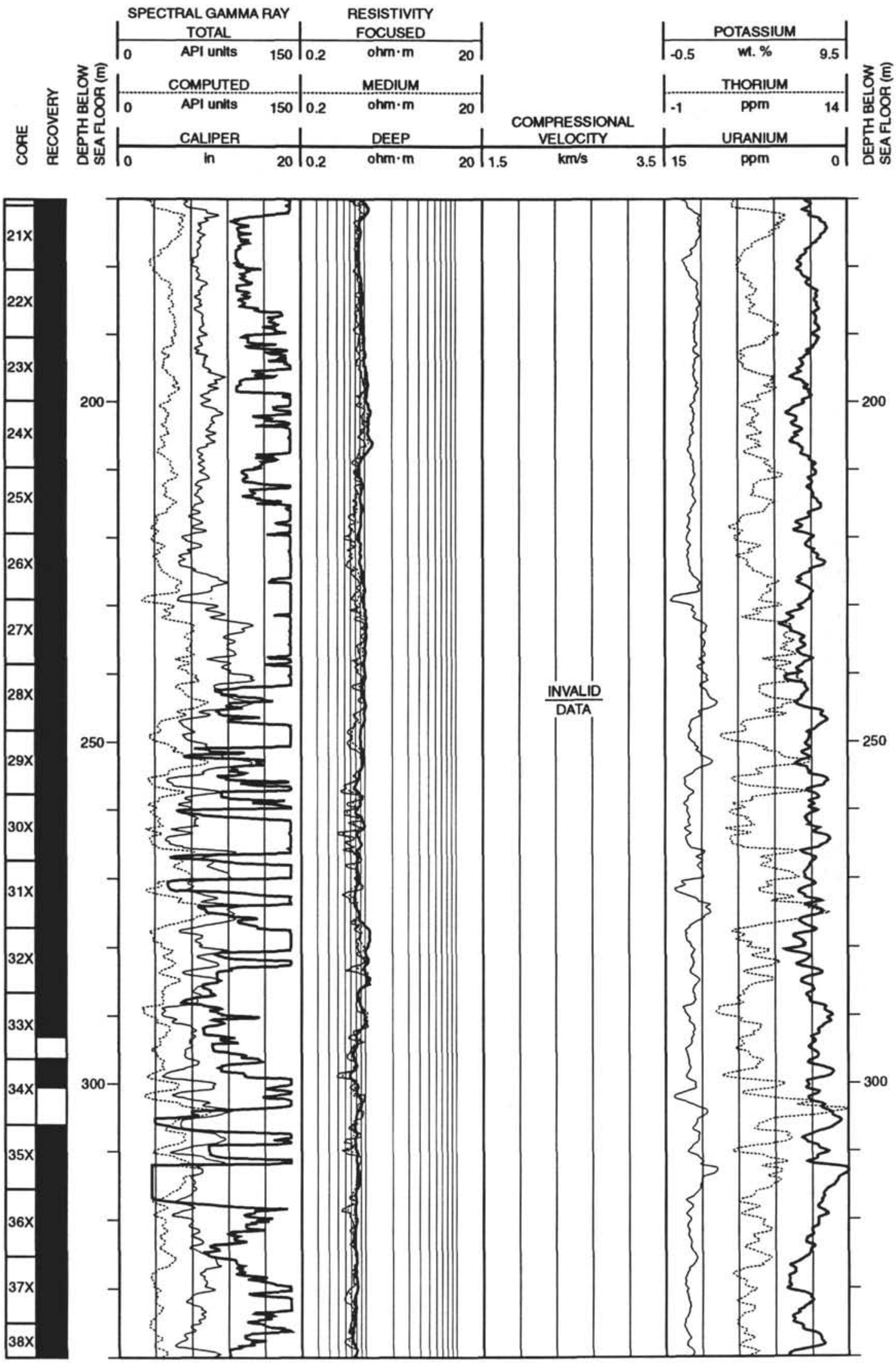

Hole 902D: Resistivity-Velocity-Natural Gamma Ray Log Summary (continued)

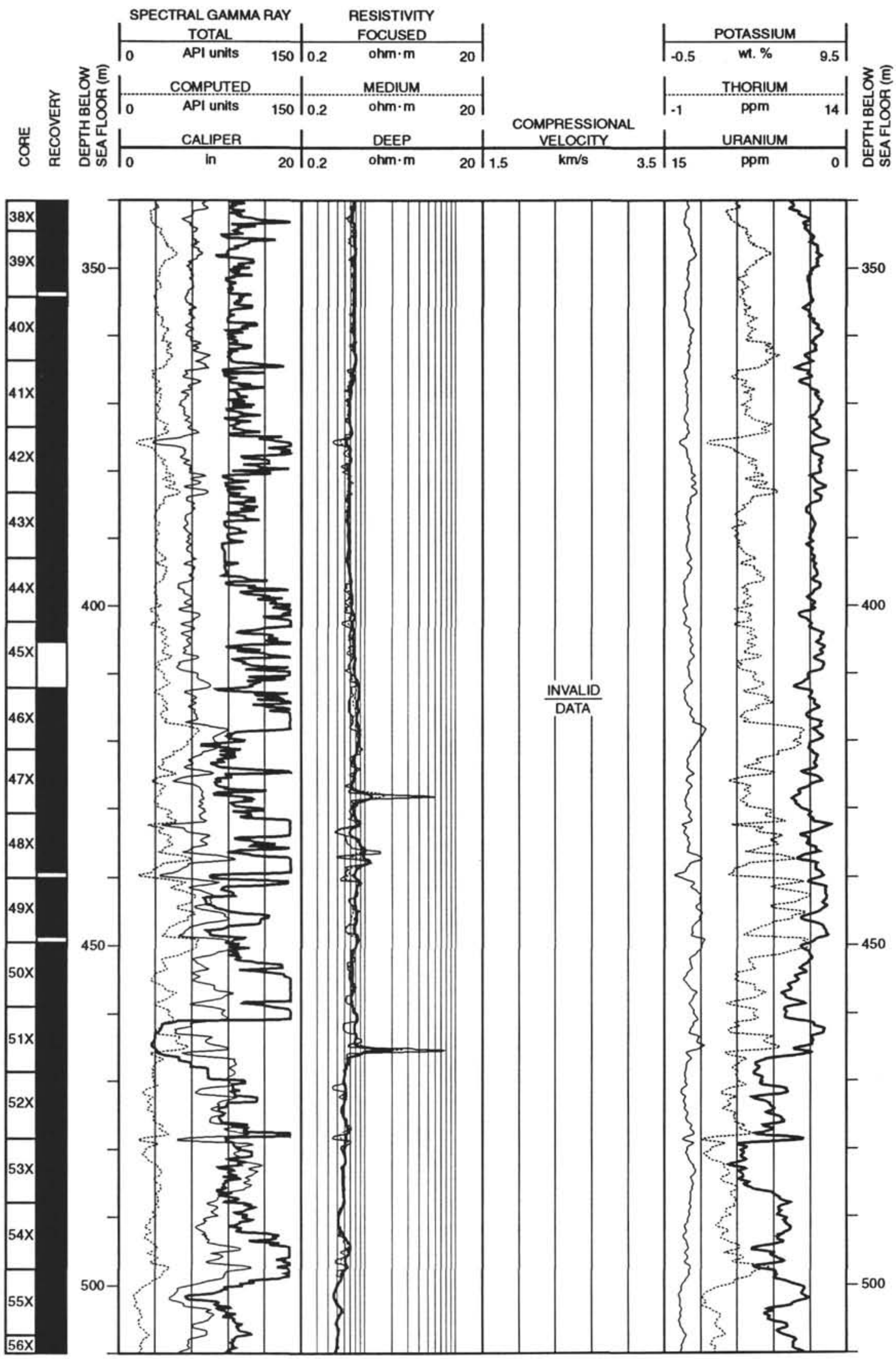

Hole 902D: Resistivity-Velocity-Natural Gamma Ray Log Summary (continued)

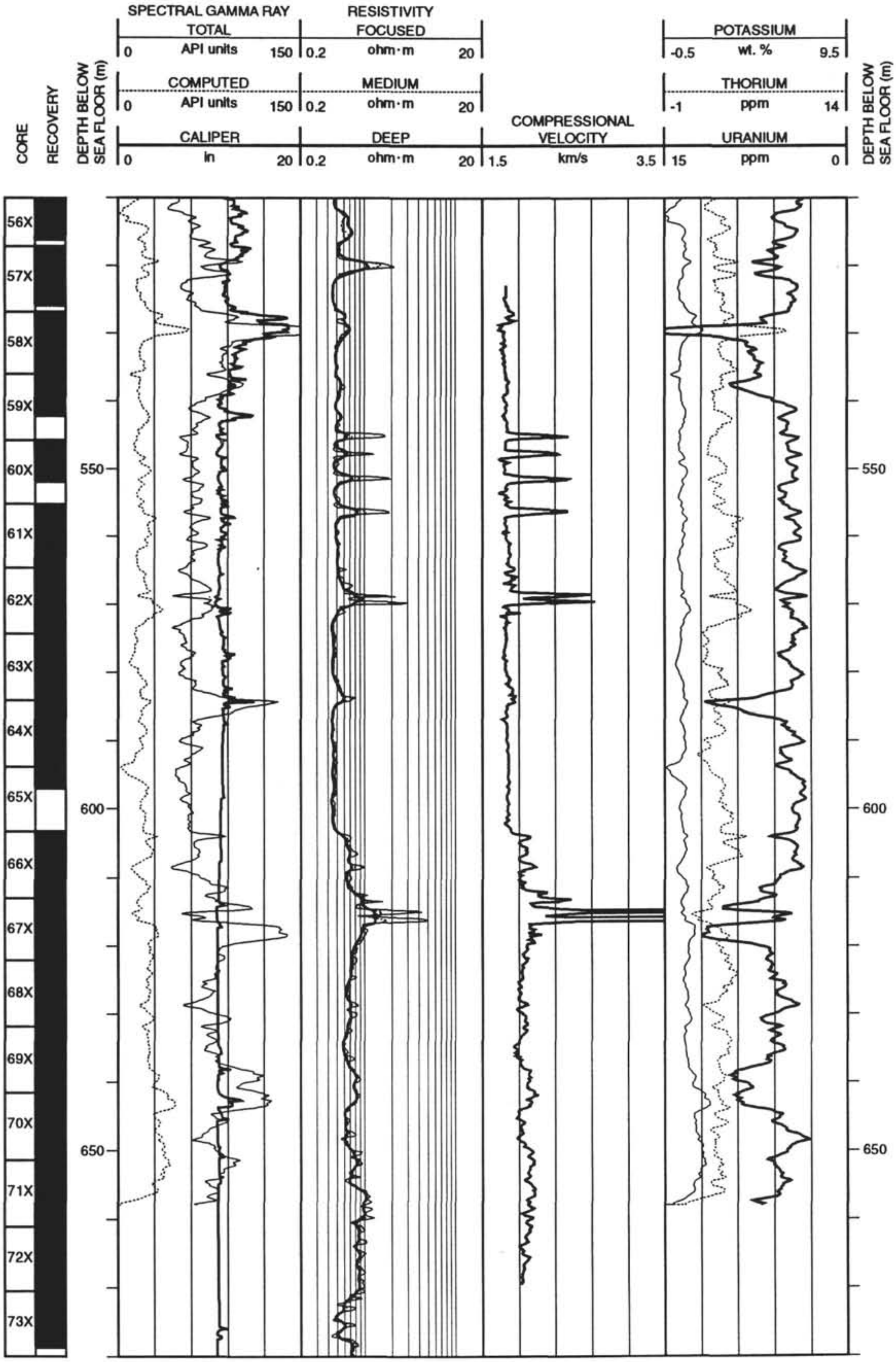

Hole 902D: Resistivity-Velocity-Natural Gamma Ray Log Summary (continued)

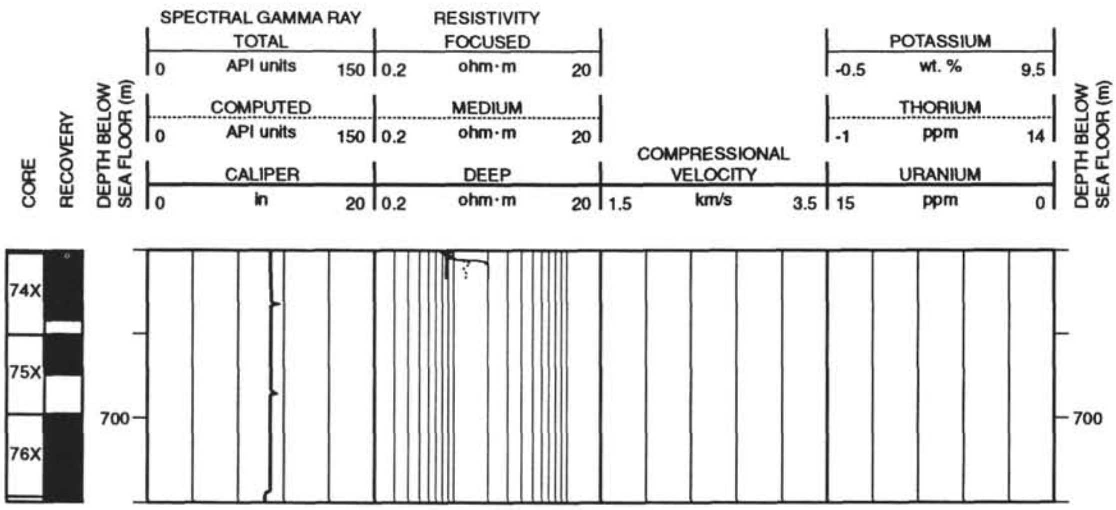

Hole 902D: Density-Porosity-Natural Gamma Ray Log Summary

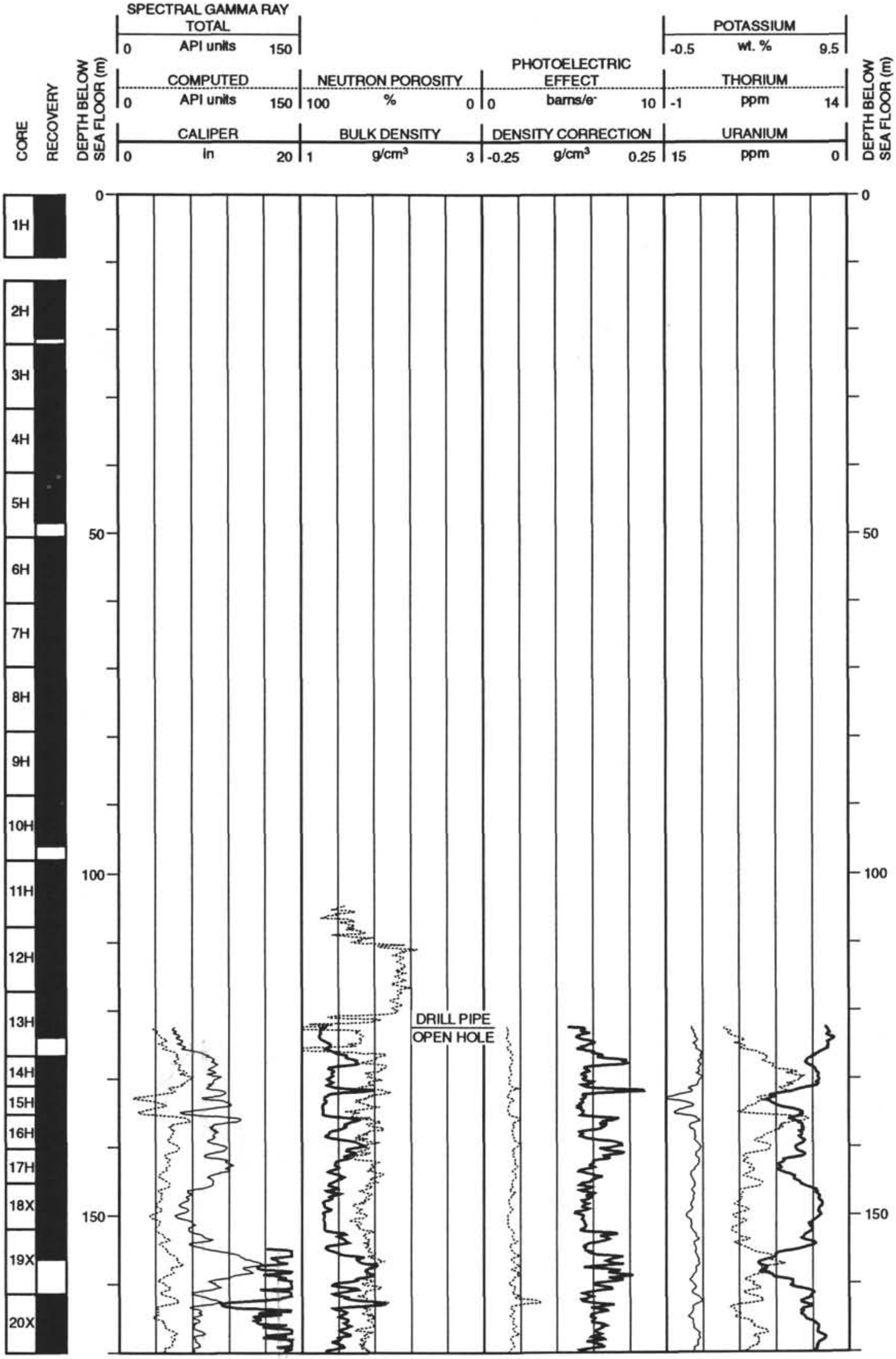

Hole 902D: Density-Porosity-Natural Gamma Ray Log Summary (continued)

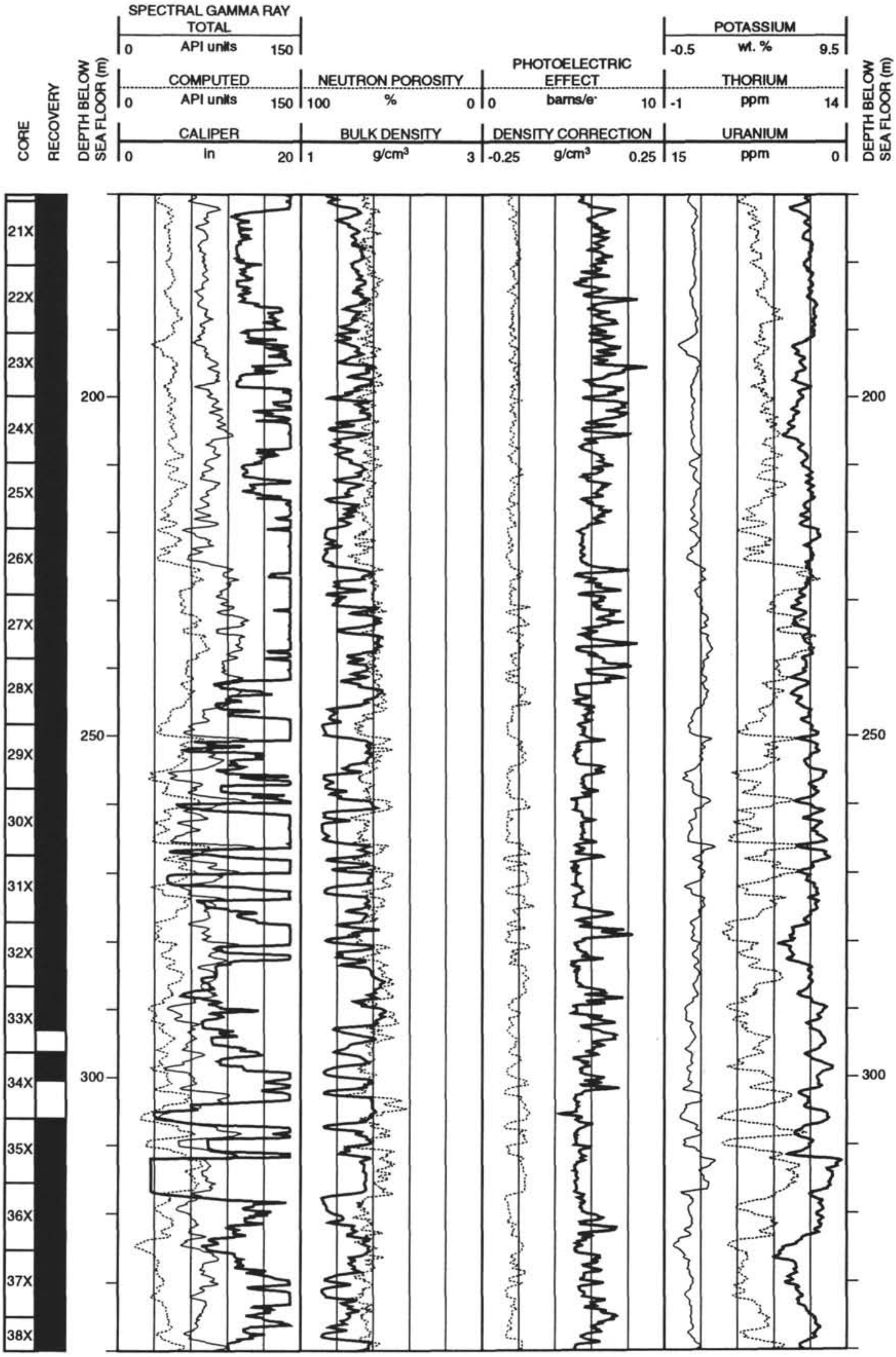

Hole 902D: Density-Porosity-Natural Gamma Ray Log Summary (continued)

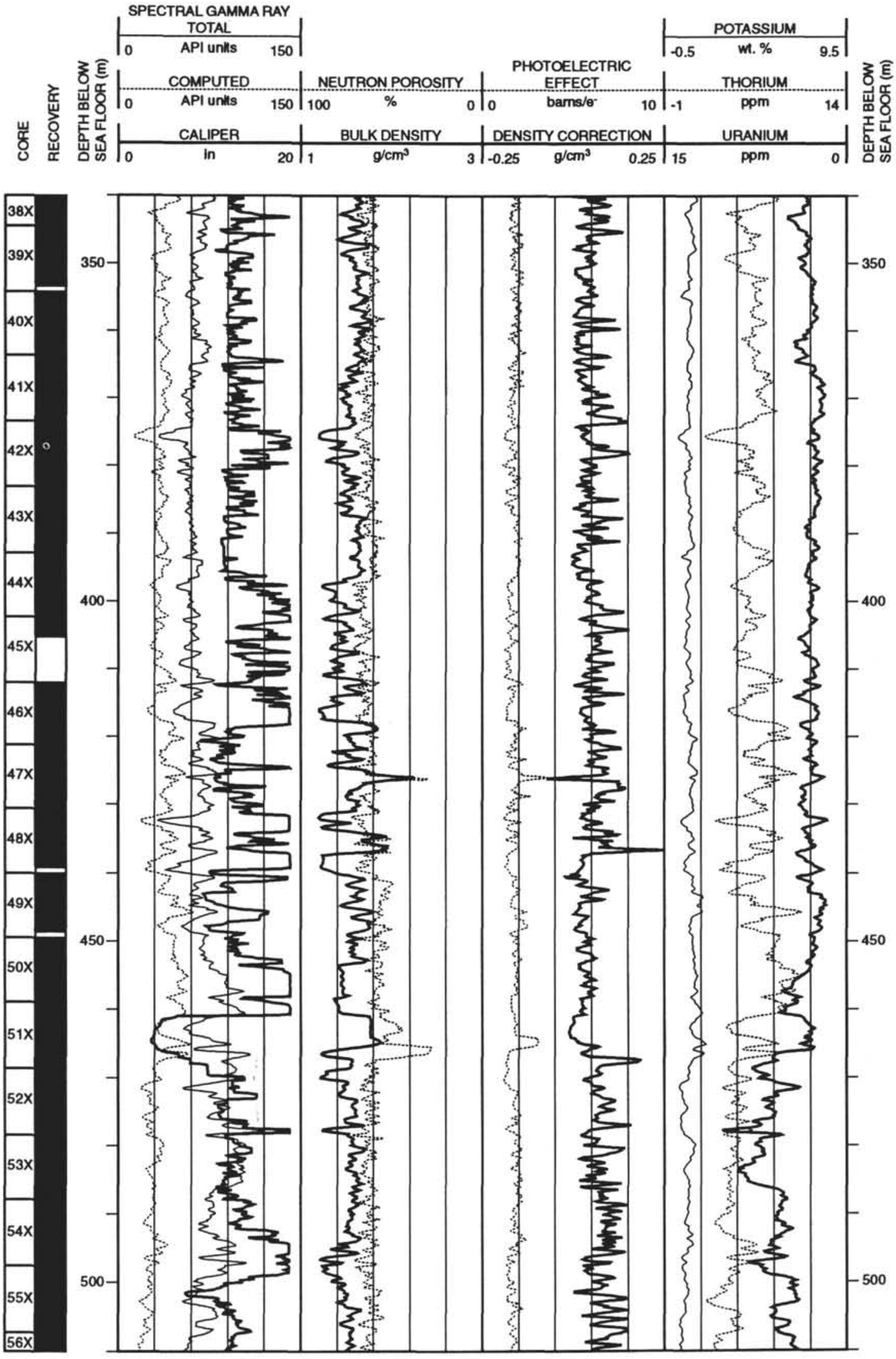

Hole 902D: Density-Porosity-Natural Gamma Ray Log Summary (continued)

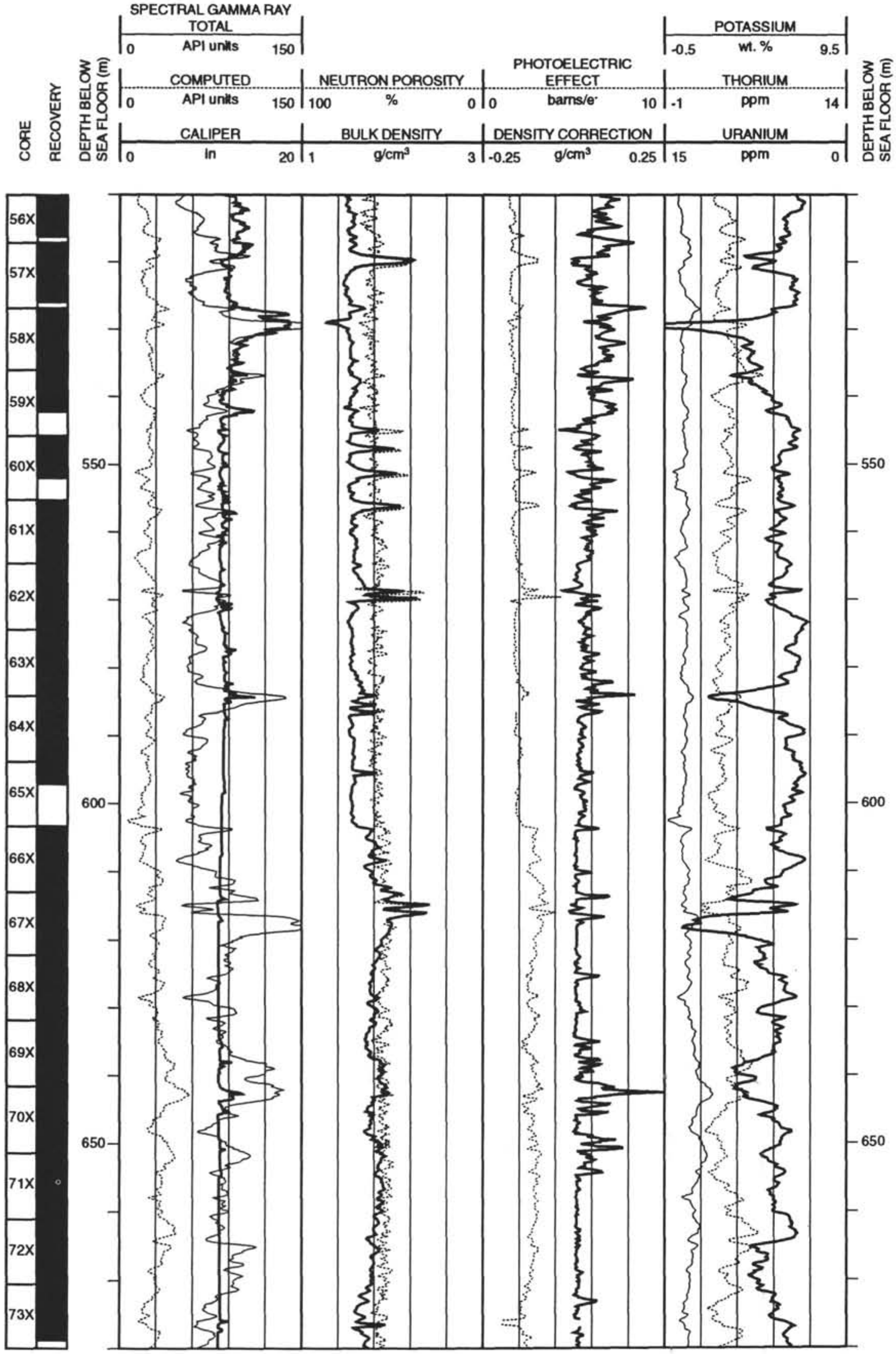

Hole 902D: Density-Porosity-Natural Gamma Ray Log Summary (continued)